Application of commercial aircraft-based observations of greenhouse gases to carbon cycle science

Dissertation

zur Erlangung des akademischen Grades doctor rerum naturalium
(Dr. rer. nat.)

durchgefürt am Max Planck Institute für Biogeochemie Jena
vorgelegt dem Rat der Chemisch-Geowissenschaftlichen Fakültat
der Friedrich-Schiller-Universtät Jena

von M.Tech. (Climate Science) Shreeya Verma geboren am
06.07.1988 in Chandigarh, India

Gutachter:
1. Prof. Dr. Kai Uwe Totsche, Friedrich-Schiller-Universität, Jena
2. Dr. habil. Christoph Gerbig, Max-Planck-Institut für Biogeochemie, Jena

Tag der Verteidigung: 23 November, 2016

Contents

List of Acronyms ..... **ix**

Definitions ..... **x**

List of Figures ..... **xi**

List of Tables ..... **xiv**

Abstract ..... **xvii**

Zusammenfassung ..... **xix**

Chapter 1: Introduction **1**

1.1 Global Carbon cycle 4

1.2 Estimating carbon sources and sinks: Top-down approach 5

1.3 Atmospheric greenhouse gas observations 7

1.4 Thesis Objectives 12

1.5 References 14

Chapter 2: The constraint of CO_2 measurements made onboard commercial-aircraft on surface-atmosphere fluxes **20**

2.1 Abstract 20

2.2 Introduction 20

2.3 Method 23

2.3.1 Jena CarboScope: Model description 23

2.3.2 Data density de-weighting 25

2.3.3 Estimation of model data mismatch error 27

2.3.4 Experimental Setup 28

2.4 Results and Discussion 32

2.4.1 Impact of BLH transport model errors on flux retrieval 32

2.4.2 Constraint on carbon budget due to IAGOS aircraft profiles 34

2.5 Summary 38

2.6 References 41

Chapter 3: Extending methane profiles from aircraft into the stratosphere for satellite total column validation **45**

3.1 Abstract 45

3.2 Introduction 46

3.3 Datasets 49

3.3.1 Integrated Forecasting system for Composition (C-IFS) 49

3.3.2 TOMCAT/SLIMCAT model 50
3.3.3 MIPAS observations of CH_4 51
3.3.4 ACE-FTS observations of CH_4 51
3.4 Results 52
3.4.1 Factors influencing stratospheric contribution to XCH_4 52
3.4.2 C-IFS and TOMCAT models 59
3.4.3 Climatology-based approaches 71
3.4.4 Satellite a-priori profile 74
3.5 Discussion and conclusions 75
3.6 References 77

Chapter 4: Using aircraft profiles for validation of satellite-based column-averaged mole fraction measurements of CO_2 83
4.1 Abstract 83
4.2 Introduction 83
4.3 Datasets 89
4.3.1 CONTRAIL CO_2 data 89
4.3.2 GOSAT-RemoTeC CO_2 observations 91
4.3.3 SCIAMACHY-BESD CO_2 observations 91
4.3.4 Integrated Forecasting system for Composition (C-IFS) 92
4.3.5 Carbon Tracker CO_2 profiles 93
4.3.6 Jena CarboScope CO_2 profiles 93
4.3.7 Weather Research and Forecasting − Greenhouse Gas Model (WRF-GHG) 93
4.4 Validation Methodology 94
4.4.1 Filtering input data 94
4.4.2 Spatial and Temporal Colocation 94
4.4.3 Vertical extension of the aircraft profile 95
4.4.4 Application of satellite a-priori and averaging kernel 96
4.4.5 Estimation of uncertainty of the computed XCO_{2ac} 96
4.5 Results 98
4.5.1 Impact of model profiles in the stratosphere on the calculation of aircraft based XCO_{2ac} 98
4.5.2 Validation results and comparison of satellite products 99
4.5.3 Model analysis: Representativeness of aircraft profiles 106
4.6 Summary and Conclusion 108
4.7 References 110
Chapter 5: Summary and outlook 115

Acknowledgements 119
Curriculum Vitae 121
Selbstständigkeitserklärung 123

List of Acronyms

ACE-FTS	Atmospheric Chemistry Experiment- Fourier Transform Spectrometer
CARIBIC	Civil Aircraft for the Regular Investigation of the atmosphere Based on an Instrument Container
CAMS	Copernicus Atmosphere Monitoring Service
CFC	Chlorofluorocarbons
CONTRAIL	Comprehensive Observation Network for TRace gases by AIrLiner
CTM	Chemical Transport Model
ECMWF	European Centre for Medium range Weather Forecasts
ECV	Essential climate variables
ENVISAT	Environmental Satellite
ERA-Interim	ECMWF Re-analysis Interim
GAW	Global Atmosphere Watch
GHG	Greenhouse Gas
GCOS	Global climate observing system
GOSAT	Greenhouse gases observing satellite
IAGOS	In-service Aircraft for a Global Observing System
C-IFS	Integrated Forecasting system for Composition
IPCC	Intergovernmental Panel on Climate Change
LPJ	Lund-Potsdam-Jena
MACC	Monitoring atmospheric Composition and Climate
MOZAIC	Measurement of Ozone and Water Vapour on Airbus in-service Aircraft
MIPAS	Michelson Interferometer for Passive Atmospheric Sounding
NCEP	National Centre for Environmental Prediction
NIES	National Institute for Environmental Studies
NOAA	National Oceanic and Atmospheric Administration
NWP	Numerical Weather Prediction
OCO-2	Orbiting Carbon Observatory-2
SCIAMACHY	SCanning Imaging Absorption SpectroMeter for Atmospheric CHartographY
TCCON	Total Carbon Column Observing Network
TOA	Top of Atmosphere
UNFCCC	United Nations Framework Convention on Climate Change
UTLS	Upper Troposphere Lower Stratosphere
WDCGG	World Data Centre for Greenhouse Gases
WMO	World Meteorological Organization

Definitions

Units

	Definition	Units
ppm	Parts per million	10^{-6} mol/mol
ppb	Parts per billion	10^{-9} mol/mol

Column-averaged Dry Air Mole Fraction (XGHG)

The ratio of the total amount of a gas species to the total amount of dry air contained in a vertical column starting at the Earth's surface and extending to the top of the atmosphere.

List of Figures

1.1: Atmospheric concentrations of important long-lived greenhouse gases over the last 2000 years.....3

1.2: An overview of the global carbon cycle showing the different reservoirs in PgC and annual mean fluxes of carbon in PgC year $^{-1}$ 4

1.3: Schematic showing the concept of using atmospheric observations in an inverse modelling set-up to estimate surface fluxes.....6

1.4: Global network of stations that contribute to the WDCGG (World Data Centre for Greenhouse Gases) under the WMO GAW programme.....7

1.5: Global Map of the CO_2 column-averaged volume mixing ratios during August 2010 as seen by GOSAT.....9

1.6: Map of scheduled airline traffic around the world (June 2009) 10

2.1: Box plot showing the model data mismatch between the TM3 analysed CO_2 fields and the vertical profiles from the CONTRAIL plotted against height.. 28

2.2: (a) Map showing the locations of the stations of the surface based measurements used in the Jena Inversion scheme. (b) Spatial distribution and number of the vertical profiles measured by the MOZAIC fleet for the TransCom3 land regions during the year 1996-2004.....30

2.3: Prior flux uncertainty for the TransCom3 regions (in PgC year^{-1}) as used in the Jena inversion scheme.....31

2.4: Taylor diagram showing the correlation coefficient, standard deviation and root mean square difference of the concatenated time series of the monthly posterior fluxes from the TransCom3 land regions.....33

2.5: Spatial maps showing the reduction in monthly CO_2 flux uncertainty (in percent) at the TransCom3 regions during the period 1996-2004 using measurements from (a) the Surface network alone (b) Five simulated IAGOS aircraft (c) Combined network (Surface + IAGOS aircraft). Panel (d) shows the net change in uncertainty reduction due to the addition of IAGOS measurements to the surface network.....35

2.6: Plots showing change in uncertainty reduction (with respect to the surface network) against the number of measurements from IAGOS aircraft for (a) Northern hemisphere (b) Tropics.....37

3.1: Mean column abundance of methane (in ppb) during June-August 2010 obtained from the C-IFS fields for (a) tropospheric partial column, (b) stratospheric partial column and (c) total column. 53

3.2: Variability (standard deviation) in the column abundance of methane (in ppb) during June-August 2010 obtained from the C-IFS model fields for (a) tropospheric partial column, (b) stratospheric partial column and (c) total column.....55

3.3: (a) Mean tropopause height (in hPa) and (b) variability (standard deviation) of tropopause height (in hPa) from the C-IFS model fields for June - August 2010. 56

3.4: Scatterplots showing the CH_4 stratospheric column mass fraction (f_{str}) against CH_4 stratospheric column mass fraction variability (σ_{str}) for different seasons of 2010.....58

3.5: Latitudinal distribution of MOZAIC aircraft profile observations (in the vicinity of airports) during the year 2004. 59

3.6: Zonal mean latitude-pressure plots of CH_4 (in ppb) for the months September to November 2010. Panel (a) shows the profiles from the MIPAS limb soundings. Panels (b) and (c) show the profiles from the C-IFS and TOMCAT models, respectively, sampled at the location and time of the MIPAS measurement. Panels (d) and (e) show the bias between the models and MIPAS measurements.. 61

3.7: Zonal mean latitude-pressure CH_4 profiles (in ppb) for the months September to November 2010 plotted against latitude. Panel (a) shows the profiles from the ACE limb soundings. Panels (b) and (c) show the profiles from the C-IFS and TOMCAT models, respectively, sampled at the location and time of the ACE measurement. Panels (d) and (e) show the bias between the models and ACE measurement.. 62

3.8: Maps showing the CH_4 concentration (in ppb) at the 10 hPa pressure level for the months September to November 2010. Panel (a) shows the CH_4 concentration as measured by MIPAS. Panels (b) and (c) show the CH_4 concentrations modeled by C-IFS and TOMCAT, respectively, sampled at the location and times of the MIPAS measurements. Panels (c) and (d) show the bias between the models and the MIPAS measurements.....64

3.9: Maps showing the CH_4 concentration (in ppb) at the 10 hPa pressure level for the months September to November 2010. Panel (a) shows the CH_4 concentration as measured by ACE. Panels (b) and (c) show the CH_4 concentration modeled by the C-IFS and TOMCAT, respectively, sampled at the location and times of the MIPAS measurements. Panels (c) and (d) show the bias between the models and the ACE measurements.....65

3.10: Zonal mean CH_4 stratospheric column bias for different seasons of the year 2010 plotted against latitude for the models (a) C-IFS and (b) TOMCAT. MIPAS data are used as reference truth.....67

3.11: Histograms showing the distribution of the stratospheric column bias with respect to MIPAS at the MOZAIC airport locations for the year 2010 for (a) C-IFS model and (b) TOMCAT model. 68

3.12: Impact of model bias correction. (a) Zonal mean CH_4 stratospheric column bias for different seasons of the year 2010 plotted against latitude. (b) Histogram showing the distribution of the stratospheric column bias in the C-IFS model at the MOZAIC airport locations. 70

3.13: Distribution of the stratospheric column bias estimated at the location of the MOZAIC airports and using FULL C-IFS as the reference truth. Panel (a) shows the bias when monthly mean fields from the C-IFS model are used for profile extension. Panels (b) and (c) depict the bias when monthly mean fields from the C-IFS model obtained using the sampling from the MIPAS and ACE instruments are used for profile extension, respectively. 72

3.14: Stratospheric column error estimated at the MOZAIC airport locations when the GOSAT CH_4 a-priori profile is used for aircraft profile extension. MIPAS data are taken as reference truth. 74

4.1: Steps involved in the validation of satellite-based column-averaged mole fraction using aircraft vertical profiles. 86

4.2: Illustration showing the problem of representativeness of slant aircraft profiles of the true vertical column as seen by the satellite. 88

4.3: Location of CONTRAIL airports used for validation. 90

4.4: Vertical profiles of CO_2 over Narita on 23 January, 2010 extended using model profiles from the Integrated Forecasting system for Composition (C-IFS), Jena CarboScope (JCS) and the Carbon Tracker (CT) model. 98

4.5: Scatter plot between XCO_{2ac} computed at the CONTRAIL airports against the collocated XCO_{2sat} from the (a) SCIAMACHY-BESD and (b) GOSAT-RemoTeC retrieval during January 2010 to October 2011. 102

4.6: Time series of XCO_{2ac} and XCO_{2sat} from the SCIAMACHY-BESD retrieval during January 2010 to October 2011. 104

4.7: Time series of XCO_{2ac} and XCO_{2sat} from the GOSAT-RemoTeC retrieval during January 2010 to October 2011.. 105

4.8: Histogram showing the distribution of the difference between the vertical column XCO_{2ac} computed at the representative location of the aircraft profile and the slant column $XCO_{2ac.}$ 106

4.9: Histogram showing the distribution of the difference between the vertical column XCO_{2ac} computed at the representative location of the aircraft profile and modelled XCO_2 in the colocation region for each aircraft profile. 107

List of Tables

3.1: Mean value and variability of the stratospheric column bias due to the different stratospheric extensions at the locations of MOZAIC airports.....69

4.1: Location and names of the CONTRAIL airports used for validation.....90

4.2: The assumed standard deviation of partial XCO_2 for each domain.....97

4.3: The average and standard deviation of the differences of aircraft-based XCO_2 calculated by using CO_2 profiles extended using different models. 99

4.4: The statistical results of comparison between satellite retrieved XCO_2 data and that computed from aircraft profiles from the CONTRAIL during the period January 2010 to October 2011…….....……....101

Abstract

Robust and sustained observations of atmospheric greenhouse gases like CO_2 and CH_4 are of great importance in order to understand the current state of the global carbon cycle and for the reliable prediction of climate change scenarios.

The current observational network is largely a combination of ground-based stations, satellite instruments and research aircraft. In recent years, a new concept has emerged in the field of global atmospheric monitoring that uses the existing commercial aviation infrastructure and deploys hi-tech instruments onboard commercial airliners. These instruments make highly precise, in-situ observations of atmospheric species at a high spatial and temporal resolution while the aircraft performs its intended task of flying people from one part of the globe to the other. Vertical profiles are measured near airports and cruise level data are obtained in the UTLS (Upper Troposphere Lower Stratosphere) region, thus providing a rich and extensive dataset for studying the chemical and physical processes in the atmosphere.

This thesis is based on greenhouse gas observations (CO_2 and CH_4) from this novel dataset and investigates two main applications of these observations that are crucial to our understanding of the global carbon cycle. These are: 1. Estimation of carbon flux sources and sinks using inverse modelling; 2. Validation of satellite-based column-averaged dry air mole fractions (XGHG).

Inverse modelling schemes are built around models that simulate the atmospheric processes and transport. These models however have large errors in the representation of vertical mixing due to convection near the surface of the Earth that get translated into errors in the retrieved flux estimates. Chapter 2 deals with this issue and shows how the use of vertical aircraft profiles as an observational constraint can help in mitigating the impact of these errors on the fluxes retrieved. The retrieved fluxes show a different response from those retrieved using ground-based measurements, with the latter showing greater sensitivity to errors in simulated vertical transport. This study therefore emphasizes the potential advantage of using aircraft vertical profiles as an observational constraint in inverse modelling studies. Further, the reduction in uncertainty of the posterior flux due to the addition of these observations to the existing ground-based observational network is quantified and is estimated to be the highest for the tropical regions.

Chapters 3 and 4 describe how these vertical profiles can be used optimally for the validation of satellite total column retrievals. Chapter 3 addresses the main drawback of using aircraft profiles for validation of total column measurements, which is their limited altitudinal extent. Therefore, prior to being used for validation of the column-averaged mole fractions as seen by the satellite, these profiles need to be extended synthetically into the stratosphere. In this chapter, three different data sources that can

be used for the extension of CH_4 aircraft profiles are evaluated in terms of the error each of them introduces to the total column mixing ratio and the recommendations for the best approach are provided. It is found that the model profiles from the ECMWF model, the Integrated Forecasting System for Composition (C-IFS) and the TOMCAT/SLIMCAT model perform better in the stratosphere in comparison with other data sources like climatology based data and the satellite a-priori profile. Application of seasonal and latitudinal bias correction to the models further improves the results.

Chapter 4 describes the general approach and methodology for using these profiles for validation of satellite-based column-averaged dry air mole fraction data. XCO_2 from two satellite products – GOSAT-RemoTeC and SCIAMACHY-BESD – are validated using the vertical profiles from the CONTRAIL project to characterize the error associated with each of the retrievals. The two products are compared in terms of the systematic and random error associated with each of them. Both the satellite retrievals are able to capture the spatial and temporal characteristics of the XCO_2 computed from aircraft. The mean bias and standard deviation in comparison with the aircraft-derived column is lower for the SCIAMACHY-BESD retrieval (0.19 ppm, 1.96 ppm) than the GOSAT-RemoTeC product (0.40 ppm, 2.01 ppm). These values are comparable to the results from other validation studies that use data from TCCON as reference truth. This highlights the utility of these data for future validation efforts. Further, this chapter deals with the question regarding the representativeness of the aircraft profiles. Since the aircraft-derived columns are not truly vertical and are obtained from profiles that span a certain horizontal distance, this source of uncertainty in the aircraft-derived column needs to be estimated and accounted for. This impact of the slant profile on the computed column is found to be small for CO_2, indicating that the assumption of vertical aircraft column is reasonable.

Overall, this thesis seeks to evaluate the potential of commercial aircraft-based observations of greenhouse gases for complementing the existing Earth observational network and gaining deeper insights into the dynamics of the global carbon cycle. Only vertical profiles that are measured near airports during the ascent and descent of the aircraft have been used. The impact of data gaps in the aircraft profiles on satellite validation and potential application of cruise level data need to be investigated further and forms the basis of the future work.

Zusammenfassung

Eine genaue kontinuierliche Messung atmosphärischer Treibhausgase wie CO_2 und CH_4 ist von großer Bedeutung für das Verständnis des globalen Kohlenstoffkreislaufes und auch für verlässliche Aussagen über den Klimawandel.

Das gegenwärtige Beobachtungsnetzwerk besteht dabei aus einer breiten Kombination von bodengestützten Messstationen, Satelliten und Forschungsflugzeugen. In den letzten Jahren entstand für das globale atmosphärische Monitoring ein neues Konzept, das die existierende Infrastruktur der kommerziellen Luftfahrt nutzt, um technisch weit entwickelte Messgeräte an Bord kommerzieller Flugzeuge einzusetzen. Diese Messgeräte ermöglichen eine sehr genaue in-situ-Beobachtung der einzelnen atmosphärischen Bestandteile mit einer hohen räumlichen und zeitlichen Auflösung in Verbindung mit der ursprünglichen Aufgabe der Flugzeuge, die Menschen von einem Ort zum anderen zu transportieren. Dabei können sowohl vertikale Profile bei den Starts und Landungen in der Nähe der Flughäfen gemessen, als auch auf Reisehöhe Messungen in der UTLS (Upper Troposphere Lower Stratosphere) durchgeführt werden. Es ergibt sich so ein reichhaltiger Datenpool an Messdaten verschiedener Bestandteile der Atmosphäre, der das Studium der chemischen und physikalischen Prozesse in der Atmosphäre ermöglicht.

Diese Dissertation verwendet Messungen der Treibhausgase (CO_2) und (CH_4) mit diesem neuartigen Beobachtungsansatz und untersucht dabei zwei Hauptapplikationen, die entscheidend für das Verständnis des globalen Kohlenstoffkreislaufes sind: 1. Bestimmung der Oberflächenaustauschflüsse mittels inverser Modellierung; 2. Validierung von satellitengestützt ermittelten Säulenmittelwerten (XGHG).

Für die inverse Modellierung werden Modelle verwendet, die den atmosphärischen Transport beschreiben. Diese Modelle haben jedoch große Fehler bei der Repräsentation der vertikalen Durchmischung durch die Konvektion in der Nähe der Erdoberfläche, was zu Unsicherheiten bei der Bestimmung der Austauschflüsse führt. Die Dissertation widmet sich in Kapitel 2 diesem Aspekt. Es wird gezeigt, wie die vertikalen Profile aus den Flugzeugmessungen als Constraints eingesetzt werden können, um den Einfluss dieser Fehler auf die Bestimmung der Flüsse zu minimieren. Die so erhaltenen A-posteriori-Flüsse unterscheiden sich von den aus Inversionen mit bodengestützten Messungen ermittelten, die eine größere Sensitivität gegenüber Fehlern im simulierten vertikalen Transport aufweisen. Diese Arbeit verdeutlicht daher den potenziellen Vorteil der Nutzung vertikaler Profile aus Flugzeugmessungen als Constraints der Beobachtungen für inverse Modellierung. Weiterhin wurde die Reduzierung der Unsicherheiten in den A-posteriori-Flüssen durch diese zusätzlich zu den existieren bodengestützten Messnetzwerk eingeführten Messungen quantifiziert. Dabei zeigte sich, dass die Reduzierung der Unsicherheiten in den tropischen Regionen am größten ist.

Kapitel 3 und 4 beschreiben wie diese vertikalen Profile optimal für die Validierung der satellitengestützten Spurengasmessungen benutzt werden können. In Kapitel 3 wird der Hauptnachteil der Benutzung von Profilen aus Flugzeugmessungen für die Validierung satellitengestützter Treibhausgasmessungen untersucht, der in den limitierten verfügbaren Messhöhen bei Flugzeugen besteht. Für die Validierung der mit Satelliten ermittelten Säulenmittelwerte der Stoffmengenverhältnisse müssen daher diese Profile synthetisch in die Stratosphäre ausgedehnt werden. In diesem Kapitel wird die synthetische Erweiterung der CH_4 Flugzeugprofile mit Hilfe von drei verschiedenen Datenquellen beschrieben. Diese wurden bezüglich der Fehlerterme des Mischungsverhältnisses der Gesamtsäule untersucht und daraus eine Empfehlung für den besten dieser Ansätze gegeben. Dabei zeigte sich, dass die Modellprofile aus dem ECMWF Modell (Integrated Forecasting System for Composition - C-IFS) und dem TOMCAT/SLIMCAT Modell in der Stratosphäre bessere Ergebnisse liefern als andere Datenquellen wie klimatologische Ansätze oder A-priori-Satellitenprofile. Die Verwendung einer saisonalen und vom Breitengrad abhängigen Bias-Korrektur in diesen Modellen führt zu einer weiteren Verbesserung der Ergebnisse.

Kapitel 4 beschreibt den generellen Ansatz und die Methodologie für die Verwendung der Profile zur Validierung der von Satelliten gemessenen Gesamtsäulen. Dabei wurde das von zwei verschiedenen Satellitenprodukten – GOSAT RemoTeC und SCIAMACHY BESD – erhaltene XCO_2 unter Nutzung der vertikalen Profile aus dem CONTRAIL Projektes validiert. So ließen sich die Fehler charakterisieren, die mit dem jeweiligen Retrieval verbunden sind. Diese beiden Satellitenprodukte wurden in Bezug auf die Terme für den systematischen und zufälligen Fehler verglichen, die mit jeden dieser beiden Produkte verbunden sind. Beide Satellitenretrievals reproduzieren die räumliche und zeitliche Charakteristik der XCO_2 Säule, die aus Profilen von Flugzeugmessungen berechnet wurde. Der mittlere Bias und die Standardabweichung zu den aus Profilen von Flugzeugmessungen ermittelten XCO_2 Säulen ist für das SCIAMACHY Retrieval (0.19 ppm, 1.96 ppm) kleiner als für das GOSAT-RemoTeC Produkt (0.40 ppm, 2.01 ppm). Diese Ergebnisse sind vergleichbar zu Resultaten anderer Validierungsstudien, die Messdaten aus dem TCCON Messnetzwerk als Referenzdaten nutzten. Dies unterstreicht die Nützlichkeit dieser Daten für zukünftige Validierungsstudien. Des Weiteren befasst sich dieses Kapitel mit der Frage, wie repräsentativ die Flugzeugprofile sind. Da die Flugzeug abgeleitete Spalten nicht wirklich vertikal sind und aus Profilen erhalten, die einen bestimmten horizontalen Abstand überspannen , diese Quelle der Unsicherheit in der Flugzeug abgeleitete Spalte muss geschätzt werden und berücksichtigt. Es hat sich gezeigt, dass die Neigung des Profils nur einen geringen Einfluss auf die berechneten Säulenmittelwerte für CO_2 hat. Die näherungsweise Annahme eines vertikalen Profils ist daher gerechtfertigt.

Zusammenfassend zielt diese Dissertation darauf ab, das Potential flugzeuggestützter Treibhausgasmessungen zur Komplementierung des existierenden Messnetzwerkes sowie zur Gewinnung tieferer Einblicke in die Dynamik des Kohlenstoffkreislaufes zu beurteilen. Es wurden nur die vertikalen Profile verwendet, die in der Nähe der Flughäfen während des Aufstieges bzw. der Landephase der Flugzeuge gemessen

wurden. Die Auswirkungen von Lücken in den Flugzeugdaten auf die Satellitenvalidierung und die mögliche Verwendung von im Horizontalflug gewonnenen Messdaten erfordern weitergehende Untersuchungen und bilden den Ausgangspunkt für zukünftige Arbeiten.

Chapter 1

Introduction

"Warming of the climate system is unequivocal ... The atmosphere and ocean have warmed, the amounts of snow and ice have diminished, sea level has risen, and the concentrations of greenhouse gases have increased... It is extremely likely that human influence has been the dominant cause of the observed warming since the mid-20th century".

-IPCC Working Group I, 2013

Global climate change is one of the greatest threats that mankind faces today. The UNFCCC defines climate change as "a change of climate which is attributed directly or indirectly to human activity that alters the composition of the global atmosphere and which is in addition to natural climate variability observed over comparable time periods." In recent years, there has been a growing consensus in the scientific community about significant global warming, based on observational evidence from direct measurements of rising surface temperatures, subsurface ocean temperatures, increasing global sea levels and retreating glaciers. These changes in the climate system are attributed to anthropogenic activities that have been going at an unprecedented rate, especially in the last few decades.

The Earth's climate system is powered by solar radiation, which is largely shortwave, lying in the visible light portion of the electromagnetic spectrum. While a part of this radiation is reflected back into space, depending on the albedo or reflectivity of the surface, a part is absorbed by the Earth and held as thermal energy. To balance this absorbed solar radiation, an equal amount of energy must be radiated back into space. The Earth's atmosphere has a greenhouse effect, which is defined as the trapping and absorption of the radiation emitted by the surface and is thus responsible for warming of the planet and rendering it habitable for life. This effect is the result of the presence of greenhouse gases such as water vapour (H_2O), carbon dioxide (CO_2), methane (CH_4) & nitrous oxide (N_2O) in the atmosphere which, by virtue of their radiative properties, absorb and reflect the Sun's rays back down to the Earth.

Since the Industrial Revolution in the 19th century there has been an increase in the amounts of these greenhouse gases in the atmosphere that has led to an intensification of the natural greenhouse effect. Human activities like fossil fuel combustion for

energy (i.e. coal and oil) and land-use practices have been responsible for altering the atmospheric composition which has directly led to more heat being retained in the atmosphere and thus an increase in global average surface temperatures (Lean and Rind, 2009). The increase in temperature is also leading to other noticeable effects on the climate system like melting of polar ice caps and submergence of coastal areas due to rise in sea levels (Hansen et al., 2011). Together these affects are known as anthropogenic (human-caused) climate change.

CO_2 and CH_4 are the two most important greenhouse gases whose concentrations are directly linked to human activities. Measurements of Antarctic ice cores show a marked increase in the concentration of these gases since the Industrial Revolution (Fig. 1.1). Global mean CO_2 concentration increased from 280 ppm to about 399.5 ppm in 2015 while CH_4 increased from 700 ppb to about 1834 ppb (IPCC, 2014). The increase in carbon dioxide in the atmosphere is mainly attributed to combustion of fossil fuels, deforestation and land-use activities (Ciais et al., 2013). Carbon dioxide is also released in natural processes such as autotrophic respiration and the decay of plant matter. Methane has a natural source in wetlands, rice paddies, the digestive systems of ruminants and termites, and organic waste deposits (such as manure, sewage and landfills) besides being emitted as a result of human activities related to agriculture, natural gas extraction through fracking, and coal mining (Kirschke et al., 2013).

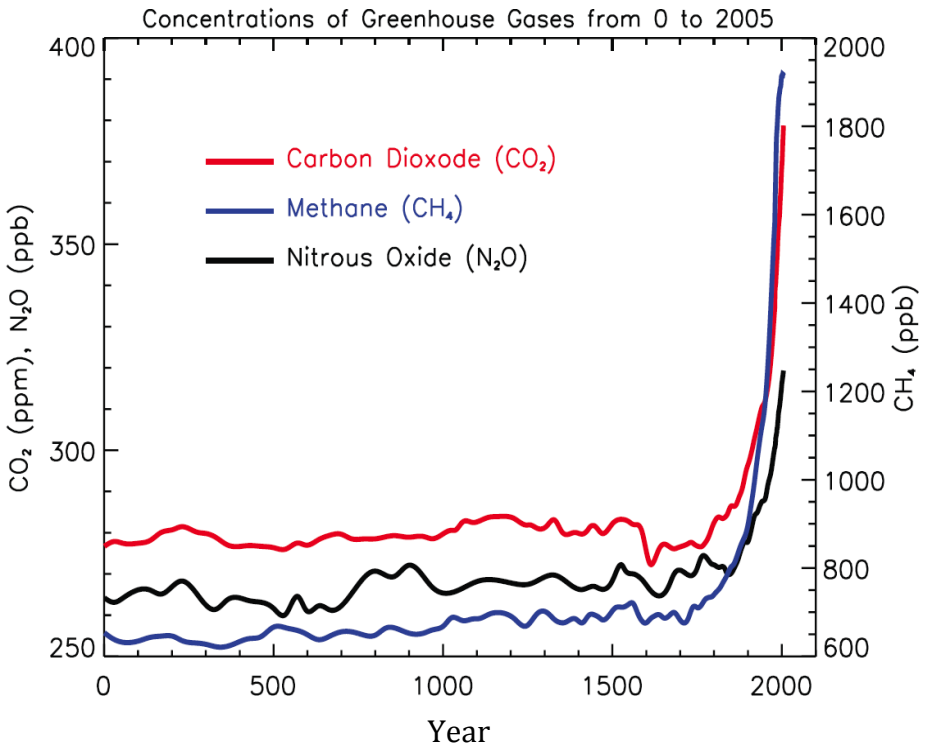

Figure 1.1: Atmospheric concentrations of important long-lived greenhouse gases over the last 2000 years (Forster et al. 2007).

In the coming years, increasing world population and its needs for energy and food production are expected to further increase greenhouse gas emissions which will lead to a further rise in their atmospheric concentrations and an associated increased radiative forcing[1] of the climate of the Earth. In order to make reliable predictions of future climate change scenarios, accurate estimates of current sources and sinks of carbon and an understanding of carbon-climate feedbacks in the Earth system are of prime importance. The sources and sinks of carbon and the sequence of processes by which it circulates between different reservoirs in the Earth System are collectively known as the Global Carbon cycle.

[1]*Radiative forcing is defined as 'The change in net (down minus up) irradiance (solar plus longwave; in W m–2) at the tropopause after allowing for stratospheric temperatures to readjust to radiative equilibrium, but with surface and tropospheric temperatures and state held fixed at the unperturbed values' (Ramaswamy et al 2001). In simple words, it is the measure of the capacity of a gas or other forcing agents to affect that energy balance, thereby contributing to climate change.*

1.1 Global Carbon cycle

Within the Earth system, carbon is present in four main reservoirs or pools:

1. Atmosphere
2. Oceans
3. Earth's crust (Lithosphere)
4. Terrestrial biosphere

Through the action of different processes and feedbacks in the climate system, carbon is circulated amongst these reservoirs. Such processes and feedbacks operating at different spatial and temporal scales are responsible for transferring large amounts of carbon from one pool to another and together form the global carbon cycle. Figure 1.2 shows the different carbon pool sizes and the associated annual carbon exchange fluxes.

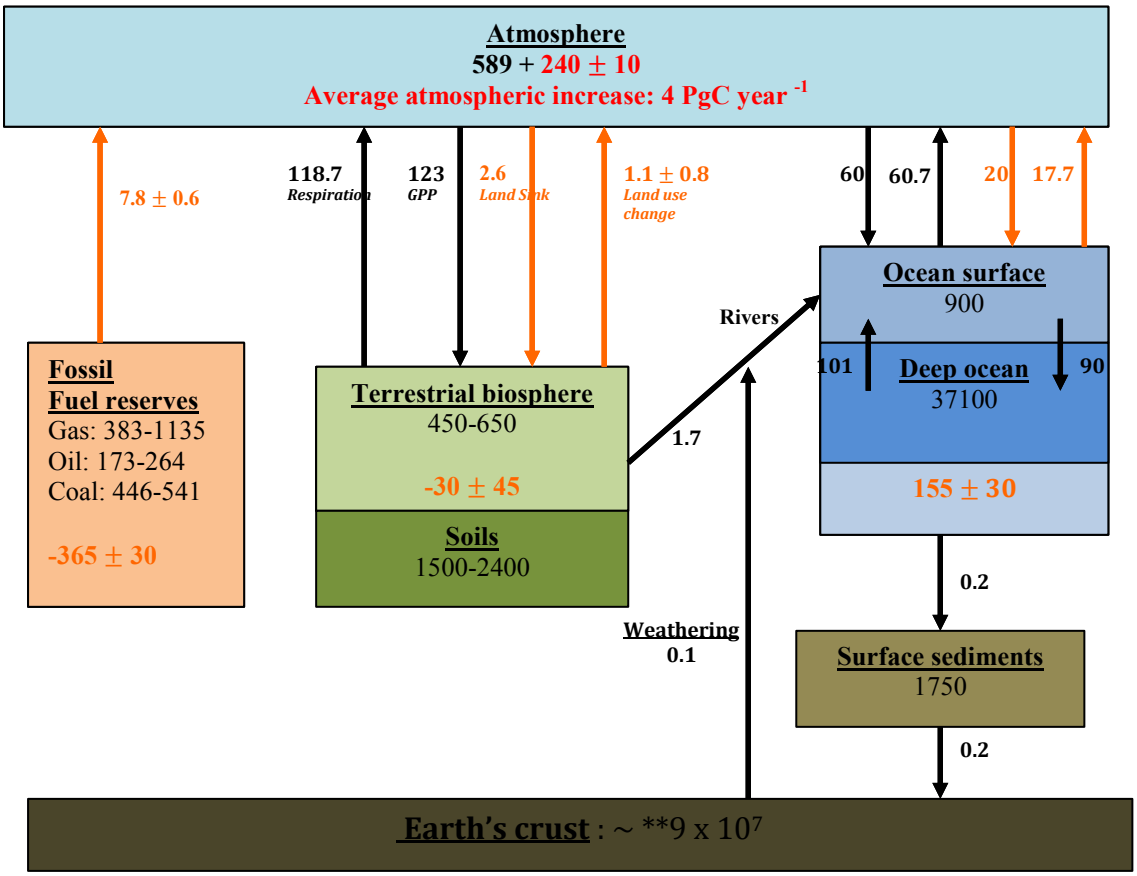

Figure 1.2 : An overview of the global carbon cycle showing the different reservoirs in PgC and annual mean fluxes of carbon in PgC year $^{-1}$ (1 PgC = 1 Petagram carbon = 10^{15} grams carbon). Fluxes and reservoir masses indicated in black correspond to the Pre-Industrial times (before 1750) and anthropogenic fluxes are indicated in orange. (Ciais et al., 2013; **: Taken from Sundquist et al., 1993.)

Carbon in the atmosphere is largely present in the form of CO_2 (about 830 PgC; Prather et al., 2012; Joos et al., 2013) with smaller amounts of CH_4 and CO. It is converted to plant biomass (450 to 650 PgC; Prentice et al., 2001) through the process of photosynthesis (Gross Primary productivity GPP: 123 ± 8 PgC year $^{-1}$; Beer et al., 2010) in the presence of sunlight. Carbon in the terrestrial biosphere is also present in wetland and permafrost soils and litter. When plants die and decay or are harvested by humans, this carbon is transferred from the terrestrial ecosystem pool back to the atmosphere as CO_2 or CH_4 (under anaerobic conditions) through the process of respiration. The Earth's crust forms the largest reservoir of carbon in the form of carbonate rocks, such as limestone, dolomites, and chalk. Atmospheric CO_2 is exchanged with the ocean through gaseous exchange, which is driven by the difference between the CO_2 partial pressure in the air and sea. This carbon is present as DIC (dissolved inorganic carbon; ~38000 PgC ; Falkowski et al., 2000 and Sarmiento and Gruber, 2006), DOC (dissolved organic carbon; ~ 685 PgC; Hansell and Carlson, 1998) and POC(particulate organic carbon ; 13-23 PgC Eglinton and Repeta, 2004). The total cumulative emissions of CO_2 between 1750 and 2011 due to fossil fuel burning amount to 375 ± 30 PgC (Ciais et al., 2013), while those from land-use practices have been estimated to be around 180 ± 80 PgC (Ciais et al., 2013). The net influx of carbon into the atmosphere due to these anthropogenic activities has created a disequilibrium in the exchange fluxes in the natural carbon cycle, thus leading to a net increase in atmospheric CO_2.

1.2 Estimating carbon sources and sinks: Top-down approach

One of the key challenges in carbon cycle science is to accurately quantify the regional carbon sources and sinks and how these will evolve within the context of a rapidly changing climate (Schimel et al., 2001). One of the popular methods for the regional quantification of greenhouse gas fluxes is the top-down or inverse modelling approach (Fig. 1.3).

This approach exploits the fact that the spatial and temporal variations of an atmospheric tracer contain information about the exchange processes between the atmosphere and the surface of the Earth. Atmospheric observations of trace gases are used in combination with knowledge of atmospheric transport and mixing to derive the carbon fluxes at the Earth's surface. Since there is a finite number of monitoring stations all over the globe, this inverse problem is highly underdetermined. Therefore, in order to obtain a realistic solution, some prior knowledge of the carbon fluxes is required. The prior flux may be inferred from sources like process based models or remote sensing data. This approach has been successfully used to infer continental and ocean-basin-scale CO_2 sources and sinks from a global network of atmospheric background stations (e.g. Gurney et al., 2002, Rödenbeck et al., 2003), as well as to

constrain the emission patterns of CH_4 (e.g. Hein et al., 1997, Houweling et al., 1999).

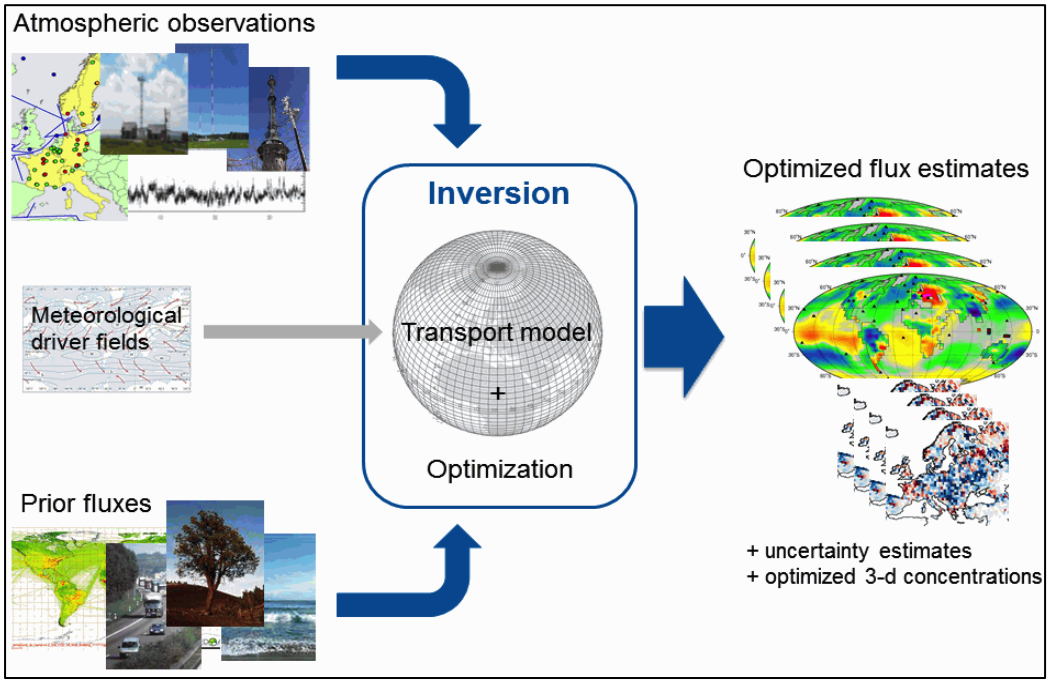

Figure 1.3: Schematic showing the concept of using atmospheric observations in an inverse modelling set-up to estimate surface fluxes. (Source: https://www.icos-cp.eu/node/53)

At present the top-down approach in general is severely limited by the small number of observing stations. The current configuration of atmospheric observing stations is sparse and unevenly distributed. The stations are generally so far apart from the major sources and sinks, that reliable flux estimation is possible only at coarse resolution and at continental scales. Consequently, the carbon budget remains poorly constrained in inversions with large discrepancies between the estimated fluxes by different studies (e.g. Fan et al., 1998; Rayner et al., 1999; Bousquet et al., 2000; Roedenbeck et al., 2003) depending on the included stations. Moreover, these estimates are also heavily dependent on the accuracy and reliability of transport models in simulating the atmospheric processes like vertical mixing (convection) and advection that link the observed mixing ratios to the surface fluxes (Gurney et al., 2002, 2003). Therefore, as the requirements grow for estimating surface fluxes, especially at sub-continental regional scales, so will the need for both, improved modelling techniques as well as a higher density of atmospheric observations on the global scale.

1.3 Atmospheric greenhouse gas observations

Earliest attempt at precise and continuous measurement of atmospheric greenhouse gases was made in the year 1958 when C. D Keeling of the Scripps Institution of Oceanography became the first to make regular measurements of atmospheric CO_2 concentrations at Mauna Loa Antarctica, and La Jolla (Keeling, 1960).

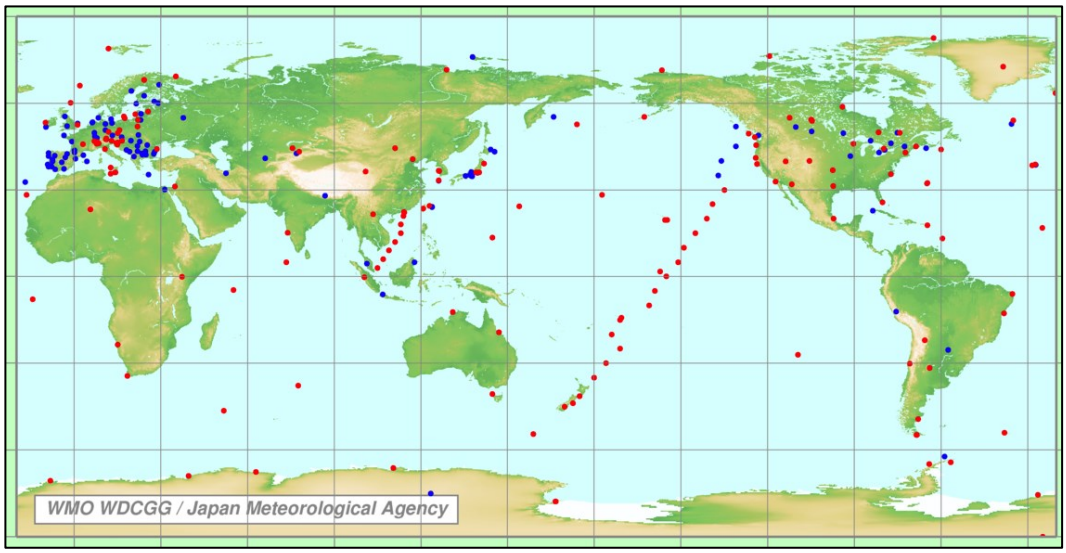

Figure 1.4: Global network of stations that contribute to the WDCGG (World Data Centre for Greenhouse Gases) under the WMO GAW programme.

At present, atmospheric GHGs are being monitored globally by a variety of observation platforms. These include ground-based stations that make routine and precise observations of atmospheric species, in-situ and flask measurements by aircraft, ships, balloons and remote sensing observations of atmospheric constituents such as those from satellites and the Total Column Carbon Observing Network TCCON (Toon et al., 2009; Wunch et al., 2011). The Global Atmosphere Watch (GAW) program of the World Meteorological Organisation (WMO) coordinates the systematic observations and analysis of atmospheric composition (www.wmo.int/gaw/). Figure 1.4 shows the global network of stations that observe atmospheric greenhouse gases as a part of the WDCGG (World Data Centre for Greenhouse Gases) under the GAW program.

The need for accurate measurements of atmospheric greenhouse gases is three-fold:
1) To better understand global carbon cycle, in particular, the exchange of greenhouse gases between the atmosphere and the biosphere and ocean through inverse modelling techniques.
2) To validate and calibrate remote sensing measurements that complement the surface based network.

3) To assess and improve present modelling capabilities as well as improvement of feedback parameterizations used in climate models for reducing predictive uncertainties.

Ground-based stations such as those operated by NOAA ESRL (United States), CSIRO (Australia) and NIES (Japan) have been providing accurate in-situ information about the atmosphere with records going back for decades. These observations are being assimilated into atmospheric models that constrain carbon source/sink scenarios (e.g. Gurney et al., 2002; Rödenbeck et al., 2003; Peters et al., 2007). However, the limitation of these surface based measurements is that they have sparse sampling and are unevenly distributed globally. For instance, the majority of the ground based stations are located in the continents of Europe and North America but tropical regions of Africa and Amazonia are not adequately covered, sometimes even lacking measurements entirely. In addition, these measurements are not likely to be representative of large areas (Haszpra et al., 1999) and provide only localized flux information.

Spaceborne measurements such as those made by GOSAT (Yokota et al., 2009), OCO-2 (Crisp et al., 2008) and SCIAMACHY (Bovensmann et al., 1999) can compensate for the sparseness of the surface based measurements since they have the ability to provide information around the world using a single instrument. These satellites provide column-averaged dry air mole fractions of CO_2 and CH_4 that can be used as an additional constraint for regional flux estimation (Rayner and O'Brian, 2001; Houweling et al., 2004; Chevallier et al., 2005; Miller et al., 2007). Figure 1.5 shows the map of the column averaged CO_2 during August 2013 from the GOSAT satellite, which is indicative of the spatial coverage of the instrument. These measurements are, however, prone to higher measurement uncertainty and systematic errors, as well as temporal heterogeneity in their sampling (Ehret and Kiemle, 2005; Galli et al., 2014; Checa-Garcia et al., 2015) that limits their use for inverse modelling of surface fluxes. These measurements therefore need to be continuously validated and calibrated using independently-obtained measurements of higher precision.

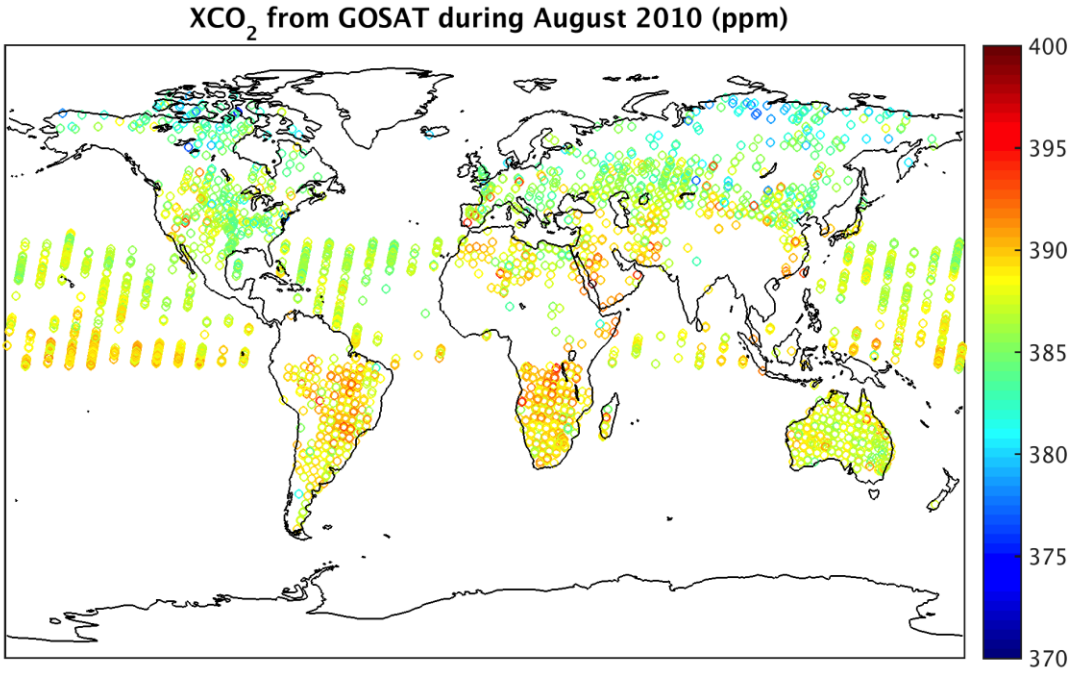

Figure 1.5: Global Map of the CO_2 column-averaged volume mixing ratios during August 2010 as seen by GOSAT

One source of validation of spaceborne instruments is a network of ground-based spectrometers, such as the Total Column Carbon Observing Network (TCCON), (Toon et al., 2009) that provide column-averaged mole fractions of CO_2, CH_4 and CO (Wunch et al., 2011, Petersen et al., 2008, Yang et al., 2002). Some recent studies such as those by Reuter et al., (2011), Parker et al., (2011) and Kulawik et al., (2016) have successfully used these remotely sensed columns for validation efforts. However, such spectral methods must also be validated and calibrated by in situ measurements having higher precision.

This is being achieved using airborne measurements, for instance, those made onboard aircraft, balloons that provide highly precise and accurate in-situ information about atmospheric composition and therefore can be used as useful validation data for remotely sensed observations (e.g. Inoue et al., 2013, de Laat et al., 2012, 2014). They can also be utilized within an inverse modelling framework as an observational constraint for estimation of surface fluxes (e.g. Patra et al., 2011, Niwa et al., 2012). In addition, these measurements can be useful for model improvement and in bias correction schemes.

Institutions like NOAA and NIES conduct regular measurements of greenhouse gases using flask-sampling technique at specific sites around the globe. These institutions

also hold campaigns that make trace gas measurements using research aircraft flights. These are precise measurements, having a high spatial and temporal resolution. The typical range of altitude at which these aircraft measure is from a few hundred meters to about 8 km. However such campaigns are sporadic since the prohibitive expense restricts the number of flights and hence the data availability.

In the past few decades, the concept of commercial aircraft as platforms for obtaining information about atmospheric composition and chemical and physical processes has emerged. There are currently nearly 400 commercial airlines operating worldwide that regularly carry millions of people from one part of the globe to another. Figure 1.6 shows a map of scheduled airline traffic around the world for June 2009, which is indicative of the extensive global-scale infrastructure of civil aviation. In such a scenario, obtaining atmospheric data by deploying sensors on a commercial aircraft, while it carries out its intended task of flying people from one part of the globe to another, is quite an attractive and cost-effective idea.

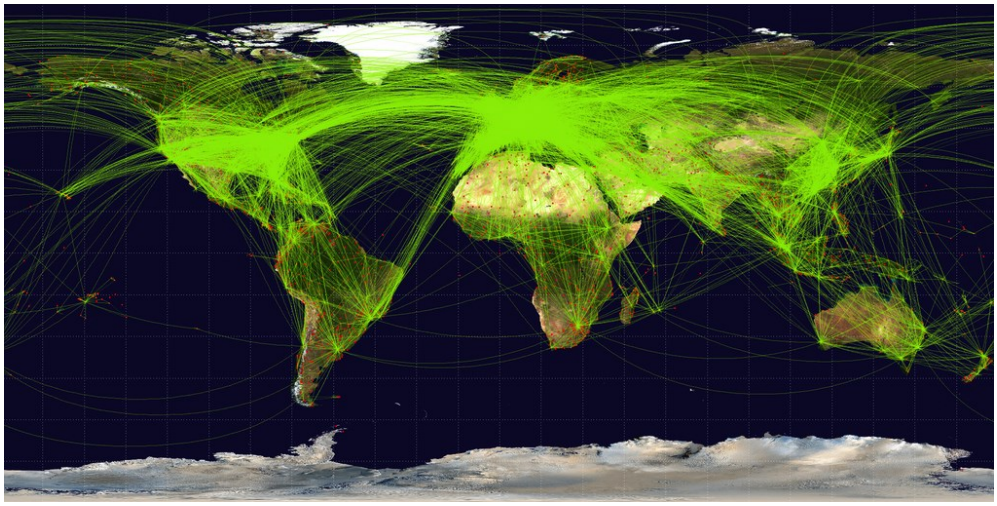

Figure 1.6: Map of scheduled airline traffic around the world (June 2009). Source: https://en.wikipedia.org/wiki/Airline

In contrast to research aircraft, commercial aircraft offer advantages like regular, long-term coverage, a global distribution and also helps overcome the limitations of cost. Detailed and continuous measurements are made during long distance flights by hi-tech instruments, thus providing a view of the horizontal and vertical distribution of the measured trace gases. These aircraft operate at an altitude of about 9-13 km, which forms the UTLS (Upper Troposphere Lower Stratosphere) region, which has great importance for climate (Solomon et al., 2010; Riese et al., 2012) and currently has very few observations. These airline observations provide vertical profiles near airports and cruise measurements that can go a long way in gaining deeper insights into atmospheric transport processes such as convection, inter-hemispheric transport and the troposphere-stratosphere exchange processes and dynamics of the UTLS

region.
The major international projects (past and ongoing) that operated global observing systems using civil aircraft are listed below:

1. MOZAIC
The Measurement of Ozone and Water Vapor by Airbus In-Service Aircraft (MOZAIC) program (Marenco et al., 1998; www.iagos.fr/ mozaic) was initiated in 1993 by European scientists, aircraft manufacturers, and airlines to collect experimental data on atmospheric composition. O_3, CO, NO_y (nitrogen oxides) and H_2O vapour were monitored using powerful instruments installed permanently onboard five Airbus 340 aircraft that made continuous and precise measurements during long-distance flights. The program ended in February 2004 and until December 2003 more than 20,000 long-range flights were made, collecting trace gas profiles at all major airports on a quasi-global scale.

2. CARIBIC
The CARIBIC (Civil Aircraft for the Regular Investigation of the Atmosphere Based on an Instrument Container, Brenninkmeijer et al., 1999; www.caribic-atmospheric.com) project was started in November 1997 as a result of collaboration between European scientific institutions and airlines. A container instrument equipped with sensors and instruments for sampling of over 60 trace gas species and aerosols is installed on an Airbus A340-600 Lufthansa aircraft every month and de-installed after four sequential flights. The time between two installations is used to analyse the samples in the laboratory and for equipment maintenance and calibration. The main species measured by the CARIBIC fleet include H_2O, CO, O_3, NO_x, NO_y, aerosols, cloud particles, CFCs, stratospheric H_2O and VOCs.

3. IAGOS
In the year 2008, the CARIBIC and MOZAIC projects were merged into a single a single infrastructure, IAGOS (In-service Aircraft for a Global Observing System) to carry out long-term and global atmospheric observations (Volz-Thomas et al., 2009; Petzold et al., 2015; www.iagos.org). Currently six IAGOS aircraft are flying measuring nearly all the atmospheric composition essential climate variables (ECVs; GCOS, 2010). CO_2 and CH_4 measurements are foreseen in the near future.

4. CONTRAIL
CONTRAIL (Comprehensive Observation Network for TRace gases by AIrLiner) is a Japanese undertaking (Machida et al., 2008; Matsueda et al., 2008; http://www.cger.nies.go.jp/contrail/) that was initiated in the year 2005. Two types of instruments, Automatic Air Sampling Equipment (ASE) based on flask sampling and the continuous CO_2 Measuring Equipment (CME), have been installed on several Boeing 747-400 and Boeing 777-200ER aircraft of JAL (Japan Airlines) with regular flights from Japan to Australia, Europe, East, South and Southeast Asia, Hawaii, and

North America. This provides significant spatial coverage, particularly in the Northern Hemisphere.

1.4 Thesis Objectives

This thesis is based on greenhouse gas observations (CO_2 and CH_4) made onboard commercial aircraft and seeks to investigate the potential of this new data stream for addressing hitherto unanswered questions and bridging the current gap in our understanding about the global carbon cycle. In particular, two main applications of these observations are discussed in detail. These are:

(a) Inverse modelling using these measurements as observational constraint for the estimation of carbon source and sinks.
(b) Utilizing the observations for improvement of quality and better error characterization of satellite-based column-averaged dry air mole fraction data (XGHG)

The work has been divided into three main chapters:

Inverse Modelling (Chapter 2)
Chapter 2 describes the suitability and application of CO_2 measurements made onboard commercial aircraft for constraining the carbon budget. The measurements are assimilated in an inverse modelling framework and the impact of errors in the transport model on the retrieved flux is estimated. This chapter highlights the advantage of using airborne measurements over those from the ground-based stations. Further, the reduction in the uncertainty of the flux estimates brought about by the use of these observations is quantified and compared to ground based observations.

Satellite validation (Chapter 3 and 4)
Chapter 3 addresses the main challenge in using aircraft vertical profiles for validation of column-averaged mole fractions i.e. their limited altitudinal extent and therefore inability to represent the full depth of the atmosphere. This study has been carried out for specifically for methane since it has a steep gradient above the tropopause due to stratospheric sink, unlike CO_2. Therefore, this gradient needs to be accurately represented when extending the aircraft profile to the total column. This chapter presents analyses of the different data sources that are available for extending aircraft vertical profiles into the stratosphere when using them for validating column-averaged mole fraction data from satellites and provides recommendations regarding the best approach.

Chapter 4 introduces the general approach and methodology for using aircraft profiles for validation of satellite-retrieved column-averaged dry air CO_2 mole fraction data (XCO_2). CO_2 measurements from the CONTRAIL campaign are used for this part of the study. Two satellite products − GOSAT RemoTeC and SCIAMACHY-BESD −

are validated using this approach and the errors in the retrieved XCO_2 with respect to those computed using the aircraft profiles are compared. Further, this chapter also investigates the issue of representativeness of the aircraft profiles-that span a certain horizontal distance - of the true vertical nadir column as seen by the satellites.

Chapter 5 summarizes the results from chapters 2,3 and 4 and discusses the future scope of work.

1.5 References

Bojinski, S., Verstraete, M., Peterson, T. C., Richter, C., Simmons, A. and Zemp, M.: The concept of essential climate variables in support of climate research, applications, and policy, Bull. Am. Meteorol. Soc., 95(9), 1431–1443, doi:10.1175/BAMS-D-13-00047.1, 2014.

Bovensmann, H., Burrows, J. P., Buchwitz, M., Frerick, J., Noël, S., Rozanov, V. V., Chance, K. V. and Goede, a. P. H.: SCIAMACHY: Mission Objectives and Measurement Modes, J. Atmos. Sci., 56(2), 127–150, doi:10.1175/1520-0469(1999)056<0127:SMOAMM>2.0.CO;2, 1999.

Brenninkmeijer, C. A. M., Crutzen, P. J., Fischer, H., Guesten, H., Hans, W., Heinrich, G., Heintzenberg, J., Hermann, M., Immelmann, T., Kersting, D., Maiss, M., Nolle, M., Pitscheider, A., Pohlkamp, H., Scharffe, D., Specht, K., and Wiedensohler, A.: CARIBIC – civil aircraft for global measurement of trace gases and aerosols in the tropopause region, J. Atmos. Oceanic Tech- nol., 16, 1373–1383, 1999.

Checa-Garcia, R., Landgraf, J., Galli, A., Hase, F., Velazco, V. A., Tran, H., Boudon, V., Alkemade, F. and Butz, A.: Mapping spectroscopic uncertainties into prospective methane retrieval errors from Sentinel-5 and its precursor, Atmos. Meas. Tech., 8(9), 3617–3629, doi:10.5194/amt-8-3617-2015, 2015.

Chevallier, F., M. Fisher, P. Peylin, S. Serrar, P. Bousquet, F.-M. Bréon, A. Chédin, and P. Ciais: Inferring CO_2 sources and sinks from satellite observations: Method and application to TOVS data, J. Geophys. Res., 110, D24309, doi:10.1029/2005JD006390, 2005

Ciais, P., Sabine, C., Govindasamy, B., Bopp, L., Brovkin, V., Canadell, J., Chhabra, A., DeFries, R., Galloway, J., Heimann, M., Jones, C., Le Quéré, C., Myneni, R., Piao, S., and Thornton, P.: Chapter 6: Carbon and Other Biogeochemical Cycles, in: Climate Change 2013 The Physical Science Basis, edited by: Stocker, T., Qin, D., and Platner, G.-K., Cambridge University Press, Cambridge, 2013.

Crisp, D., Miller, C., and DeCola, P.: NASA Orbiting Carbon Observatory; measuring the column averaged carbon dioxide mole fraction from space, J. Appl. Remote Sens., 2, 023508, doi:10.1117/1.2898457, 2008.

De Laat, A. T. J., Dijkstra, R., Schrijver, H., Nédélec, P., & Aben, I. : Validation of six years of SCIAMACHY carbon monoxide observations using MOZAIC CO profile measurements. Atmospheric Measurement Techniques, *5*(9), 2133–2142. doi:10.5194/amt-5-2133-2012, 2012.

De Laat, A. T. J., Aben, I., Deeter, M., Nédélec, P., Eskes, H., Attié, J. L., Ricaud, P., Abida, R., El Amraoui, L. and Landgraf, J.: Validation of nine years of MOPITT V5 NIR using MOZAIC/IAGOS measurements: Biases and long-term stability, Atmos. Meas. Tech., 7(11), 3783–3799, doi:10.5194/amt-7-3783-2014, 2014.

Eglinton, T. I. and Repeta, D. J.: Organic Matter in the Contemporary Ocean, in Treatise on Geochemistry: Second Edition, vol. 8, pp. 151–189, 2013.

Ehret, G. and Kiemle, C.: Requirements definition for future DIAL instruments, Study report ESA-CR(P)-4513, ESA, Noordwijk, The Netherlands, 2005.

Falkowski, P.: Falkowski et al - The Global Carbon Cycle - A Test of Our Knowledge of Earth as a System - Science.pdf, Science, 291(2000), 290–296, doi:10.1126/science.290.5490.291, 2013.

Forster et al., P.: 2: Changes in Atmospheric Constituents and in Radiative Forcing, in Climate Change 2007: The Physical Science Basis, p. 137. [online] Available from: https://www.ipcc.ch/pdf/assessment-report/ar4/wg1/ar4-wg1-chapter2.pdf, 2007.

Galli, A., Guerlet, S., Butz, A., Aben, I., Suto, H., Kuze, A., Deutscher, N. M., Notholt, J., Wunch, D., Wennberg, P. O., Griffith, D. W. T., Hasekamp, O. & Landgraf, J.: The impact of spectral resolution on satellite retrieval accuracy of CO_2 and CH_4 Atmospheric Measurement Techniques, *7*(4), 1105–1119. doi:10.5194/amt-7-1105-2014, 2014.

GCOS: Implementation plan for the global observing system for climate in support of the UNFCCC (2010 update). GCOS Rep. 138, 186 pp. [Available online at www.wmo.int/pages/prog/gcos /Publications/gcos-138.pdf.], 2010

Gurney, K. R., Law, R. M., Denning, a S., Rayner, P. J., Baker, D., Bousquet, P., Bruhwiler, L., Chen, Y.-H., Ciais, P., Fan, S., Fung, I. Y., Gloor, M., Heimann, M., Higuchi, K., John, J., Maki, T., Maksyutov, S., Masarie, K., Peylin, P., Prather, M., Pak, B. C., Randerson, J., Sarmiento, J., Taguchi, S., Takahashi, T. and Yuen, C.-W.: Towards robust regional estimates of CO2 sources and sinks using atmospheric transport models., Nature, 415(February), 626–630, doi:10.1038/415626a, 2002.

Hansell, D.A., and C.A. Carlson: Deep-ocean gradients in the concentration of dissolved organic carbon. Nature, 395, 263–266, 1998

Hansen, J., Sato, M., Kharecha, P. and Von Schuckmann, K.: Earth's energy imbalance and implications, Atmos. Chem. Phys., 11(24), 13421–13449, doi:10.5194/acp-11-13421-2011, 2011.

Haszpra, L.: On the representativeness of carbon dioxide measurements, J. Geophys. Res. Atmos., 104(D21), 26953–26960, doi:10.1029/1999JD900311, 1999.

Houweling, S., Breon, F.-M., Aben, I., Roedenbeck, C., Gloor, M., Heimann, M., and Ciais, P.: Inverse modeling of CO_2 sources and sinks using satellite data: a synthetic inter-comparison of measurement techniques and their performance as a func- tion of space and time, Atmos. Chem. Phys., 4, 523–538, doi:10.5194/acp-4-523-2004, 2004.

IPCC Climate Change 2014: Synthesis Report. Contribution of Working Groups I, II and III to the Fifth Assessment Report of the Intergovernmental Panel on Climate Change [Core Writing Team, R.K. Pachauri and L.A. Meyer (eds.)]. IPCC, Geneva, Switzerland, 151 pp, 2014

Makoto, I., Isamu, M., Osamu, U., Yuki, M., Yukio, Y., Tatsuya, Y., Toshinobu, M., Yousuke, S., Hidekazu, M., Colm, S., Pieter P., T., Arlyn E., A., Sebastien C., B., Tomoaki, T. and Shuji Kawakami and Prabir K., P.: Validation of XCO_2 derived from SWIR spectra of GOSAT TANSO-FTS with aircraft measurement data, Atmospheric Chemistry and Physics, Atmos. Chem. Phys., 13(19), 9771–9788, doi:10.5194/amt-7-2987-2014, 2013.

Keeling, C. D.: The Concentration and Isotopic Abundances of Carbon Dioxide in the Atmosphere, Tellus, 12(2), 200–203, doi:10.1111/j.2153-3490.1960.tb01300.x, 1960.
Kirschke, S. et al: Three decades of global methane sources and sinks, Nat. Geosci., 6, 813–823, 2013.

Kulawik, S., Wunch, D., O'Dell, C., Frankenberg, C., Reuter, M., Oda, T., Chevallier, F., Sherlock, V., Buchwitz, M., Osterman, G., Miller, C. E., Wennberg, P. O., Griffith, D., Morino, I., Dubey, M. K., Deutscher, N. M., Notholt, J., Hase, F., Warneke, T., Sussmann, R., Robinson, J., Strong, K., Schneider, M., De Mazière, M., Shiomi, K., Feist, D. G., Iraci, L. T. and Wolf, J.: Consistent evaluation of ACOS-GOSAT, BESD-SCIAMACHY, CarbonTracker, and MACC through comparisons to TCCON, Atmos. Meas. Tech., 9(2), 683–709, doi:10.5194/amt-9-683-2016, 2016.

Lean, J. L. and Rind, D. H.: How will Earth's surface temperature change in future decades?, Geophys. Res. Lett., 36(15), doi:10.1029/2009GL038932, 2009.

Machida, T., Matsueda, H., Sawa, Y., Nakagawa, Y., Hirotani, K., Kondo, N., Goto, K., Nakazawa, T., Ishikawa, K. and Ogawa, T.: Worldwide Measurements of Atmospheric CO2 and Other Trace Gas Species Using Commercial Airlines, J. Atmos. Ocean. Technol., 25, 1744–1754, doi:10.1175/2008JTECHA1082.1, 2008.

Matsueda, H., Machida, T., Sawa, Y., Nakagawa, Y., Hirotani, K., Ikeda, H., Kondo, N., and Goto, K.: Evaluation of atmospheric CO_2 measurements from new flask air sampling of JAL airliner observations, Pap. Meteorol. Geophys., 59, 1–17, 2008.

Marenco, A., Thouret, V., Nédélec, P., Smit, H., Helten, M., Kley, D., Karcher, F., Simon, P., Law, K., Pyle, J., Poschmann, G., Von Wrede, R., Hume, C. and Cook, T.: Measurement of ozone and water vapor by Airbus in-service aircraft: The MOZAIC airborne program, an overview, J. Geophys. Res., 103(D19), 25631, doi:10.1029/98JD00977, 1998.

Miller, C. E., Crisp, D., DeCola, P. L., Olsen, S. C., Randerson, J. T., Michalak, A. M., Alkhaled, A., Rayner, P., Jacob, D. J., Suntharalingam, P., Jones, D. B. A., Denning, A. S., Nicholls, M. E., Doney, S. C., Pawson, S., Boesch, H., Connor, B. J., Fung, I. Y., O'Brien, D., Salawitch, R. J., Sander, S. P., Sen, B., Tans, P., Toon, G. C., Wennberg, P. O., Wofsy, S. C., Yung, Y. L. and Law, R. M.: Precision requirements for space-based XCO_2 data, J. Geophys. Res. Atmos., 112(10), doi:10.1029/2006JD007659, 2007.

Niwa, Y., MacHida, T., Sawa, Y., Matsueda, H., Schuck, T. J., Brenninkmeijer, C. A. M., Imasu, R. and Satoh, M.: Imposing strong constraints on tropical terrestrial CO_2 fluxes using passenger aircraft based measurements, J. Geophys. Res. Atmos., 117(11), doi:10.1029/2012JD017474, 2012.

Pak, B. C. and Prather, M. J.: CO_2 source inversions using satellite observations of the upper troposhere, Geophys. Res. Lett., 28, 4571–4574, 2001.

Parker, R., Boesch, H., Cogan, A., Fraser, A., Feng, L., Palmer, P. I., Messerschmidt, J., Deutscher, N., Griffith, D. W. T., Notholt, J., Wennberg, P. O. and Wunch, D.: Methane observations from the Greenhouse Gases Observing SATellite: Comparison to ground-based TCCON data and model calculations, Geophys. Res. Lett., 38(15), doi:10.1029/2011GL047871, 2011.

Patra, P. K., Niwa, Y., Schuck, T. J., Brenninkmeijer, C. A. M., MacHida, T., Matsueda, H. and Sawa, Y.: Carbon balance of South Asia constrained by passenger aircraft CO_2 measurements, Atmos. Chem. Phys., 11(9), 4163–4175, doi:10.5194/acp-11-4163-2011, 2011.

Petersen, A. K., Warneke, T., Lawrence, M. G., Notholt, J. and Schrems, O.: First ground-based FTIR observations of the seasonal variation of carbon monoxide in the tropics, Geophys. Res. Lett., 35(3), doi:10.1029/2007GL031393, 2008.

Petzold, A., Thouret, V., Gerbig, C., Zahn, A., Brenninkmeijer, C. A. M., Gallagher, M., Hermann, M., Pontaud, M., Ziereis, H., Boulanger, D., Marshall, J., Nédélec, P., Smit, H. G. J., Friess, U., Flaud, J.-M., Wahner, A., Cammas, J.-P. and Volz-Thomas, A.: Global-scale atmosphere monitoring by in-service aircraft – current achievements and future prospects of the European Research Infrastructure IAGOS, Tellus B, 67(0), 13801, doi:10.5194/acp-7-4953-2007, 2015.

Ramaswamy, V., Boucher, O., Haigh, J., Haughustaine, D., Haywood, J., Myhre, G.: Radiative forcing of climate change, in Climate Change 2001: The Scientific Basis, pp. 349–416. [online] Available from: http://www.grida.no/publications/other/ipcc_tar/?src=/climate/ipcc_tar/wg1/index.htm , 2001.

Rayner, P. J. and O'Brien, D. M.: The utility of remotely sensed CO_2 concentration data in surface source inversions, Geophys. Res. Lett., 28(1), 175–178, doi:10.1029/2000GL011912, 2001.

Reuter, M., Bovensmann, H., Buchwitz, M., Burrows, J. P., Connor, B. J., Deutscher, N. M., Griffith, D. W. T., Heymann, J., Keppel-Aleks, G., Messerschmidt, J., Notholt, J., Petri, C., Robinson, J., Schneising, O., Sherlock, V., Velazco, V., Warneke, T., Wennberg, P. O. and Wunch, D.: Retrieval of atmospheric CO_2 with enhanced accuracy and precision from SCIAMACHY: Validation with FTS measurements and comparison with model results, J. Geophys. Res. Atmos., 116(4), doi:10.1029/2010JD015047, 2011.

Riese, M., Ploeger, F., Rap, A., Vogel, B., Konopka, P., Dameris, M. and Forster, P.: Impact of uncertainties in atmospheric mixing on simulated UTLS composition and related radiative effects, J. Geophys. Res. Atmos., 117(16), doi:10.1029/2012JD017751, 2012.

Rödenbeck, C., Houweling, S., Gloor, M. and Heimann, M.: CO2 flux history 1982–2001 inferred from atmospheric data using a global inversion of atmospheric transport, Atmos. Chem. Phys., 3(6), 1919–1964, doi:10.5194/acp-3-1919-2003, 2003.

Sarmiento, J. L. and Gruber, N.: Ocean Biogeochemical Dynamics, Carbon N. Y., 67, doi:10.1063/1.2754608, 2006.

Schimel, D. S., House, J. I., Hibbard, K. a, Bousquet, P., Ciais, P., Peylin, P., Braswell, B. H., Apps, M. J., Baker, D., Bondeau, a, Canadell, J., Churkina, G., Cramer, W., Denning, a S., Field, C. B., Friedlingstein, P., Goodale, C., Heimann, M., Houghton, R. a, Melillo, J. M., Moore, B., Murdiyarso, D., Noble, I., Pacala, S. W., Prentice, I. C., Raupach, M. R., Rayner, P. J., Scholes, R. J., Steffen, W. L. and Wirth, C.: Recent patterns and mechanisms of carbon exchange by terrestrial ecosystems., Nature, 414(6860), 169–172, doi:10.1038/35102500, 2001.

Solomon, S., Rosenlof, K. H., Portmann, R. W., Daniel, J. S., Davis, S. M., Sanford, T. J. and Plattner, G.-K.: Contributions of stratospheric water vapor to decadal changes in the rate of global warming, Science. 327(5970), 1219–1223, doi:10.1126/science.1182488, 2010.

Toon, G. C., Blavier, J.-F. L., Washenfelder, R. A., Wunch, D., Katrynski, K., Wennberg, P. O., Connor, B. J., Sherlock, V., Griffith, D. W. . T., Deutscher, N. M. and Notholt, J.: Total Column Carbon Observing Network (TCCON), Adv. Imaging, JMA3, doi:10.1364/FTS.2009.JMA3, 2009.

Volz-Thomas, A., J.-P. Cammas, C. A. M. Brenninkmeijer, T. Machida, O. Cooper, C. Sweeney, and A. Waibel,: Civil Aviation Monitors Air Quality and Climate. EM Magazine, Air & Waste Manage. Assoc., 16-19, 2009

Wunch, D., Toon, G. C., Blavier, J.-F. L., Washenfelder, R. A., Notholt, J., Connor, B. J., Griffith, D. W. T., Sherlock, V. and Wennberg, P. O.: The Total Carbon Column Observing Network, Philos. Trans. R. Soc. A Math. Phys. Eng. Sci., 369(1943), 2087–2112, doi:10.1098/rsta.2010.0240, 2011.

Yang, Z., Toon, G. C., Margolis, J. S. and Wennberg, P. O.: Atmospheric CO_2 retrieved from ground-based solar spectra, Geophys. Res. Lett., 29(9), 1339, doi:10.1029/2001GL014537, 2002.

Yokota, T., Yoshida, Y., Eguchi, N., Ota, Y., Tanaka, T., Watanabe, H. and Maksyutov, S.: Global Concentrations of CO_2 and CH_4 Retrieved from GOSAT: First Preliminary Results, Sola, 5, 160–163, doi:10.2151/sola.2009-041, 2009.

Chapter 2

The constraint of CO_2 measurements made onboard commercial aircraft on surface-atmosphere fluxes

2.1 Abstract

Inaccurate representation of atmospheric processes by transport models is a dominant source of uncertainty in inverse analyses and can lead to large discrepancies in the retrieved flux estimates. This study investigates the impact of uncertainties in vertical transport as simulated by atmospheric transport models on fluxes retrieved using vertical profiles from aircraft as an observational constraint. The numerical experiments are based on synthetic data with realistic spatial and temporal sampling of aircraft measurements. The impact of such uncertainties on the flux retrieved using the ground-based network with those retrieved using the aircraft profiles are compared. The results indicate that the posterior flux retrieved using aircraft profiles is less susceptible to errors in boundary layer height as compared to the ground-based network. This highlights the benefit of utilizing atmospheric observations made onboard aircraft over surface measurements for flux estimation using inverse methods. Further, synthetic vertical profiles of CO_2 are used in an inversion to estimate the potential of these measurements, which will be made available through the In-Service Aircraft for a Global Observing System (IAGOS) project in future, in constraining the regional carbon budget. Results from these simulations show that the regions tropical Africa and temperate Eurasia, that are under constrained by the existing surface based network, will benefit the most from these measurements, the reduction on posterior flux uncertainty being about 7 to 10 %.

2.2 Introduction

Reliable prediction of climate change scenarios requires a thorough understanding the carbon-climate feedbacks in the Earth system and accurately estimating current sources and sinks of carbon is of prime importance. While it is impossible to measure these directly everywhere around the globe, we may estimate these using the 'top-down' approach employing atmospheric observations in combination with knowledge of atmospheric transport and prior knowledge of the fluxes by inverse modelling. The inverse modelling scheme exploits the fact that the spatial and temporal variations of atmospheric trace gases like CO_2 contain information about the exchange processes

between the atmosphere and the surface of the Earth. Unfortunately, the estimates of surface fluxes using this approach are prone to large uncertainties that can largely be attributed to imperfections in the transport models and insufficient data coverage by the observation network.

Atmospheric transport models use meteorological input like wind fields to link the observed atmospheric concentrations of tracers to the estimated fluxes at the surface of the Earth. These models are not able to perfectly simulate atmospheric transport processes, which results in uncertainties in the retrieved surface fluxes (Law et al., 1996, 2008; Gerbig et al., 2003; Stephens et al., 2007; Lauvaux et al., 2009; Houweling et al., 2010). One of the dominant sources of transport model uncertainty is the inaccurate representation of the vertical mixing near the surface of the Earth and hence the boundary layer height. An accurate simulation of the vertical mixing in the boundary layer accurately is critical since it is this part of the atmosphere where most observations are made and that lies closest to the carbon sources and sinks. Hence, misrepresentation of transport in the boundary layer can lead to significant biases in modelled tracer mixing ratios as well as the retrieved fluxes (Denning et al. 1996; 2008; Yi et al., 2004; Ahmadov et al., 2009).

Furthermore, a weak observational constraint due to insufficient atmospheric data is also an important factor that causes large errors in retrieved fluxes. Lack of measurements in the atmosphere or an unevenly distributed observation network of observation can result in a poorly constrained regional carbon budget (Gurney et al., 2002). Hence in addition to improved transport models, an enhanced global network of atmospheric measurements is indispensable for more accurate and precise estimation of surface fluxes using inverse modelling.

The current global measurement network of greenhouse gases combines in-situ measurements made by the ground-based stations and satellite instruments measuring column-averaged dry air mixing ratios remotely. While ground based measurements are highly precise, the main limitation of these measurements is the sparse and uneven spatial coverage (Bousquet et al., 2006; Marquis and Tans, 2008). While parts of Europe and North America dispose of a fairly high data coverage from the surface-based observation network, the tropical regions of Amazonia, Africa, remote regions of tundra, and Siberia are not adequately covered, sometimes even lacking measurements entirely. In addition, these measurements are often not representative of large areas and provide information only at the local scale (Haszpra et al., 1999). Satellites largely overcome this drawback of ground-based measurements since they have the ability to provide information around the world using a single instrument. However, they have their constraints, too, which limits their use for accurate flux estimation using inverse methods: Space borne measurements are still somewhat limited by higher measurement uncertainty and systematic errors, as well as temporal heterogeneity in their sampling (Ehret and Kiemle, 2005; Galli et al., 2014; Checa-Garcia et al., 2015)

The use of commercial aircraft as platforms for obtaining information about the physical and state and chemical composition of the atmosphere is a rather new concept. IAGOS (In-Service Aircraft for a Global Observing System) is a European Research Infrastructure that deploys sensors on commercial airliners that make regular in-situ measurements of the atmosphere. The project is an extension and continuation of the MOZAIC (Measurement of Ozone and Water Vapour on Airbus in-service Aircraft) project (Marenco et al., 1998) that was initiated in the year 1993. Detailed and continuous measurements are made during long distance flights by onboard instruments, thus providing a view of the horizontal and vertical distribution of the measured trace gases at high temporal and spatial resolution. The last MOZAIC aircraft was deactivated in October 2014; currently six IAGOS aircraft are flying. IAGOS provides observations with applications in the field of atmospheric modelling and for validation of satellite observations. There are a number of species that are currently being measured by IAGOS aircraft like CO, O_3, NO_x, NO_y and aerosols. Measurement of greenhouse gases CO_2 and CH_4 is foreseen in the near future. Thus IAGOS provides for the measurement of a large number of the Essential Climate Variables (ECVs) pertaining to atmospheric composition, as defined by GCOS (Global Climate Observing System) in 2010 as necessary in order to understand the complex feedback mechanisms of the climate system.

Some recent studies have utilized measurements made onboard of commercial aircrafts in order to better understand their impact on the dynamics of the carbon cycle. Niwa et al., (2012) examined the impact of commercial aircraft based on measurements from CONTRAIL (Comprehensive Observation Network for Trace gases by Airliner) on the overall carbon budget constraint and the flux uncertainties. Patra et al., (2011) used measurements from the CARIBIC (Civil Aircraft for the Regular Investigation of the atmosphere Based on an Instrument Container) project as well as the CONTRAIL project to estimate regional CO_2 fluxes in the tropics. Both studies focused specifically on the estimation of the tropical terrestrial fluxes. So far, the suitability of aircraft vertical profiles and their treatment when using them into inversions, given the transport modelling errors related to vertical mixing has not been addressed so far.

In this chapter, synthetic data are used to investigate theoretically the impact of transport model uncertainties associated with boundary layer height on the fluxes retrieved by using commercial aircraft profiles in an inverse modelling set-up. The synthetic data are generated using a forward run of the TM3 transport model (Heimann and Körner, 2003) and have the temporal and spatial sampling of the measurements made during the MOZAIC project. The idea is to examine how closely the posterior flux obtained using the synthetic aircraft measurements as constraint captures the trends and variability in the flux that is used to generate the synthetic data. This allows for the estimation of the impact of the inaccurate, simulated vertical mixing.
In the second part of this work, the potential of CO_2 observations that will be onboard

the IAGOS fleet for constraining the regional carbon budget and reducing posterior flux uncertainties is assessed. Only the time, location and uncertainty of the measurements are used for the simulations. Since flight routes of commercial aircraft undergo little changes with time, it is reasonable to estimate the constraint that will be brought about by IAGOS aircraft using the sampling from MOZAIC, its predecessor project.

The goal of this study is to investigate the following main questions:

1. What is the impact of boundary layer height uncertainty in the transport models on the retrieved fluxes when profile information from aircraft is used in the inversions?
2. What impact will these measurements have on the overall carbon budget constraint and how big is the reduction in flux uncertainty?
3. Which areas will benefit the most from these measurements?

The chapter is organized as follows: Section 2.3 describes the methods used that include description of the inversion scheme (Section 2.3.1), the data-weighting scheme used in the model (Section 2.3.2), estimation of the model representation error (Section 2.3.3) and the experimental set-up (Section 2.3.4). In section 2.4, the results from the simulations are presented and the conclusions are discussed in Section 2.5.

2.3 Method

2.3.1 Jena CarboScope: Model description

Jena CarboScope (or the Jena Inversion System) (Roedenbeck et al., 2005) is a Bayesian inversion framework that is used to estimate trace gas fluxes at the surface of the Earth from measured atmospheric concentrations and knowledge of atmospheric transport. It employs the global atmospheric tracer model TM3 to simulate atmospheric transport (Heimann and Körner, 2003). In this study, the model simulations are carried out at a $4° \times 5°$ spatial resolution using the ERA-Interim (European Centre for Medium Range Weather Forecasts (ECMWF) Reanalysis-Interim) meteorology.

In the following, a brief description of the inversion system is provided (described in more detail in Roedenbeck et al., (2005)). Observed atmospheric mixing ratios $\mathbf{C}_{obs}$, are compared to modelled atmospheric mixing ratios $\mathbf{C}_{mod}$, based on a prior estimate of the surface fluxes. The modelled atmospheric mixing ratio at a specific location is obtained by the multiplication of the linear atmospheric transport operator **A** computed by the transport model with the flux field **f** and the addition of the initial

atmospheric mixing ratio $\mathbf{C}_{ini}$

$$\mathbf{C}_{\mathrm{mod}} = \mathbf{Af} + \mathbf{C}_{\mathrm{ini}} \quad (2.1)$$

Since the problem is ill posed and thus does not result in a unique solution, a further constraint is added based upon prior knowledge of the fluxes and their correlations in space and time. The additional constraints on the a-priori flux field consist of a fixed flux term $\mathbf{f}_{fix}$ and an adjustable flux term $\mathbf{f}_{adj}$. Therefore,

$$\mathbf{f} = \mathbf{f}_{\mathrm{fix}} + \mathbf{f}_{adj} \quad (2.2)$$

The term $\mathbf{f}_{fix}$ represents the a-priori expectation value, $\langle\mathbf{f}_{pri}\rangle$ while $\mathbf{f}_{adj}$ determines the deviations around $\langle\mathbf{f}_{pri}\rangle$ (Gaussian distributed). The adjustable term is composed of matrix **F** and vector $\mathbf{p}_{inv}$ i.e. $\mathbf{f}_{adj}=\mathbf{F}.\ \mathbf{p}_{inv}$. The matrix **F** comprises all the a- priori information about flux uncertainties and correlations while the vector $\mathbf{p}_{inv}$ is a vector of adjustable parameters, each of which scales one of the columns of matrix **F**. Therefore, $\mathbf{p}_{inv}$ determines the relative strength of the adjustments around $\langle\mathbf{f}_{pri}\rangle$**.** Each element of vector $\mathbf{p}_{inv}$ is assumed to have zero mean and unit variance.

Thus, the modelled atmospheric mixing ratio can thus be written as:

$$\mathbf{C}_{\mathrm{mod}} = \mathbf{C}_{\mathrm{mod,fix}} + \mathbf{Af}_{\mathrm{adj}} \quad (2.3)$$

where

$$\mathbf{C}_{\mathrm{mod,fix}} = \mathbf{Af}_{\mathrm{fix}} + \mathbf{C}_{\mathrm{ini}} \quad (2.3a)$$

The concentration mismatch between observed and modelled values is defined as

$$\mathbf{m} = \mathbf{C}_{\mathrm{obs}} - \mathbf{C}_{\mathrm{mod}} \quad (2.4)$$

The aim of the inversion system is to optimize the adjustable part of the posterior flux, $\mathbf{f}_{post}$, with respect to the **m**, according to Bayes' Theorem. $\mathbf{Q}_c$ is defined as the error covariance matrix of the atmospheric mixing ratio mismatch. Its diagonal elements represent the combined measurement and modelling errors for each observation i.e. $\sigma_{i,tot} = \sqrt{{\sigma_{mod}}^2 + {\sigma_{meas}}^2}$

The off-diagonal elements would represent the correlations between the measurement errors or between the modelling errors. Nevertheless, due to the difficulties in characterizing error correlations, each observation is assumed independent so the off-diagonal elements are set to zero. In order to scale the impact of the a-priori constraint on the Bayesian inversion the factor **μ** is used. It determines the ratio between the a-priori information and data constraints. For **μ** equal to 0 no prior information is used for minimizing the cost function. For high values of **μ** the a-priori flux distribution has a high impact on the minimization of the cost function.

Therefore, according to Bayes' law of conditional probability

$$\mathrm{Prob}(\mathbf{f}_{\mathrm{post}} \mid \mathbf{m}) = \mathrm{Prob}\,(\mathbf{m} \mid \mathbf{f}_{\mathrm{post}})\,.\,\mathrm{Prob}\,(\mathbf{f}_{\mathrm{post}})\,/\mathrm{Prob}(\mathbf{m}) \quad (2.5)$$

Where

$$\mathrm{Prob}(\mathbf{m} \mid \mathbf{f}_{\mathrm{post}}) \propto \exp(-\tfrac{1}{2}\mathbf{m}^{\mathbf{T}}\ \mathbf{Q}_{\mathrm{c}}^{-1}\mathbf{m}) \quad (2.5a)$$

$$\mathrm{Prob}(\mathbf{f}_{\mathrm{post}}) \propto \exp\,(-\tfrac{\mu}{2}\ \mathbf{f}_{\mathrm{post}}^{\mathbf{T}}.\,\mathbf{f}_{\mathrm{post}}) \quad (2.5b)$$

Thus, $\mathrm{Prob}(\boldsymbol{f}_{post} \mid \boldsymbol{m})$ needs to be maximized with respect to $\mathbf{f}_{post}$. This can be expressed in terms of a cost function **J** defined as:

$$\mathbf{J} = -\ln\left(\mathrm{Prob}\left(\mathbf{f_{post}} \mid \mathbf{m}\right)\right) \tag{2.6}$$

$$= \frac{1}{2}\mathbf{m^T Q_c^{-1} m} + \frac{\mu}{2}\mathbf{f_{post}^T f_{post}} + \mathrm{C} \tag{2.7}$$

The difference between the modelled $\mathbf{C}_{mod}$ and observed $\mathbf{C}_{obs}$, $\mathbf{m}$ is used to calculate the observation-based term of a cost function which forms the first term of Eq. (2.7); taking into account the measurement and model representation errors. $\frac{\mu}{2}\mathbf{f_{post}^T f_{post}}$ describes the a-priori flux constraints. The additive constant C subsumes all parameter independent terms, such as those arising from Prob ($\mathbf{m}$) and from the normalization of the distribution. This cost function is minimized iteratively using the adjoint of the atmospheric transport model, as the number of observations and variables to constrain is very large, therefore prohibiting the calculation of an analytical solution.

2.3.2 Data density de-weighting

The existing observation network consists of a number of ground-based stations that measure at different temporal frequencies. Measurements of greenhouse gases can either be made continuously by using stationary instruments that analyse the current concentration (*in situ*), or by collecting air samples in glass flasks or metals tanks and measuring the concentrations later back in the laboratory. While stations based on flask observations have measurements made once per week, there also exist a growing number of continuously measuring stations with data provided typically half hourly or hourly. For the aircraft profiles, the profile measurements are made over a period of approximately 30-40 minutes during the ascent or descent of the aircraft. Therefore many of the measurements made by surface stations in a single day or in a single aircraft profile cannot be treated as independent of each other. This means that the errors of such measurements are likely to be correlated with each other over certain temporal scales. To account for this fact in the simulations, the error of correlated measurements is enhanced (or "inflated"), so that their contribution to the cost function is reduced. In this way the impact of continuous observations from a single station has a comparable impact on the cost function as less frequent flask observations from another station.

In the Jena inversion scheme, these error correlations between measurements are accounted for using a data density 'de-weighting' scheme. It assigns a weight to the error associated with every measurement computed based on certain pre-defined criteria. For surface network sites, to avoid a higher impact of the more frequent continuous observations compared to the less frequent flask observations, the data density weighting considers, for every observation, the number of observations $\mathbf{N}_{surf}$ within the same week. The total uncertainty for that observation increases by a factor

of $\sqrt{N_{surf}}$ to:

$$\sigma_i = \sqrt{N_{surf}}\, \sigma_{i,tot} \tag{2.8}$$

where σ_i represents the elements of the error covariance matrix $\mathbf{Q}_c$ and $\sigma_{i,tot}$ is the total uncertainty associated with measurement i ($\sigma_{i,tot} = \sqrt{\sigma_{mod}^2 + \sigma_{meas}^2}$ where σ_{mod} is the transport model error and σ_{meas} is the measurement error). These $\mathbf{N}_{surf}$ measurements have their errors correlated and this error inflation by a factor of $\sqrt{N_{surf}}$ helps lessen the impact of measurements that are not independent of each other. In other words, the data de-weighting controls the value of $\mathbf{N}_{surf}$ that scales the value of the error associated with each measurement and hence its contribution to the cost function.

The aircraft is a moving platform, which means that the aircraft profiles span a considerable horizontal and vertical distance while making measurements. Therefore, in contrast to a fixed station, the CO_2 concentration along the profile can be expected to de-correlate due to distance, even if taken within a short period of time. This fact needs to be incorporated in the de-weighting scheme. Thus, for the aircraft profiles the de-weighting scheme is implemented in such a way that a spatial de-correlation between measurements in addition to the temporal de-correlation as explained above is included.

For the aircraft measurements, $\mathbf{N}_{aircraft}$ is defined to be the number of measurements that lie in a 4-D (3D space and time) window instead of just those lying within a 1-week interval as used for the surface stations. Measurements that lie within this 4-D window are taken to have their errors correlated with each other, but taken independent of those that lie outside of it. The 4-D space is defined using the following criteria:

1. Temporal de-correlation length is taken to be 1 week, to be consistent with the treatment of the station data.
2. Horizontal spatial de-correlation distance is set at +/-500 km for measurements within the first 700-mbar from the surface and +/-1000 km for the ones above the 700-mbar height.

These values of spatial correlation lengths are used since they are comparable to the grid size that we use for the simulations and sub-grid scale processes cannot be resolved by the transport model. The 700-mbar pressure level represents approximately the maximum of a typical boundary layer height and separates the boundary layer part of the atmospheric column (which is more closely coupled to surface fluxes by fast vertical mixing and hence has a shortened correlation length) from the free troposphere part of the column.

2.3.3 Estimation of model data mismatch error

Model representation error or model-data mismatch can be defined as the mismatch between point observations assimilated in the model and the model simulated spatial averages (Engelen et al., 2002). This error needs to be pre-specified in inversion framework. In the Jena inversion scheme, a representation error that varies with altitude is used. This is because the mismatch is likely to be higher for measurements that lie closer to the surface while the models perform better for higher altitudes that are not affected as directly by the fluxes. The functional dependency of the mismatch with altitude is computed using data from the CONTRAIL project (Machida et al., 2008).

For this, observations from CONTRAIL are compared against TM3 "reanalysed CO_2 fields" (i.e., atmospheric CO_2 fields simulated by the tracer transport model from surface fluxes previously optimized against CO_2 data, such that these fields closely match the data and interpolate in between them). The difference gives the model-data mismatch (*mdm*) at every level for each airport where CONTRAIL aircraft fly. The statistics have been aggregated onto a 1-km resolution for this analysis. In order to obtain a typical *mdm* at every level of a profile the median of the standard deviation of the *mdm* at each level across all airports that have at least 20 data points is used. Figure 2.1 shows a box plot that is thus obtained. An exponential curve is then fitted to the median values at each level:

$$\mathrm{mdm} = \mathrm{a}e^{\mathrm{bz}} + \mathrm{c} \qquad (2.9)$$

where we obtain a= 2.85 ppm, b= -0.4, and c= 3.18 ppm.

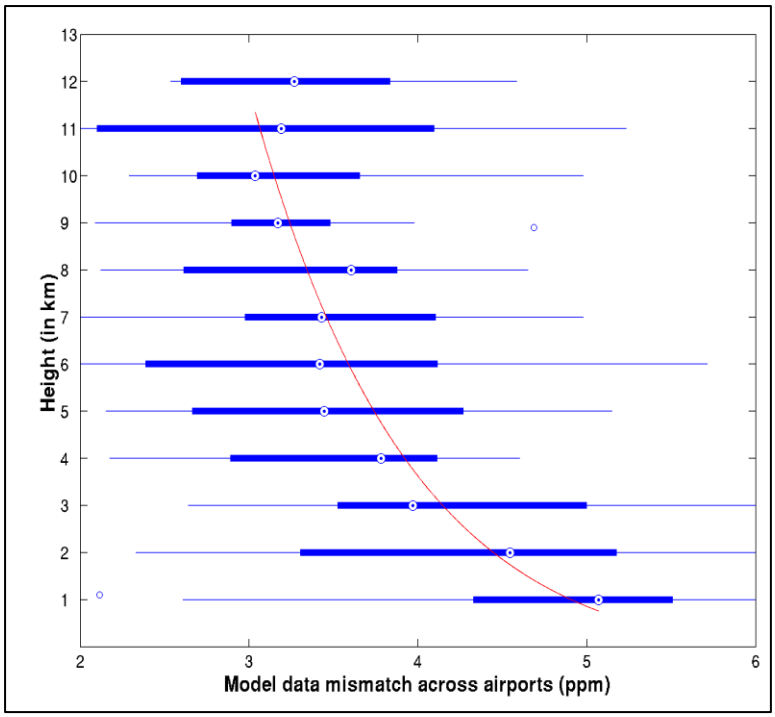

Figure 2.1: Box plot showing the model data mismatch between the TM3 analysed CO_2 fields and the vertical profiles from the CONTRAIL plotted against height. The red line shows the exponential curve fitted to the median of the standard deviation of the model data mismatch.

2.3.4 Experimental Setup

Synthetic data at the times and locations of the MOZAIC profiles and the ground network sites are generated to both investigate the impact of boundary layer height errors and assess the impact the addition of aircraft observations has on flux retrievals. For the forward run, fluxes from the BIOME-BGC biosphere model (Thornton et al., 2005) are used in order to get realistic mixing ratios at the locations of aircraft profiles and the surface stations. These fluxes form the "true flux". The MOZAIC aircraft profiles consist of measurements provided at approximately every 150 m altitude starting at 75 m and going typically up to an altitude of 9-10 km. Cruise level data is not used for this study because of the fact that most of these measurements are made around the tropopause region, and the model skill in accurately representing the transport at that altitude and linking those measurements via vertical transport to fluxes at the surface is limited (Deng et al., 2015)

Since the profiles generated by the forward run of the transport model use the ERA-Interim meteorology, the boundary layer height represented by these profiles is that of ERA-Interim. This is the "true" boundary layer height denoted by $BLH_{true.}$ In order to simulate the vertical-mixing-related imperfections in the transport models, new

profiles with a "wrong" boundary layer height need to be generated. This is achieved by modifying these profiles in such a way that they represent a new boundary layer height that is different from BLH_{true}. BLH_{model} denotes this "wrong" boundary layer height.. In order to do this the approach as implemented by Kretschmer et al., (2012) is used. This approach assumes that errors in the simulated boundary layer height are caused by incorrect vertical distribution of CO_2 in a given atmospheric column, such that the total column concentration remains unchanged. The CO_2 between the free troposphere and boundary layer part of the atmospheric column is redistributed in such a way that the BLH for the profile changes to $BLH_{model.}$ In this study, the BLH_{model} obtained from the NCEP (National Centres for Environmental Prediction) meteorology. In order to compute the boundary layer height the Bulk Richardson Number method (Seibert et al., 2000) was used.

The effect of vertical mixing errors in transport models on flux retrieval is analysed with three groups of experiments:
S: Simulation with only the surface-based observation network.
A: Simulation using only the IAGOS aircraft profiles.
C: Simulation with the combined network: surface-based observation network augmented with the measurements from IAGOS.
For each of these simulations, two types of inversions are carried out:

a. Original profiles (Control case)
b. Reshuffled profiles.

Experiments S (a), A (a) and C (a) represent scenarios where the boundary layer height is well known. Experiments S (b), A (b) and C (b) simulate the realistic case where the vertical mixing in the transport model is imperfect. The monthly posterior fluxes are analysed for one year (2000). The surface network consists of 49 sites (Fig. 2.2 (a)) and the IAGOS observation network consists of measurements from five IAGOS aircraft (Fig. 2.2(b)). The prior flux used for the inverse simulations is different and independent from the true flux used to generate the pseudo data and is obtained from the Lund-Potsdam-Jena (LPJ) dynamic global vegetation model (Sitch et al., 2003)

In the second part of the study, the reduction in posterior flux uncertainty brought about by the use of IAGOS vertical profiles as a constraint on the carbon budget is estimated. Simulations are carried out where the surface-based observation network is augmented by one or more IAGOS aircraft. These simulations do not require the synthetic data that as used in the first part of this study since the inversion system solves for the resultant posterior flux uncertainties based upon only the measurement time, location and the uncertainties of the prior fluxes and the measurements (model-data mismatch). The uncertainty reduction is computed for the monthly mean posterior fluxes aggregated over the TransCom3 land regions (Gurney et al., 2000). It is expressed as the following:

a. Surface stations used in the inversion

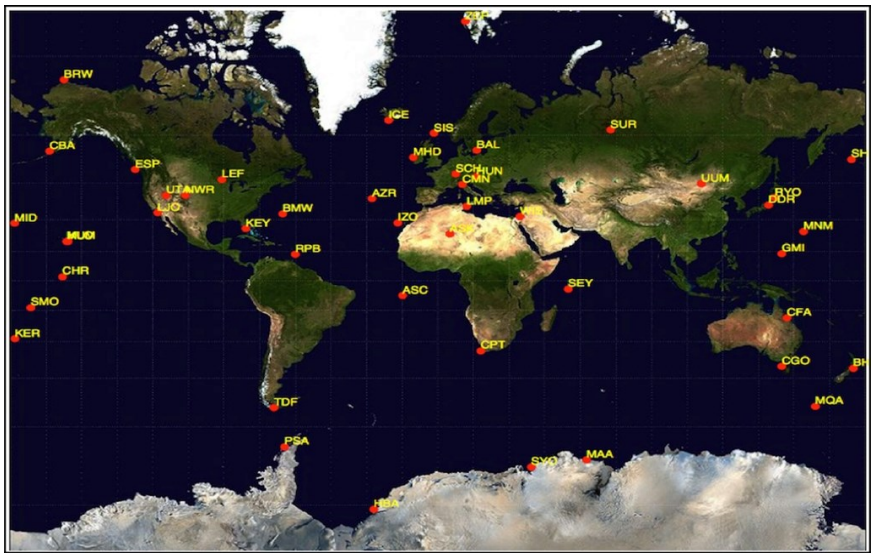

b. Vertical profiles measured by MOZAIC aircraft

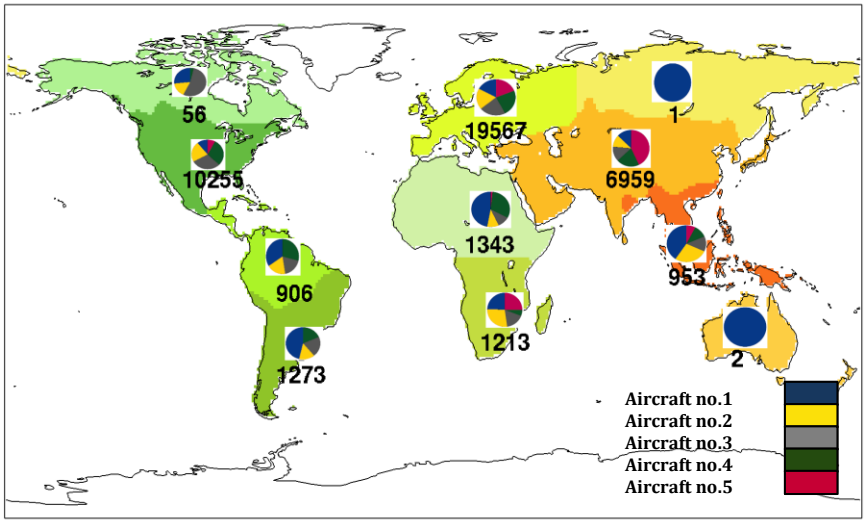

Figure 2.2: (a) Map showing the locations of the stations of the surface based measurements used in the Jena inversion scheme. (b) Spatial distribution and number of the vertical profiles measured by the MOZAIC fleet for the TransCom3 land regions during the year 1996-2004.

$$\text{Uncertainty Reduction (in percent)} = \left(1 - \frac{\text{posterior uncertainty}}{\text{prior uncertainty}}\right) \times 100\ \% \quad (2.10)$$

It is defined as the extent to which the error in the flux field is modified by the inversion. It is dependent on both the prior uncertainty as well as the observation coverage and is a measure of the accuracy of the posterior fluxes estimated by the inversion.

Figure 2.3 shows the prior uncertainty used by the Jena inversion scheme for the different TransCom3 regions. We focus on the years 1996-2004 because of sufficient data availability from MOZAIC during this period. This period also has some data gaps representing times when one or more aircraft are not flying. This helps give a more realistic quantification of the uncertainty reduction brought about by the use of these data.

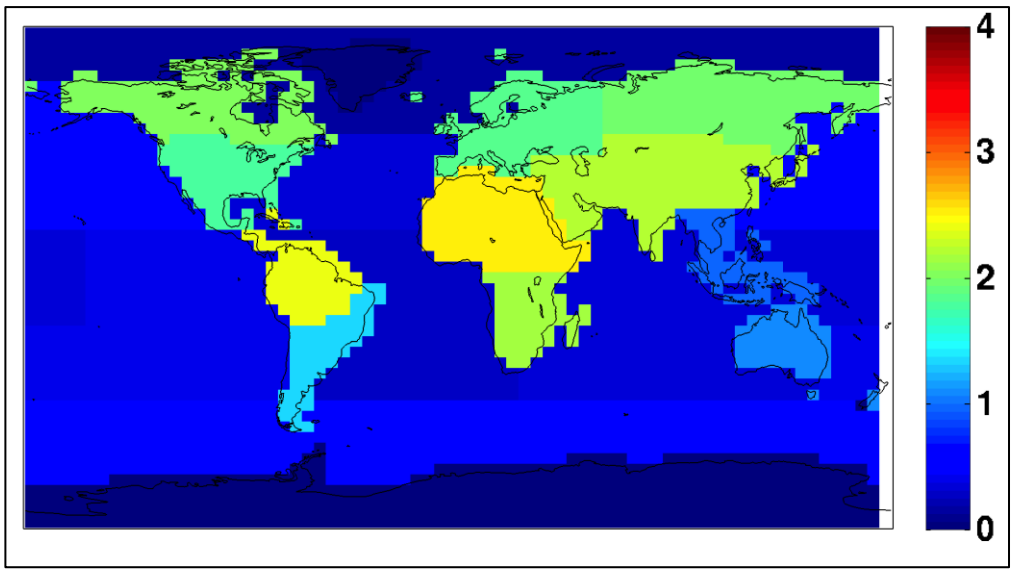

Figure 2.3: Prior flux uncertainty for the TransCom3 regions (in PgC year^{-1}) as used in the Jena inversion scheme.

2.4 Results and Discussion

2.4.1 Impact of BLH transport model errors on flux retrieval

Monthly posterior fluxes for the TransCom3 land regions are analysed and compared to the "true" flux, which is the flux that is used to generate the pseudo data. The time series of the posterior flux for all regions is concatenated to form a single time series in order to obtain a single diagnostic metric for the whole globe. The statistics for comparison between the different simulations are represented on a Taylor diagram as shown in Fig. 2.4.

It is observed that that the transport model errors related to vertical mixing, as simulated using the reshuffling method, affect the flux retrieved from measurements made at surface stations differently than those retrieved using aircraft profiles. There is a large impact of the simulated vertical mixing errors on the flux retrieved using the surface measurements with and without the boundary layer height uncertainties incorporated in the experiments as shown by points Sb and Sa respectively.

The posterior flux standard deviation, root-mean-square difference and correlation coefficient values with respect to the true flux change from 1.90 PgC $year^{-1}$, 0.65 PgC $year^{-1}$ and 0.95 respectively for the simulation Sa to 2.39 PgC $year^{-1}$, 1.76 PgC $year^{-1}$ and 0.69 for simulation Sb. On the other hand, the erroneous vertical mixing has nearly no impact on the flux retrieval using aircraft profile measurements. The standard deviation, root-mean-square difference and correlation coefficient values of 1.81 PgC $year^{-1}$, 0.70 PgC $year^{-1}$, 0.94 change only marginally to 1.82 PgC $year^{-1}$, 0.72 PgC $year^{-1}$ and 0.94 shown by the overlap of the points Aa and Ab.

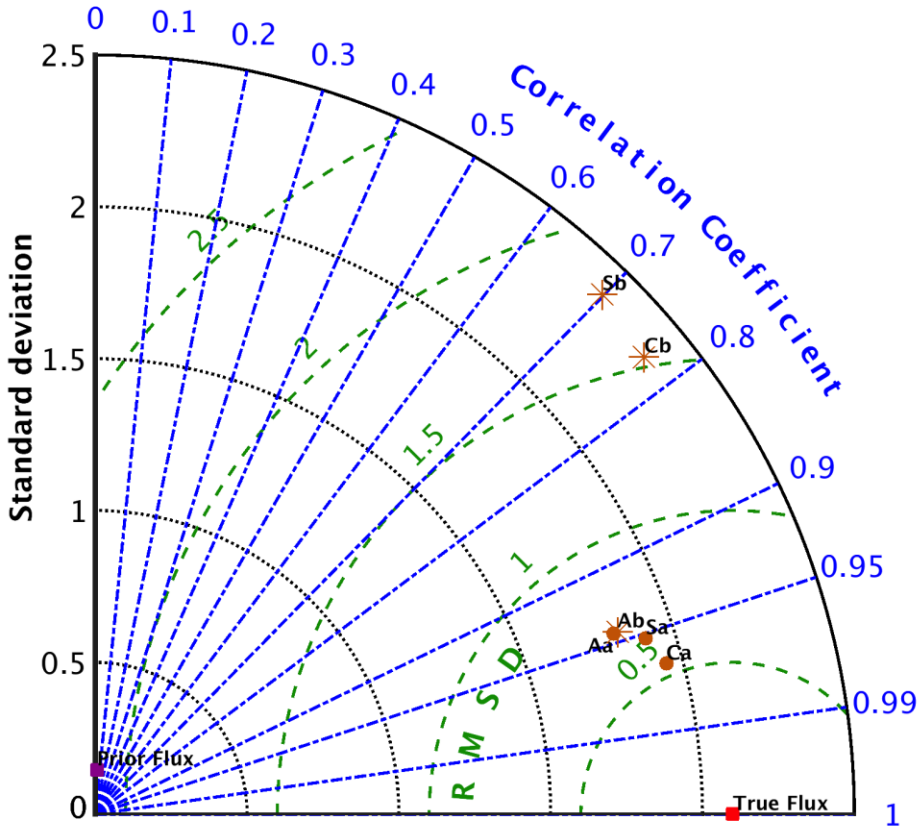

Figure 2.4: Taylor diagram showing the correlation coefficient, standard deviation and root mean square difference of the concatenated time series of the monthly posterior fluxes from the TransCom3 land regions. Points S, A, C represent the simulations using measurements from only the surface stations, only the aircraft profiles and the combined network (Surface + Aircraft) respectively. 'a' denotes the control case simulation with well known boundary layer height while 'b' denotes simulations using reshuffled profiles with "wrong" boundary layer height.

This difference in the response of the flux retrieved using observations from the two different measurement platforms to vertical mixing error can be explained as follows: The aircraft profiles, by virtue of their vertical extent, constrain the inversion using observations at nearly all tropospheric layers over which the total column CO_2 abundance remains constant since CO_2 is well mixed in the troposphere. The impact of vertical transport near the surface is solely to redistribute the tracer mass in the atmospheric column between the different layers of the atmosphere, keeping the total column abundance unchanged. In other words, due to this redistribution the loss of tracer mass in the boundary layer is compensated by the gain in mass in the free troposphere and vice versa. Therefore, any change in the vertical distribution of the tracer at these levels is not likely to impact the total tracer mass in the profile that constrains the inversion and hence the resultant posterior flux retrieved using these measurements. The surface station measurements, on the other hand, are made at a

single altitude, generally within the boundary layer and hence, any change in the boundary layer height due vertical mixing, is likely to cause an impact on the modelled mixing ratio at the measurement altitude which is used to constrain the inversion and hence in the flux retrieved by the inversion. The posterior flux shows less sensitivity to boundary layer height errors in the transport model when aircraft profiles are used as constraint while surface measurements are more likely to be affected by these errors, which translates into errors in the retrieved flux.
Points Ca and Cb in Fig. 2.4 show the impact of the boundary layer error on the flux retrieved using the combined observation network that uses measurements from both the surface network and the aircraft profiles. By using the combined observation network, a similar sensitivity of the posterior flux to boundary layer uncertainty is observed as by the surface based network alone (Points Sa and Sb). This means that the effect of the surface network dominates the flux retrieval and indicates that the surface network stations largely contribute to the sensitivity of the retrieved flux to the uncertainty of the boundary layer height. It can also be seen that the addition of aircraft measurements leads to an improved estimate of the surface flux. This is shown by points Ca and Cb being closer to the true flux than points Sa and Sb respectively. It implies that the addition of the aircraft measurements to the surface based network improves the constraint on the carbon budget as compared to the surface network alone.

2.4.2 Constraint on carbon budget due to IAGOS aircraft profiles

In this section, the constraint that will be brought about by the aircraft measurements of CO_2 from IAGOS on the regional carbon budget is quantified (Fig. 2.5). For this, the reduction in the uncertainty of the posterior fluxes in relation to the prior fluxes is assessed. It should be noted that while the uncertainty reduction alone may not be robust, similarly computed uncertainty reductions can be robustly compared.

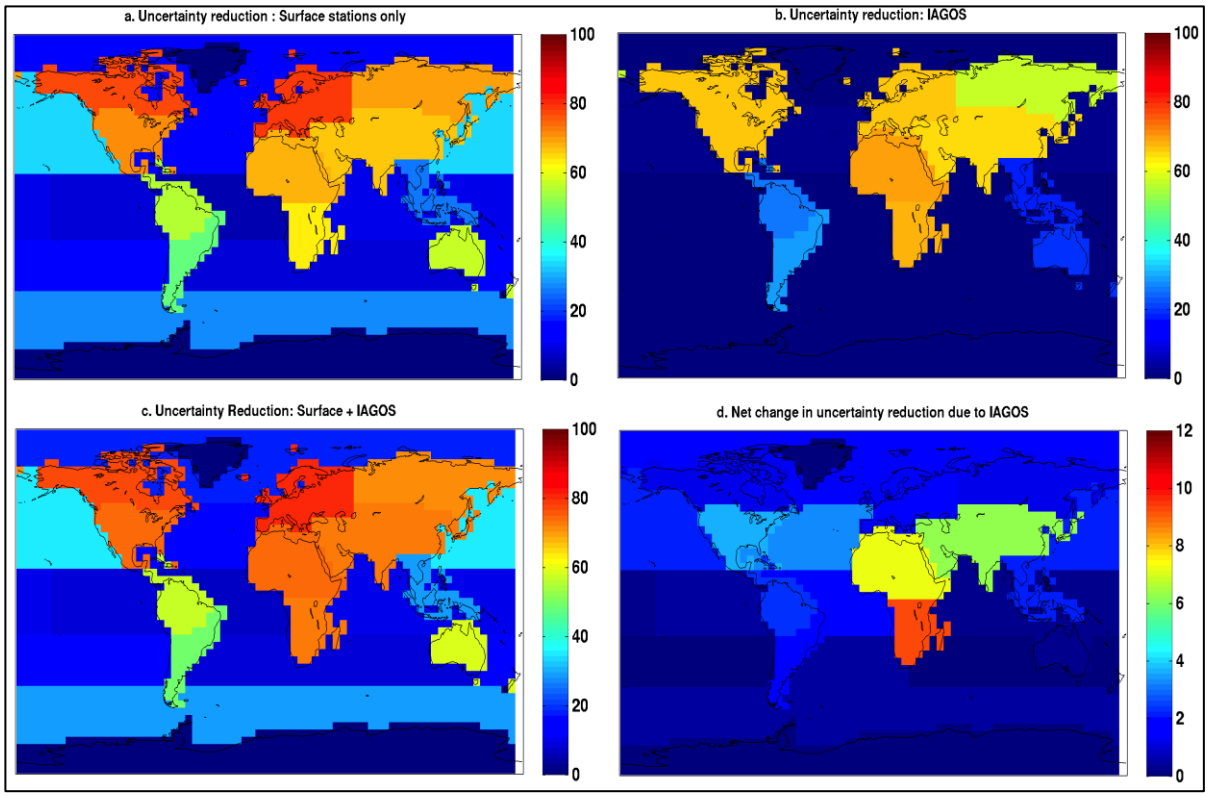

Figure 2.5: Spatial maps showing the reduction in monthly CO_2 flux uncertainty (in percent) at the TransCom3 regions during the period 1996-2004 using measurements from (a) the Surface network alone (b) Five simulated IAGOS aircraft (c) Combined network (Surface + IAGOS aircraft). Panel (d) shows the net change in uncertainty reduction due to the addition of IAGOS measurements to the surface network.

Figure 2.5(a) shows the flux uncertainty reduction of the monthly mean flux over the TransCom3 regions when only the surface based observational network is used in the inversion. The largest constraint due to the surface network alone is observed in Europe and North America. The European and Temperate North American regions have a dense and extensive network of surface observations and hence the reduction in flux uncertainty is as high as about 85 %. In addition, remote observations are also responsible for bringing about a constraint on the fluxes in the neighboring regions due to the effect of wind transport (horizontal advection). For instance, the high value of the uncertainty reduction over North American boreal regions (75 %), inspite of insufficient surface stations in that region, can be attributed to the impact of the westerly winds that cause a constraint in the region due to the effect of remote observations made in Temperate North America. Using the same argument, dense observations over Europe can help constrain surface fluxes from the Eurasian boreal region due to the effect of transport (advection) by the westerlies.

Figure 2.5(b) shows the uncertainty reduction only due to the pseudo profiles from five simulated IAGOS aircraft. Europe, temperate North American regions show an uncertainty reduction of about 70 %. These regions are those where most of the

aircraft profiles are measured due to large air traffic between the two continents by the airlines participating in MOZAIC/IAGOS. These measurements are also able to constrain boreal North America (70 %) and boreal Eurasia (55 %), regions with few or no IAGOS measurements. The African continent shows a high reduction in flux uncertainty (75 %). Regions of South America and Tropical Asia exhibit a low constraint ranging between 20 % and 35 %, due to fewer aircraft profiles measured in these regions in addition to the impact of advection by the easterly winds.

Figure 2.5(c) shows the uncertainty reduction map for the case when pseudo profiles IAGOS aircraft are added to the surface based network. The combined observation network almost completely constrains the regions of Europe and Temperate North America, the uncertainty reduction value being close to 90 %. Tropical Asia shows the least constraint in the fluxes with the combined network since it is not adequately covered by either of the networks- surface or the commercial aircraft. The net impact of adding the profiles from IAGOS to the existing network is shown in Fig 2.5(d), which is the difference between the uncertainty reduction values for the TransCom3 land regions with and without the aircraft profiles. Tropical and Eurasian temperate regions show the greatest change in the constraint in the posterior fluxes on addition of pseudo observations from IAGOS (about 7 to 10 %). These are regions that are poorly constrained by the surface based network. So, addition of aircraft measurements results in the largest improvement in posterior flux uncertainty in these regions. On the other hand, for regions already well constrained by the surface network, for example North America and Europe, the simulated constraint due to the IAGOS CO_2 measurements is very small (less than 1 %).

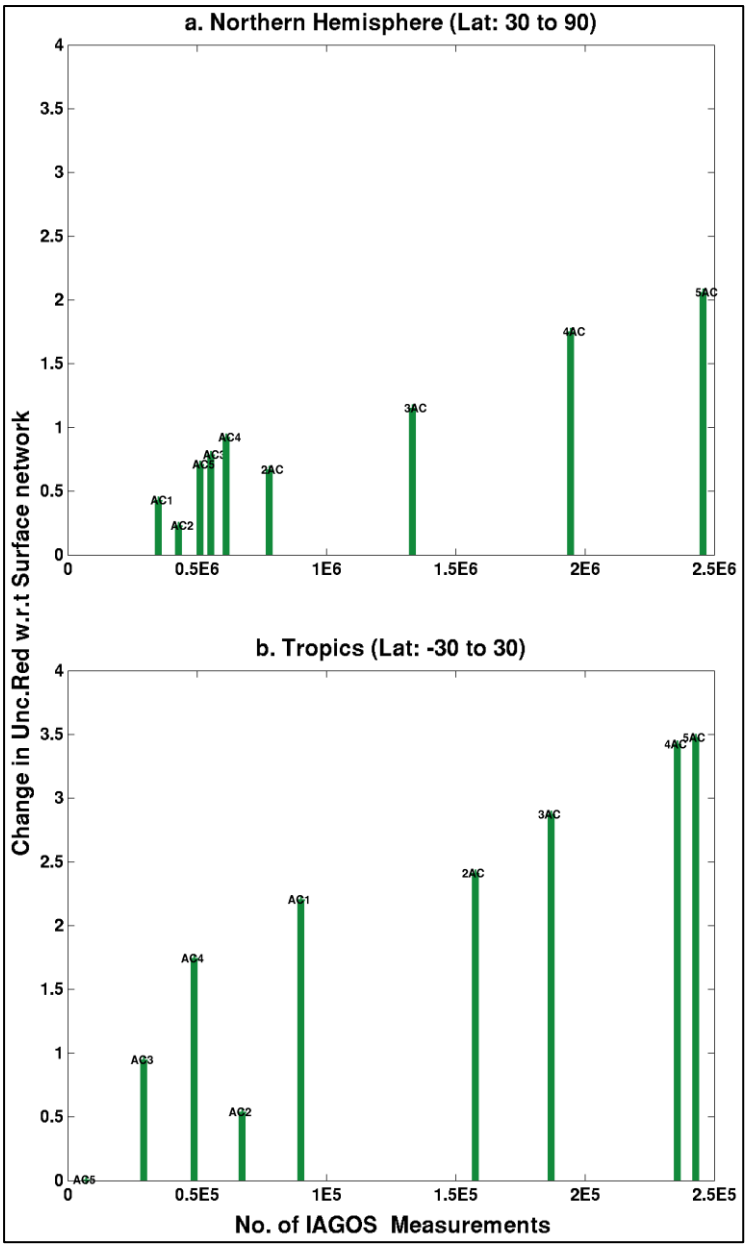

Figure 2.6: Plots showing change in uncertainty reduction (with respect to the surface network) against the number of measurements from IAGOS aircraft for (a) Northern hemisphere (b) Tropics. ACi (i=1 to 5) refers to the simulation using measurements from aircraft number i. jAC(j=2 to 5) refers to simulations that use measurements from j number of aircraft. Note that the scaling of the x-axis differs by a factor ten between (a) and (b).

Further, the constraint due to the aircraft measurements on aggregated spatial scales is investigated by examining the change in uncertainty reduction on the addition of pseudo measurements from IAGOS for the Northern hemisphere (30° N to 90° N), Tropics (-30° S to 30° S) and Southern hemisphere (-90° S to -30° S) (Fig. 2.6).
The zero measurements point on the x-axis of Fig 2.6(a) and 2.6(b) indicates the case where only the existing observation network sites have been used into the inversion but no IAGOS profiles have been used. The change in the uncertainty reduction for the northern hemisphere posterior uncertainty increases from 0.5 % when measurements from one simulated IAGOS aircraft are used, to 2 % from measurements from five aircraft. The Tropics, on the other hand, show a comparable trend and increase in the change of flux uncertainty with however up to 10 times fewer measurements than in the Northern hemisphere. This is likely to be due to the fact that unlike the Northern hemisphere, the tropics are not well constrained by the existing network hence the addition of IAGOS profiles leads to considerable constraint on the surface fluxes. The southern hemisphere (not shown), which is largely ocean, does not gain much from these measurements since they are very few in number and are not sufficient to constrain the region. Hence almost no change is seen in the uncertainty reduction due to aircraft measurements. Thus, it can be concluded that the overall impact of IAGOS measurements based upon this sampling is highest for the tropical region. This indicates that the greatest incremental increase in knowledge of fluxes would be gained by instrumenting aircraft flying preferentially tropical routes. It is however noteworthy, that the saturation of posterior uncertainty values as the number of measurements approaches the maximum value, does not imply that there would be no further benefit of adding measurements from more than from five aircraft. The figure is indicative of the information gained solely on aggregated spatial scales and it is very likely that on smaller scales there is added benefit of having more measurements.

2.5 Summary

Transport models that drive the inversion schemes often have a poor representation of the near surface vertical mixing causing large errors in the retrieved fluxes. In this study, the impact of such transport model uncertainties on the fluxes simulated using aircraft profiles as constraint in an inverse modelling set up is investigated. Only errors in near-surface vertical mixing have been considered. Those due to imperfect representation of other processes like advection and deep convection have not been accounted for. The simulation results show that the flux retrieved using aircraft profiles when the boundary layer height is well known has the same statistical metrics as the flux retrieved when the boundary layer height is erroneous. This shows that posterior fluxes retrieved using aircraft profiles show no sensitivity to the boundary layer height errors as simulated in the experiments. This behaviour of the retrieved

flux is compared to that obtained using the surface measurements as constraint. These measurements are usually in the boundary layer part of the atmosphere and therefore a much higher mismatch between the flux retrieved using correct versus erroneous boundary layer height in terms of the standard deviation, root-mean-square difference and correlation parameters is observed. In other words, this shows that the transport model uncertainties related to boundary layer height are very likely to be translated to the posterior flux when surface measurements are used as constraint in the inversion while these errors are not propagated to the retrieved flux when the aircraft profiles are used. This is likely to be due to the fact that vertical transport, whose effect we simulate by the redistribution of the tracer mass in the model profile at the location of the airports and surface stations, only redistributes the tracer mass between the boundary layer height and the free tropospheric part keeping the total tracer mass constant. The loss (or gain) of the tracer mass in the profile in the boundary layer part of the profile is compensated by the gain (or loss) in the free tropospheric part of the profile. Since aircraft profile measurements extend all the way from the surface to the free tropospheric part of the atmosphere, the net impact of the complete reshuffled profile remains comparable to that of the original. This effect of redistribution, on the other hand, is not observed for the surface station measurements since they are made within the boundary layer and hence, error in the estimation of the boundary layer height will impact the modelled mixing ratio that constrains the inversion. These results demonstrate the benefit of aircraft measurements over those made by ground-based stations for flux estimation using transport models that cannot resolve the boundary layer perfectly. Although only the errors in fluxes due to vertical mixing are accounted for in the simulations, it can be concluded that flux estimation using aircraft profiles is expected to be more robust when aircraft profiles are used as constraint since the contribution of the boundary layer height uncertainty to the overall transport model error is likely to reduce. While improved transport models are an imperative for achieving more accurate estimates of surface fluxes, the potential benefit of aircraft profiles over ground based measurements, as shown by the simulations conducted in this study, provides a simple and flexible approach of dealing with and eliminating the impact of boundary layer height uncertainties due to vertical mixing and diminishing the overall impact of transport model errors on retrieved fluxes. In addition to this, aircraft profiles would also provide valuable information to drive model development.

Furthermore, on estimating the impact that the CO_2 measurements made onboard the IAGOS fleet are likely to have on the regional carbon budget once they are available, we find that the net CO_2 flux uncertainty reduction using the IAGOS measurements is likely to be highest in the Tropics and the Eurasian temperate regions. These are regions that are not well covered by the existing surface based observation network and hence the addition of aircraft measurements brings about the largest constraint. The change in the uncertainty reduction in these regions is between 7 to 10 percent. In contrast, the European and North American continents, which have good data coverage by the surface, based network show little or no change in flux uncertainty due to added measurements from IAGOS.

It must be borne in mind that since the MOZAIC/IAGOS aircraft profiles are measured near the airports, which form areas of high anthropogenic emissions, it is likely that these observations are not truly representative of large areas. This fact has been taken into account, in this study, in a conservative way by estimating the model data mismatch uncertainty using the difference between CO_2 profiles from the CONTRAIL project and reanalysed TM3 fields (Sect. 2.3.3). However, better approaches for addressing this question of representativeness of aircraft profiles exist, for example, those described by Boschetti et al., (2015).

In summary, this study demonstrates the benefit and application of aircraft profile measurements in an inverse modelling framework to enhance our current knowledge about the distribution of carbon sources and sinks at the Earth's surface. Exploiting the potential advantage of this new data stream can help circumvent the problem of transport model related uncertainties in flux estimates to a great extent. In addition to that, these observations can also prove to be crucial to bridging the gap in our understanding of carbon cycle dynamics in hitherto under-sampled regions of the world.

2.6 References

Ahmadov, R., Gerbig, C., Kretschmer, R., Ko¨rner, S., Ro¨denbeck, C., Bousquet, P., and Ramonet, M.: Comparing high resolution WRF-VPRM simulations and two global CO_2 transport models with coastal tower measurements of CO_2, Biogeosciences, 6, 807–817, doi:10.5194/bg-6-807-2009, 2009.

Bousquet, P., Ciais, P., Miller, J. B., Dlugokencky, E. J., Hauglus- taine, D. A., Prigent, C., Van der Werf, G. R., Peylin, P., Brunke, E. G., Carouge, C., Langenfelds, R. L., Lathiere, J., Papa, F., Ramonet, M., Schmidt, M., Steele, L. P., Tyler, S. C., and White, J.: Contribution of anthropogenic and natural sources to atmospheric methane variability, Nature, 443, 439–443, 2006.

Checa-Garcia, R., Landgraf, J., Galli, A., Hase, F., Velazco, V. A., Tran, H., et al.: Mapping spectroscopic uncertainties into prospective methane retrieval errors from Sentinel-5 and its precursor. Atmospheric Measurement Techniques, 8(9), 3617–3629. doi:10.5194/amt-8-3617-2015, 2015

Deng, F., Jones, D. B. A., Walker, T. W., Keller, M., Bowman, K. W., Henze, D. K., Nassar, R., Kort, E. A., Wofsy, S. C., Walker, K. A., Bourassa, A. E. and Degenstein, D. A.: Sensitivity analysis of the potential impact of discrepancies in stratosphere-troposphere exchange on inferred sources and sinks of CO_2, Atmos. Chem. Phys., 15(20), 11773–11788, doi:10.5194/acp-15-11773-2015, 2015.

Denning, A. S., Randall, D. A., Collatz, G. J. and Sellers, P. J.: Simulations of terrestrial carbon metabolism and atmospheric CO_2 in a general circulation model. Part 2: Simulated CO2 concentrations, Tellus B, 48(4), 543–567, doi:10.1034/j.1600-0889.1996.t01-1-00010.x, 1996.

Denning, A. S., Zhang, N., Yi, C. X., Branson, M., Davis, K., Kleist, J., and Bakwin, P.: Evaluation of modeled atmospheric boundary layer depth at the WLEF tower, Agr. Forest Meteorol.,148, 206–215, 2008.

Ehret, G. and Kiemle, C.: Requirements definition for future DIAL instruments, Study report ESA-CR(P)-4513, ESA, Noordwijk, The Netherlands, 2005.

Engelen, R. J., Denning, a S. and Gurney, K. R.: On error estimation in atmospheric CO2 inversions, J. Geophys. Res. Atmos., 107, ACL 10–1–ACL 10–13, doi:10.1029/2002JD002195, 2002.

Galli, A., Guerlet, S., Butz, A., Aben, I., Suto, H., Kuze, A., Deutscher, N. M., Notholt, J., Wunch, D., Wennberg, P. O., Griffith, D. W. T., Hasekamp, O. & Landgraf, J.: The impact of spectral resolution on satellite retrieval accuracy of CO_2 and CH_4 *Atmospheric Measurement Techniques*, *7*(4), 1105–1119. doi:10.5194/amt-7-1105-2014, 2014.

Gerbig, C., Lin, J. C., Wofsy, S. C., Daube, B. C., Andrews, a. E., Stephens, B. B., Bakwin, P. S. and Grainger, C. a.: Toward constraining regional-scale fluxes of CO_2 with atmospheric observations over a continent: 1. Observed spatial variability from airborne platforms, J. Geophys. Res. Atmos., 108(D24), n/a–n/a, doi:10.1029/2002JD003018, 2003.

Gurney, K. R., Law, R. M., Denning, a S., Rayner, P. J., Baker, D., Bousquet, P., Bruhwiler, L., Chen, Y.-H., Ciais, P., Fan, S., Fung, I. Y., Gloor, M., Heimann, M., Higuchi, K., John, J., Maki, T., Maksyutov, S., Masarie, K., Peylin, P., Prather, M., Pak, B. C., Randerson, J., Sarmiento, J., Taguchi, S., Takahashi, T. and Yuen, C.-W.: Towards robust regional estimates of CO_2 sources and sinks using atmospheric transport models., Nature, 415(February), 626–630, doi:10.1038/415626a, 2002.

Gurney, K., Law, R., Rayner, P., and A.S. Denning, "TransCom 3 Experimental Protocol," Department of Atmospheric Science, Colorado State University, USA, Paper No. 707, 2000.

Haszpra, L.: On the representativeness of carbon dioxide measurements, J. Geophys. Res. Atmos., 104(D21), 26953–26960, doi:10.1029/1999JD900311, 1999.

Heimann, H., Körner, S.: The global atmospheric tracer model TM3. Technical Reports - Max-Planck-Institut für Biogeochemie 5, pp. 13, 2003

Houweling, S., Aben, I., Breon, F.-M., Chevallier, F., Deutscher, N., Engelen, R., Gerbig, C., Griffith, D., Hungershoefer, K., Macatangay, R., Marshall, J., Notholt, J., Peters, W., and Serrar, S.: The importance of transport model uncertainties for the estimation of CO_2 sources and sinks using satellite measurements, Atmos. Chem. Phys., 10, 9981–9992, doi:10.5194/acp-10-9981- 2010, 2010.

Law, R. M., Rayner, P. J., Denning, A. S., Erickson, D., Fung, I. Y., Heimann, M., Piper, S. C., Ramonet, M., Taguchi, S., Taylor, J. A., Trudinger, C. M. and Watterson, I. G.: Variations in modeled atmospheric transport of carbon dioxide and the consequences for CO_2 inversions, Global Biogeochem. Cycles, 10(4), 783–796, doi:10.1029/96GB01892, 1996.

Law, R. M., Matear, R. J., and Francey, R. J.: Saturation of the Southern Ocean CO_2 sink due to recent climate change, Science, 319, 570a–570a, 2008.

Lauvaux, T., Pannekoucke, O., Sarrat, C., Chevallier, F., Ciais, P., Noilhan, J. and Rayner, P. J.: Structure of the transport uncertainty in mesoscale inversions of CO_2 sources and sinks using ensemble model simulations, Biogeosciences, 6(6), 1089–1102, doi:10.5194/bg-6-1089-2009, 2009.

Machida, T., Matsueda, H., Sawa, Y., Nakagawa, Y., Hirotani, K., Kondo, N., Goto, K., Nakazawa, T., Ishikawa, K. and Ogawa, T.: Worldwide Measurements of Atmospheric CO2 and Other Trace Gas Species Using Commercial Airlines, J. Atmos. Ocean. Technol., 25, 1744–1754, doi:10.1175/2008JTECHA1082.1, 2008.

Marquis, M. and Tans, P.: CLIMATE CHANGE: Carbon Crucible, Science (80-.)., 320(5875), 460–461, doi:10.1126/science.1156451, 2008.

Marenco, A., Thouret, V., Nédélec, P., Smit, H., Helten, M., Kley, D., Karcher, F., Simon, P., Law, K., Pyle, J., Poschmann, G., Von Wrede, R., Hume, C. and Cook, T.: Measurement of ozone and water vapor by Airbus in-service aircraft: The MOZAIC airborne program, an overview, J. Geophys. Res., 103(D19), 25631, doi:10.1029/98JD00977, 1998.

Niwa, Y., MacHida, T., Sawa, Y., Matsueda, H., Schuck, T. J., Brenninkmeijer, C. A. M., Imasu, R. and Satoh, M.: Imposing strong constraints on tropical terrestrial CO_2 fluxes using passenger aircraft based measurements, J. Geophys. Res. Atmos., 117(11), doi:10.1029/2012JD017474, 2012.

Patra, P. K., Niwa, Y., Schuck, T. J., Brenninkmeijer, C. A. M., MacHida, T., Matsueda, H. and Sawa, Y.: Carbon balance of South Asia constrained by passenger aircraft CO 2 measurements, Atmos. Chem. Phys., 11(9), 4163–4175, doi:10.5194/acp-11-4163-2011, 2011.

Rödenbeck, C., Houweling, S., Gloor, M. and Heimann, M.: CO_2 flux history 1982–2001 inferred from atmospheric data using a global inversion of atmospheric transport, Atmos. Chem. Phys., 3(6), 1919–1964, doi:10.5194/acp-3-1919-2003, 2003.

Rödenbeck, C. : Estimating CO2 sources and sinks from atmospheric mixing ratio measurements using a global inversion of atmospheric transport. Technical Report 6, Max Planck Institute for Biogeochemistry, Jena, 2005.

Seibert P, F Beyrich, SE Gryning, S Joffre, A Rasmussen, and P Tercier. 2000. “Review and Intercomparison of Operational Methods for the Determination of the Mixing Height.” Atmospheric Environment 34(7):1001–1027.

Sitch, S., Smith, B., Prentice, I. C., Arneth, A., Bondeau, A., Cramer, W., Kaplan, J. O., Levis, S., Lucht, W., Sykes, M. T., Thonicke, K. and Venevsky, S.: Evaluation of ecosystem dynamics, plant geography and terrestrial carbon cycling in the LPJ dynamic global vegetation model, Glob. Chang. Biol., 9(2), 161–185, doi:10.1046/j.1365-2486.2003.00569.x, 2003.

Stephens, B. B., Gurney, K. R., Tans, P. P., Sweeney, C., Peters, W., Bruhwiler, L.,

Ciais, P., Ramonet, M., Bousquet, P., Nakazawa, T., Aoki, S., Machida, T., Inoue, G., Vinnichenko, N., Lloyd, J., Jordan, A., Heimann, M., Shibistova, O., Langenfelds, R. L., Steele, L. P., Francey, R. J. and Denning, A. S.: Weak northern and strong tropical land carbon uptake from vertical profiles of atmospheric CO_2., Science, 316(5832), 1732–5, doi:10.1126/science.1137004, 2007.

Thornton, P. E., S. W. Running, and E. R. Hunt. : Biome-BGC: Terrestrial Ecosystem Process Model, Version 4.1.1. Data model. Available on-line [http://www.daac.ornl.gov] from Oak Ridge National Laboratory Distributed Active Archive Center, Oak Ridge, Tennessee, U.S.A., doi:10.3334/ORNLDAAC/805, 2005

Yi, C., Davis, K. J., Bakwin, P. S., Denning, A. S., Zhang, N., Desai, A., Lin, J. C. and Gerbig, C.: Observed covariance between ecosystem carbon exchange and atmospheric boundary layer dynamics at a site in northern Wisconsin, J. Geophys. Res. D Atmos., 109(8), doi:10.1029/2003JD004164, 2004.

Chapter 3

Extending methane profiles from aircraft into the stratosphere for satellite total column validation

3.1 Abstract

Airborne observations of greenhouse gases are a very useful reference for validation of satellite-based column-averaged dry air mole fraction data. However, since the aircraft data are available only up to about 9-13 km altitude, these profiles do not fully represent the depth of the atmosphere observed by satellites and therefore need to be extended synthetically into the stratosphere. In the near future, observations of CO_2 and CH_4 made from commercial aircraft are expected to be available through the In-Service Aircraft for a Global Observing System (IAGOS) project. In this study, three different data sources that are available for the stratospheric extension of aircraft profiles are analysed by comparing the error introduced by each of them into the total column and recommendations regarding the best approach are provided. First, CH_4 fields from two different models of atmospheric composition - the European Centre for Medium-Range Weather Forecasts (ECMWF) Integrated Forecasting System for Composition (C-IFS) and the TOMCAT/SLIMCAT 3-D chemical transport model are analysed. Secondly, scenarios that simulate the effect of using CH_4 climatologies such as those based on balloons or satellite limb soundings are considered. Thirdly, the impact of using a-priori profiles used in the satellite retrievals for the stratospheric part of the total column is assessed. The results show that the models considered in this study have a better estimation of the stratospheric CH_4 as compared to the climatology-based data and the satellite a-priori profiles. Both the C-IFS and TOMCAT models have a bias of about -9 ppb at the locations where tropospheric vertical profiles will be measured by IAGOS. The C-IFS model, however, has a lower random error (6.5 ppb) than TOMCAT (12.8 ppb). These values are well within the minimum desired accuracy and precision of satellite total column XCH_4 retrievals (10 ppb and 34 ppb, respectively). In comparison, the a-priori profile from the University of Leicester Greenhouse Gases Observing Satellite (GOSAT) Proxy XCH_4 retrieval and climatology-based data introduce larger random errors in the total column, being limited in spatial coverage and temporal variability. Furthermore, the bias in the models varies with latitude and season. Therefore, applying appropriate bias correction to the model fields before using them for profile extension is expected to further decrease the error contributed by the stratospheric part of the profile to the total column.

3.2 Introduction

Space-based observations of atmospheric greenhouse gases hold great potential for gaining a better understanding of the dynamics of the global carbon cycle. Satellite measurements such as those from the Greenhouse Gases Observing Satellite (GOSAT) provide column-averaged dry air mole fractions of CO_2 (XCO_2) and CH_4 (XCH_4) (Yokota et al., 2009, Yoshida et al., 2011) that can be used in inverse simulations to estimate carbon sources and sinks at the Earth's surface along with their spatial and temporal distributions.

A precondition for the use of satellite-based total column observations in inverse modelling studies is that these measurements must be sufficiently accurate and precise. Rayner and O'Brien (2001) have shown that the precision requirement for remotely sensed total column-averaged CO_2 abundances to be useful in constraining surface fluxes is less than 1 % (3-4 ppm), while others (e.g. Miller et al., 2007) suggest even more stringent requirements (1-2 ppm). For total column abundance of CH_4, the required precision of these measurements is around 34 ppb or less (Buchwitz et al., 2011). Hence, before these space-based observations can be used for flux estimation, they must be validated and calibrated using independently obtained measurements of even higher precision.

To this end, in-situ measurements made by sensors deployed on aircraft have proved to be extremely useful. These measurements are currently being used in addition to ground-based remotely sensed column-averaged mole fraction data such as those from the Total Carbon Column Observing Network (TCCON), a network of ground-based Fourier Transform Spectrometers that provides valuable reference data for validation of satellite total column retrieval, currently at 23 sites across the globe (Wunch et al., 2011). However, these data further depend on in-situ measurements made from aircraft or AirCore (Karion et al., 2010) for validation and calibration (Wunch et al., 2010; Geibel et al., 2012).

There have been a number of recent studies that have used airborne measurements from commercial aircraft and research aircraft campaigns. Inoue et al., (2016) used TCCON measurements for bias correcting total column XCH_4 and XCO_2 retrievals from GOSAT and further verified the approach using aircraft measurements. Inoue et al., (2013) and Miyamoto et al., (2013) were focused on validation of GOSAT XCO_2 while de Laat et al., (2012) and de Laat et al., (2014) presented a validation approach using commercial aircraft profiles for CO measurements from SCIAMACHY and MOPITT respectively. While both commercial aircraft and research aircraft provide accurate, high-resolution in-situ atmospheric information, operational commercial aircraft measurements have the added advantage of global coverage and availability over long periods of time (Petzold et al., 2015). The In-Service Aircraft for a Global Observing System (IAGOS) project is a recently established European Research Infrastructure conducting long-term observations of atmospheric species with the help

of sensors deployed onboard commercial aircraft. While currently it provides for the measurement of species like carbon monoxide (CO), ozone (O_3), water vapour (H_2O), nitrogen oxides (NO_x, NO_y) and aerosols, measurements of carbon dioxide (CO_2) and methane (CH_4) is also foreseen in the near future.

One of the limitations of aircraft profiles as a source of reference data for validation of total column data is that their altitudinal extent does not represent the full depth of the atmosphere observed by the satellites. The profiles generally do not extend much above the tropopause and have to be extended further into the stratosphere using other sources of information in order to compute the total column abundance. These sources could include model output (de Laat et al., 2012), climatologies based on balloon-borne measurements that measure above the tropopause up to about 30 km altitude (Geibel et al., 2012), satellite limb soundings (Inoue et al., 2014) or the stratospheric portion of the a-priori profile used in the satellite retrieval. Therefore, in order to be able to use the aircraft profiles for validation of satellite columns, we need to choose an appropriate data source for profile extension based on a sound evaluation of the available options and the uncertainty that each of them introduces to the total column.

In this context, CH_4 poses more challenges than some other tracers like CO and CO_2. CH_4 is a critical driver of stratospheric chemistry and is known to have a stratospheric sink due to oxidation reactions with OH (hydroxyl) and Cl (chlorine) radicals. This fact makes the choice of the stratospheric extension extremely crucial for CH_4 when using aircraft profiles for validation of total column observations. This is because, although the stratosphere has a small mass relative to the total column, chemical losses in the stratosphere result in a steep gradient in the CH_4 mixing ratio with height. Misrepresentation of this gradient in the stratospheric extent can have a major impact on the calculated column-averaged concentration. Wunch et al., (2010) showed that the contribution of the error from the unsampled part of the atmosphere above the highest altitude of the aircraft profiles is the largest towards the error in the total column. Therefore, we need to reasonably estimate and, if possible, reduce the error associated with the stratospheric extension of the aircraft profile. In order to do that a good understanding of the stratospheric dynamics and variability is critical.

So far an analysis of the impact of using different extensions has not been performed and most validation studies using aircraft profiles have used only one data source for the extension of the aircraft column. In this study, three different potential candidates that can be used as stratospheric extensions for CH_4 are analysed by quantifying and characterizing the error associated with each. These are: model output, climatologies based on balloon or satellite limb soundings and a-priori profiles from satellite retrievals. The main idea is to quantify the contribution of the bias and variability in the stratospheric column from each of these data sources on the total column abundance of CH_4 and, on the basis of this analysis, provide recommendations regarding which of the data sources to use. Regional differences in the applicability of the approach are examined, and regions that prove particularly difficult are identified.

The uncertainty from each of these data sources is computed using reference data from satellite limb measurements from the Michelson Interferometer for Passive Atmospheric Sounding (MIPAS) (Fischer et al., 2008; Raspollini et al., 2006) instrument which was in operation between 2000 and 2012 and formed a part of the core payload of Envisat (Environmental Satellite). In order to get realistic estimates and distribution of the stratospheric uncertainty introduced in XCH_4, the magnitude of the error associated with each data source is estimated at real aircraft profile locations coming from the Measurement of OZone and water vapour by AIrbus in-service airCraft (MOZAIC) project (Marenco et al., 1998). The project started in 1993 with the aim of collecting O_3, H_2O, CO and NO_y data with the help of high tech sensors deployed onboard five long-range commercial airliners. This project is the predecessor of the IAGOS project and hence the sampling is expected to be comparable to that from IAGOS.

The model output analysed in this study is obtained from two models:
1. The Integrated Forecasting system for Composition (C-IFS) (Flemming et al., 2015; Massart et al., 2014) is a comprehensive, state of the art numerical weather prediction (NWP) and Earth-system model developed at the European Centre for Medium - Range Weather Forecasts (ECMWF). It models the dynamics of the atmosphere and the physical processes that influence the weather as well as the atmospheric composition. Data assimilation of meteorological and atmospheric CH_4 observations from the SRON product of GOSAT (Butz et al., 2010) is used in order to produce a global atmospheric CH_4 analysis based on an optimal estimation of the state of the atmosphere.

2. The TOMCAT/SLIMCAT model (Chipperfield, 1999, 2006), a 3-D offline chemistry transport model that simulates the temporal and spatial distribution of chemical tracers in the troposphere and stratosphere. The model has a detailed chemistry scheme and is driven by winds and temperature fields obtained from the ERA-Interim meteorological reanalysis.

As a sanity check, the model profiles are also compared to that obtained using CH_4 profiles from the ACE-FTS instrument (Bernath et al., 2005) on the Canadian satellite SCISAT-1, launched in August 2003 with the main goal of studying the chemical and dynamical processes that impact stratospheric ozone depletion.

Since climatology-based data are long-term averages, generally with sparse spatial coverage,the impact of using these data for the stratosphere by simulating the effect of temporal averaging and reduced spatial coverage on the stratospheric column error is investigated. For this, the error introduced by the following is analysed: 1) Monthly mean CH_4 fields from the C-IFS model. 2) Monthly mean C-IFS fields based on sampling as that of the (a) ACE-FTS and (b) MIPAS instruments for the stratosphere. This helps to quantify how much uncertainty is introduced if there is a poorer representation of the CH_4 variability in the data and if the spatial coverage of the data

is low. Further, it helps determine if it is better to use the full variability of CH_4 from a (potentially biased) model rather than the lower-bias monthly means lacking temporal variability from mean satellite fields. It is noteworthy that the idea behind option 2) is to not compare the impact of using the profiles from the two instruments per se, since MIPAS is no longer flying and hence cannot be used for profile extension in the future, but to evaluate the effect of the different type of sampling from the two instruments i.e. ACE-FTS-like (sparse) and MIPAS-like (dense). Since there is no realistic "truth" of MIPAS or ACE measurements at all times and all places throughout the month, here the full C-IFS fields are treated as the truth and compared to monthly mean fields derived from the C-IFS sampled at the MIPAS and ACE-FTS locations and times. Thus, for this part of the study, no actual climatology data are used and only the uncertainty introduced by the sampling and averaging is assessed. The computed error in the two cases is then re-calculated with respect to MIPAS using the bias in the full C-IFS fields obtained from comparison with MIPAS.

Lastly, the stratospheric column uncertainty from using the a-priori profile of the satellite retrieval for profile extension is estimated. This is achieved using the University of Leicester GOSAT Proxy XCH_4 retrieval (Parker et al., 2011).

The layout of the chapter is as follows. Section 3.3 describes the different datasets used in the study as well as the methodology and approach. Section 3.4 presents the details of the stratospheric column error estimation and comparison of the different profile extensions. Section 3.5 presents the discussion and conclusions of the results.

3.3 Datasets

3.3.1 Integrated Forecasting system for Composition (C-IFS)

The Integrated Forecasting System for Composition (C-IFS) is a comprehensive NWP Earth system model developed at the ECMWF. It uses 4D-Var (Rabier et al., 2000) to assimilate data from a wide range of different observation networks and satellite instruments into the model in order to produce optimal estimates of the state of the atmosphere. In addition to this, monitoring of atmospheric composition and modelling of greenhouse gases has also been incorporated into the IFS (Flemming et al., 2015; Massart et al., 2014) as a part of the Copernicus Atmosphere Monitoring Service (CAMS, https://atmosphere.copernicus.eu) and previously the Monitoring of Atmospheric Composition and Climate (MACC, mac.copernicus-atmosphere.eu) projects.

The C-IFS model uses surface CH_4 fluxes and loss rate prescribed from inventories and climatologies. The CH_4 fluxes are those used as priors for flux estimation in the

study by Bergamaschi et al., (2009), except for anthropogenic fluxes which are obtained from the EDGAR 4.2 database (Janssens-Maenhout et al., 2012) for the year 2008, and biomass burning emissions which are taken from the CAMS GFAS data set (Kaiser et al., 2012). For the chemical sink in the troposphere and the stratosphere, the climatological chemical loss rates from Bergamaschi et al., (2009) are used. These are based on OH fields optimised with methyl chloroform using the TM5 model (Krol et al., 2005) and prescribed concentrations of the stratospheric radicals using the 2-D photochemical Max Planck Institute model.

In this study, the tropopause height is diagnosed using the humidity gradient from the C-IFS model. The tropopause height is used to separate the tropospheric and stratospheric partial columns of CH_4. The CH_4 analysis product from C-IFS that includes the assimilation of the GOSAT CH_4 product from SRON (Butz et al., 2010) has been used in this study. The model run has a horizontal Gaussian grid with a resolution of TL255 (~80 km), but the output are averaged onto a regular 1° × 1° grid. The model has 60 vertical levels from the surface up to 0.1 hPa. Temporal resolution of the CH_4 analysis fields is 6 hours. The meteorological reanalysis products are used as input for a number of offline transport models and since it provides data at a high vertical and horizontal resolution, it has also been used as a reference for the development of some CTMs, e.g. TOMCAT/SLIMCAT (described below) and TM5 (Krol et al., 2005).

3.3.2 TOMCAT/SLIMCAT model

TOMCAT/SLIMCAT is a three-dimensional off-line chemical transport model (CTM) first described by Chipperfield et al., (1993). The model is driven using prescribed winds and temperatures and simulates the abundances of chemical and aerosol tracers in the troposphere and stratosphere. The TOMCAT model has been used extensively for chemistry and transport studies in the stratosphere and troposphere (e.g., Stockwell et al., 1999; Monks et al., 2012; Richards et al., 2013; Chipperfield et al., 2015). The TOMCAT version, as used here, employs a hybrid σ-p vertical coordinate system. Tracer advection is based on a conservation of second-order moments scheme described in Prather (1986) and convective transport is based on the mass flux scheme of Tiedtke (1989). In general the model has a flexible vertical and horizontal resolution. The SLIMCAT model was developed later as the 'stratosphere only' version of the TOMCAT model using a hybrid σ-θ vertical coordinate system. The SLIMCAT model was further developed and extended downwards to include the tropospheric levels to form the unified TOMCAT/SLIMCAT model (Chipperfield, 2006) allowing a choice of the vertical coordinate system.
In this study, output has been taken from a TOMCAT simulation with the moderate horizontal resolution of 2.8° × 2.8° with 32 vertical levels from the surface to 0.1 hPa.

The model has a detailed interactive stratospheric chemistry scheme with explicit simulation of the CH_4 loss reactions. The model run started in 1979 and was forced by 6-hourly ECMWF ERA-Interim reanalyses. The tropospheric mixing ratios of long-lived source gases, including CH_4, N_2O and halocarbons, were specified from monthly global mean observations. The temporal resolution of the available gridded model output is 6 hours.

In the subsequent sections of this chapter, the TOMCAT/SLIMCAT model will be referred to as 'TOMCAT'. The results of the TOMCAT simulation are complementary to those from the C-IFS model in the sense that they are obtained from a computationally inexpensive forward CTM, which has no additional constraint such as chemical data assimilation.

3.3.3 MIPAS observations of CH_4

MIPAS is a Fourier transform infrared limb emission spectrometer on the Envisat (Environmental Satellite) that was operational between 2002 and 2012 (Fischer et al., 2008; Raspollini et al., 2006). It provided trace gas information of a number of species mainly in the upper tropospheric, stratospheric, and mesospheric levels measuring continuously and providing nearly global coverage in a single day. From 2002 to 2004 MIPAS operated at a high spectral resolution mode (Glatthor et al., 2005), while from 2005 to 2012 its operation was based on the reduced spectral resolution (Chauhan et al., 2009; von Clarmann et al., 2009b)

In this study, CH_4 profiles for the year 2010, from the V5R_CH4_224 version retrieved with the IMK/IAA (Institut für Meteorologie und Klimaforschung, Karlsruhe/Instituto de Astrofisica de Andalucia, Granada) MIPAS scientific level 2 processor are used. The retrieval algorithm is described in detail in Pleininger et al., (2015). These CH_4 profiles are validated in Pleininger et al., (2016). In order to use the profiles as reference truth for comparison with the CH_4 profiles from the C-IFS and TOMCAT models, they are interpolated to the model grid before comparison.

3.3.4 ACE-FTS observations of CH_4

The ACE-FTS is a limb-sounding instrument on the SCISAT-1 satellite that was launched in August 2003 (Bernath et al., 2005). The satellite operates on a high inclination (74°), circular low Earth orbit. The ACE – FTS instrument is currently operational in a solar occultation mode covering a latitudinal range of 85° S to 85° N. It measures temperature, pressure profiles along with concentrations of a number of trace gas species at the upper tropospheric levels to about 150 km. During the retrieval process, the temperature and pressure profiles are retrieved first, which are

subsequently used to retrieve the volume mixing ratios of the atmospheric species. The detailed retrieval algorithm is described in Boone et al., (2005). For this study, level 2 version 3.5 CH_4 data for the year 2010 has been used as a reference for comparison with model CH_4 profiles.

3.4 Results

3.4.1 Factors influencing stratospheric contribution to total column XCH_4

First, the spatial distribution of the stratospheric CH_4 column abundance is analysed and those regions are identified where the total column is most sensitive to stratospheric column variability. The pressure-weighted column averaged dry air mole fraction of CH_4 is computed using the CH_4 fields from the C-IFS model for the year 2010. The profile is then separated into two parts and the tropospheric and stratospheric partial column averaged mole fractions are computed for which the 6-hourly tropopause information from the C-IFS model is used.

Figure 3.1 shows the column-averaged abundance of CH_4 for the stratospheric and tropospheric partial columns as well as the total column for the months June to August, 2010. This figure shows that for the tropical regions, the spatial variability of the total column XCH_4 is largely driven by the tropospheric CH_4 column abundance, which can be attributed to spatial variability in surface fluxes. In the northern hemisphere, the equator-to-pole gradient of the stratospheric CH_4 column is opposite to that of the tropospheric CH_4 column such that the stratosphere acts to smooth the overall tropics-pole gradient in the total column.

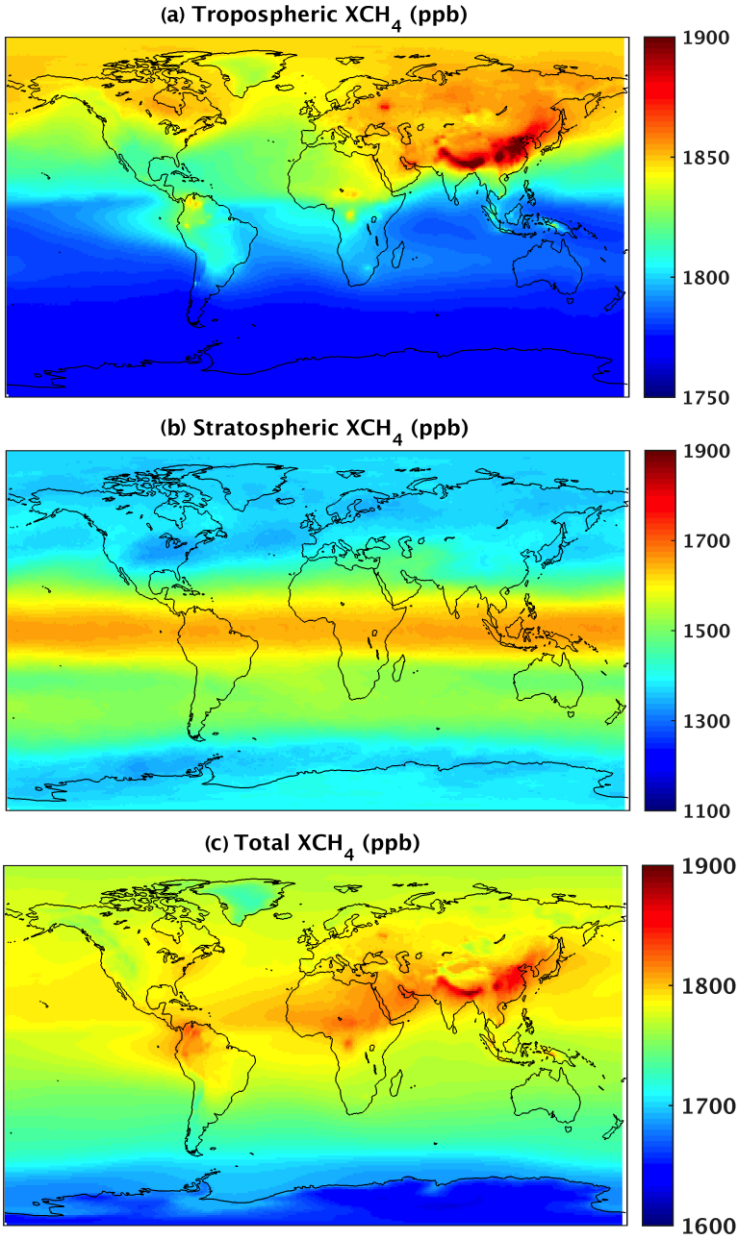

Figure 3.1: Mean column abundance of methane (in ppb) during June-August 2010 obtained from the C-IFS fields for (a) tropospheric partial column, (b) stratospheric partial column and (c) total column. Note the different colour scales in the three panels.

Figure 3.2 shows the variability of the two partial columns and the total column CH_4 over the three-month period. It can be seen that the tropospheric column variability is largest around the Tibetan plateau region. The highlands of the Tibetan plateau are regions of high tropopause variability due to their high elevation (between 3000 and 8848 m above sea level) which cause strong stratosphere-troposphere interaction events like tropopause folds to occur. These events can cause stratospheric air to be transported into the troposphere, which is responsible for the variability of the

tropospheric and stratospheric partial column. The tropospheric column variability in this region is as high as 40 ppb while in most other regions of the world the tropospheric CH_4 values remain comparatively constant where the variability is less than 15 ppb. The variability in the tropospheric column is also large for regions that form the CH_4 hotspots such as wetlands and rice-growing regions of Bangladesh, India, and China, and anthropogenic emissions, possibly exacerbated by wildfires in 2010, in western Russia.

The stratospheric column variability on the other hand has a zonal distribution. This is because the variability of the stratospheric column is directly linked to the tropopause height (Fig. 3.3). As expected, the mean tropopause height is higher in the tropics (90-100 hPa) than at extra-tropical and polar latitudes (>150 hPa). In the high- and mid-latitudes, especially in areas at the edge of the southern hemisphere polar vortex, the spatial gradient of the tropopause is at its maximum. The tropopause, therefore, interacts with the jet stream and extratropical weather systems, causing it to move up and down. The vertical movement of the tropopause results in areas of high tropopause height variability during the austral winter months (Fig. 3.3(b)), which therefore impact the variability in the stratospheric column. During months of boreal winter (not shown), this effect is shifted to the Northern Hemisphere. On the other hand, since the tropical tropopause is rather flat and has a weak spatial gradient, it causes little or no variability in the stratospheric partial column except in the Tibetan highland region (90 ppb).

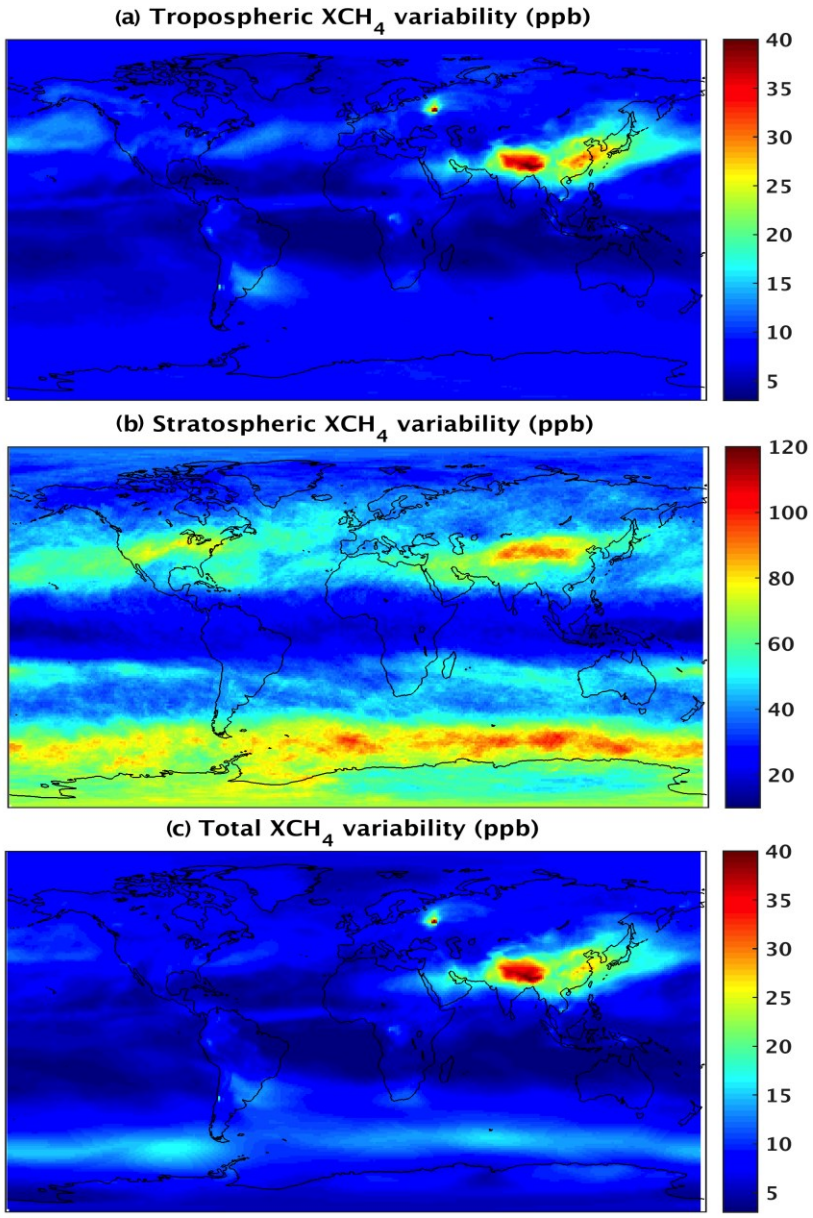

Figure 3.2: Variability (standard deviation) in the column abundance of methane (in ppb) during June-August 2010 obtained from the C-IFS model fields for (a) tropospheric partial column, (b) stratospheric partial column and (c) total column. Note the different colour scales in the three panels.

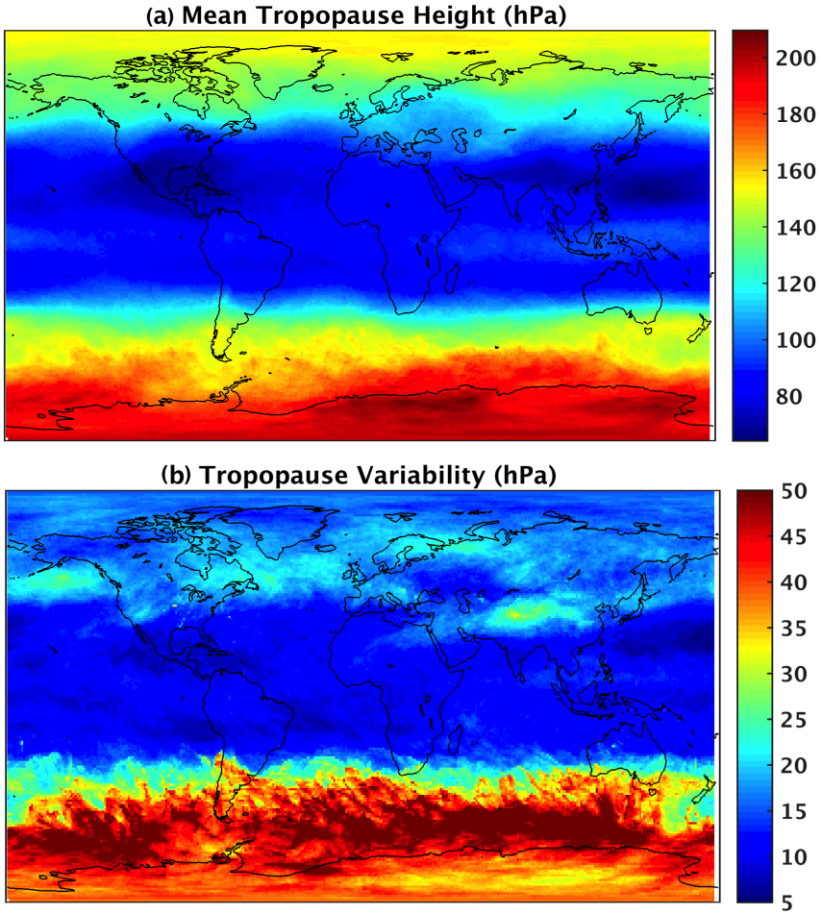

Figure 3.3: (a) Mean tropopause height (in hPa) and (b) variability (standard deviation) of tropopause height (in hPa) from the C-IFS model fields for June - August 2010.

The impact of the stratosphere on total column XCH_4, is largely linked to two factors: (i) the mass of CH_4 in the stratosphere relative to that in the total column and (ii) its associated variability due to dynamical processes in the atmosphere such as the movement of the tropopause. This means that the contribution of the uncertainties in the stratospheric CH_4 to the total column XCH_4 is likely to be significant in regions where at least one of the two driving factors is high. For regions where both these factors are low, the XCH_4 value is less sensitive to uncertainties in the stratospheric CH_4 component. A qualitative analysis of how these two driving factors vary spatially during the different seasons of the year is performed to identify regions where the stratospheric processes directly influence the total column and regions where the impact is not significant.

Two quantities are defined:

$$\text{CH}_4 \text{ mass fraction } (f_{str}) = \frac{\text{mass of CH}_4 \text{ in the stratospheric column (in kg)}}{\text{mass of CH}_4 \text{ in the total column (in kg)}} \quad (3.1)$$

$$\text{CH}_4 \text{ mass fraction variability } (\sigma_{str}) = \text{Standard deviation of } f_{str} \quad (3.2)$$

In the context of extending the aircraft measured profiles into the stratosphere, it can be said that if an aircraft profile is present in regions having both low f_{str} and low σ_{str}, the total column is likely to be less sensitive to the choice of data source used as an assumption for the stratosphere. Figure 3.4 shows the C-IFS stratospheric CH_4 mass fraction f_{str} plotted against its variability σ_{str} for five different latitude bands during the different seasons. Overall, the tropics are regions with both low f_{str} and low σ_{str} throughout the year, while the extra-tropical and high-latitude regions have high values for either one or both of these factors, making the computed value of the total column in these regions more sensitive to the CH_4 variability in the stratosphere. During the austral winter months, the Southern Hemisphere shows particularly high variability in the stratospheric CH_4 that is likely to be due to the impact of the polar vortex dynamics.

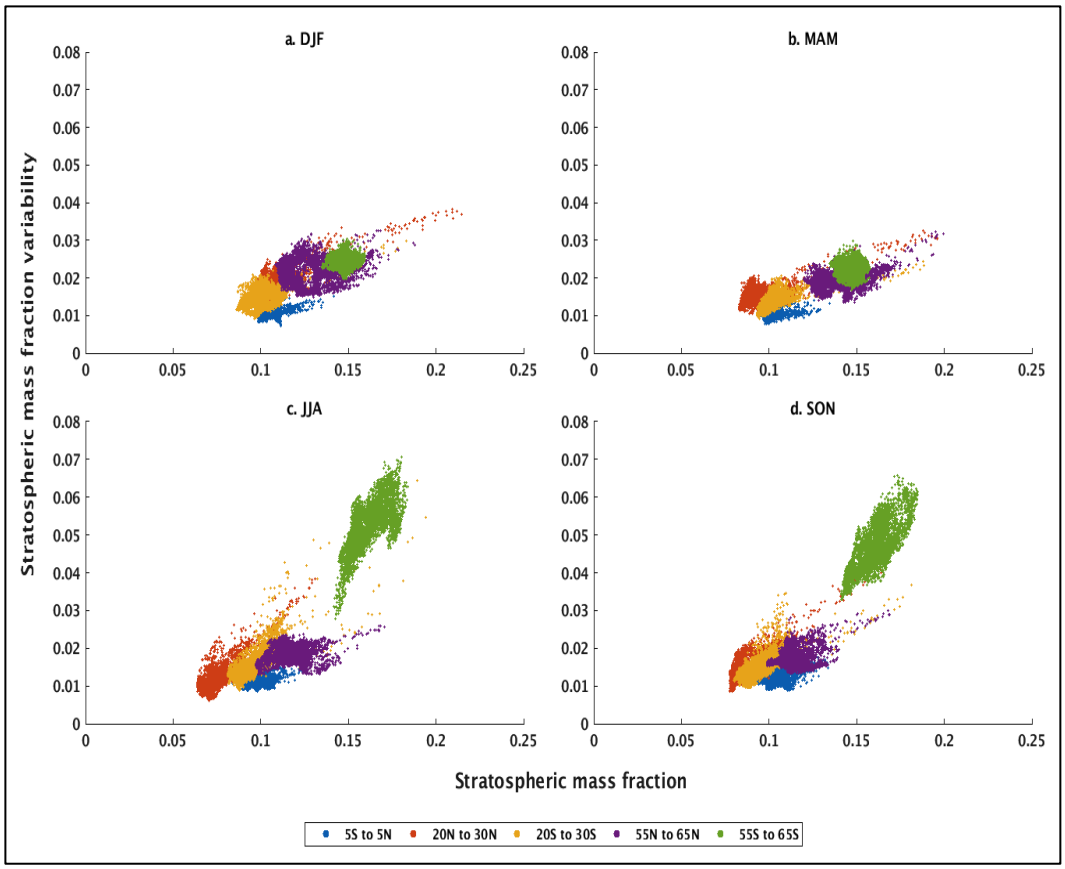

Figure 3.4: Scatterplots showing the CH_4 stratospheric column mass fraction (f_{str}) against CH_4 stratospheric column mass fraction variability (σ_{str}) for (a) December-February, (b) March-May, (c) June-August and (d) September-November months of 2010. The colour shading indicates different latitude bands.

Figure 3.5 shows the latitudinal distribution of airports visited by the MOZAIC fleet during one year (2004), reflecting the typical yearly MOZAIC flight statistics. While almost all the profiles are measured in the Northern Hemisphere, they are mostly concentrated in the mid-latitude region (between 40° N and 55° N). This is because of the large air traffic between Europe and North America by the airlines participating in MOZAIC. Of all the MOZAIC profiles measured in one year, only a small fraction falls within the tropical region (about 17 %). It is thus reasonable to infer that for the commercial aircraft profiles with sampling comparable to MOZAIC, the stratospheric variability is critical to determining the total column CH_4 abundance and needs to be accounted for using an appropriate method of profile extension into the stratosphere.

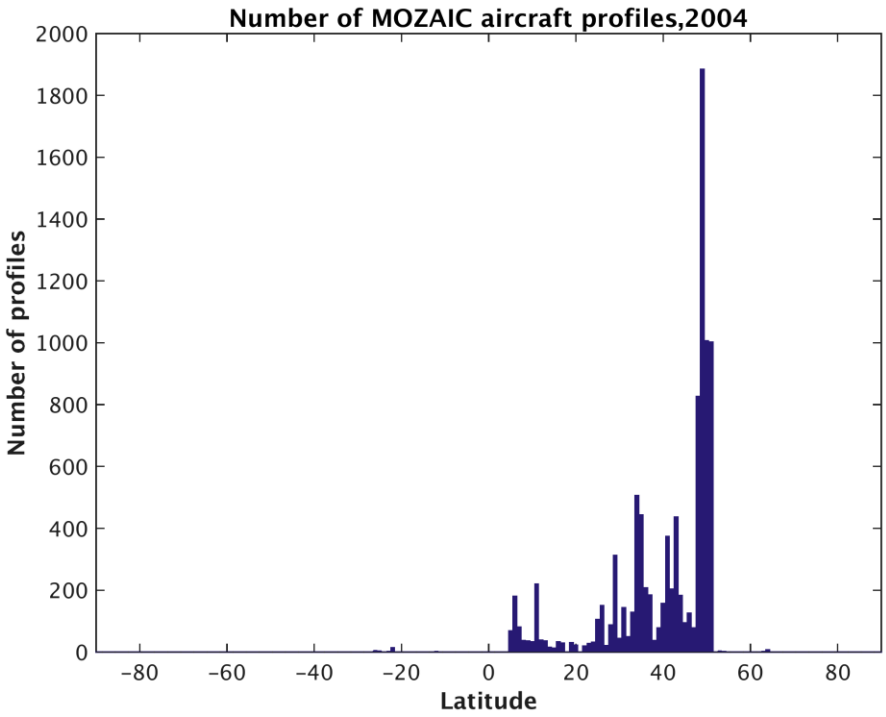

Figure 3.5: Latitudinal distribution of MOZAIC aircraft profile observations (in the vicinity of airports) during the year 2004.

In the following sections, the uncertainty introduced in the total column at the MOZAIC airport locations using the model output, climatology data and a-priori profile as stratospheric extensions is compared.

3.4.2 C-IFS and TOMCAT models

Model profiles from C-IFS and TOMCAT models are compared to coincident satellite observations from MIPAS. These measurements are independent since these are not assimilated into the models. The 6-hourly model profiles are interpolated to the time and location of the satellite observed soundings - linear in time and closest neighbour in space. The MIPAS profiles are then interpolated onto the coarser model vertical grids. Averaging kernel information of the limb satellite instrument is not applied to the coincident model profiles since the impact is not expected to be significant (Laeng et al., 2015; Ridolfi et al., 2011). In order to make a true comparison between the stratospheric levels of the profile simulated by the two models we use the C-IFS tropopause height for identifying and analysing the stratospheric levels for the TOMCAT model. Because the TOMCAT model is driven by winds from ERA-Interim, this definition of the tropopause height should be consistent with the transport of TOMCAT.

Comparison of zonal mean model profiles and coincident satellite observations for the months September to November is shown in Fig. 3.6 and 3.7. The C-IFS is biased high compared to the observed value from MIPAS in the lower stratosphere just above the tropopause (at around 100 hPa) by about 80-100 ppb during the months of September to November (Fig. 3.6(d)). This bias reverses in sign and increases to about 200 to 300 ppb in the middle stratosphere (10 hPa pressure level). In the tropical latitudes this bias shifts to the upper layers of the stratosphere (around 1 hPa). Furthermore, a comparison between Fig. 3.6(a) and 3.6(b) shows that the C-IFS model simulates a steeper vertical gradient in the CH_4 concentration in the stratosphere as compared to that observed by MIPAS.

The comparison between TOMCAT and MIPAS for the same period shows that TOMCAT is biased high by about 100 ppb compared to the MIPAS soundings in the lower stratosphere (100 hPa). In the middle stratosphere (10 hPa) the bias reverses in sign (-100 to -200 ppb in the Southern Hemisphere and around -50 ppb in the Northern Hemisphere mid-latitudes) and again becomes positive (~100 ppb) in the upper stratospheric layers. Thus, the positive and negative bias patterns in the stratospheric levels occur alternately. Also the gradient in the CH_4 concentration in the stratospheric levels as simulated by TOMCAT is more comparable to the observations and is not as steep as that modelled by C-IFS.

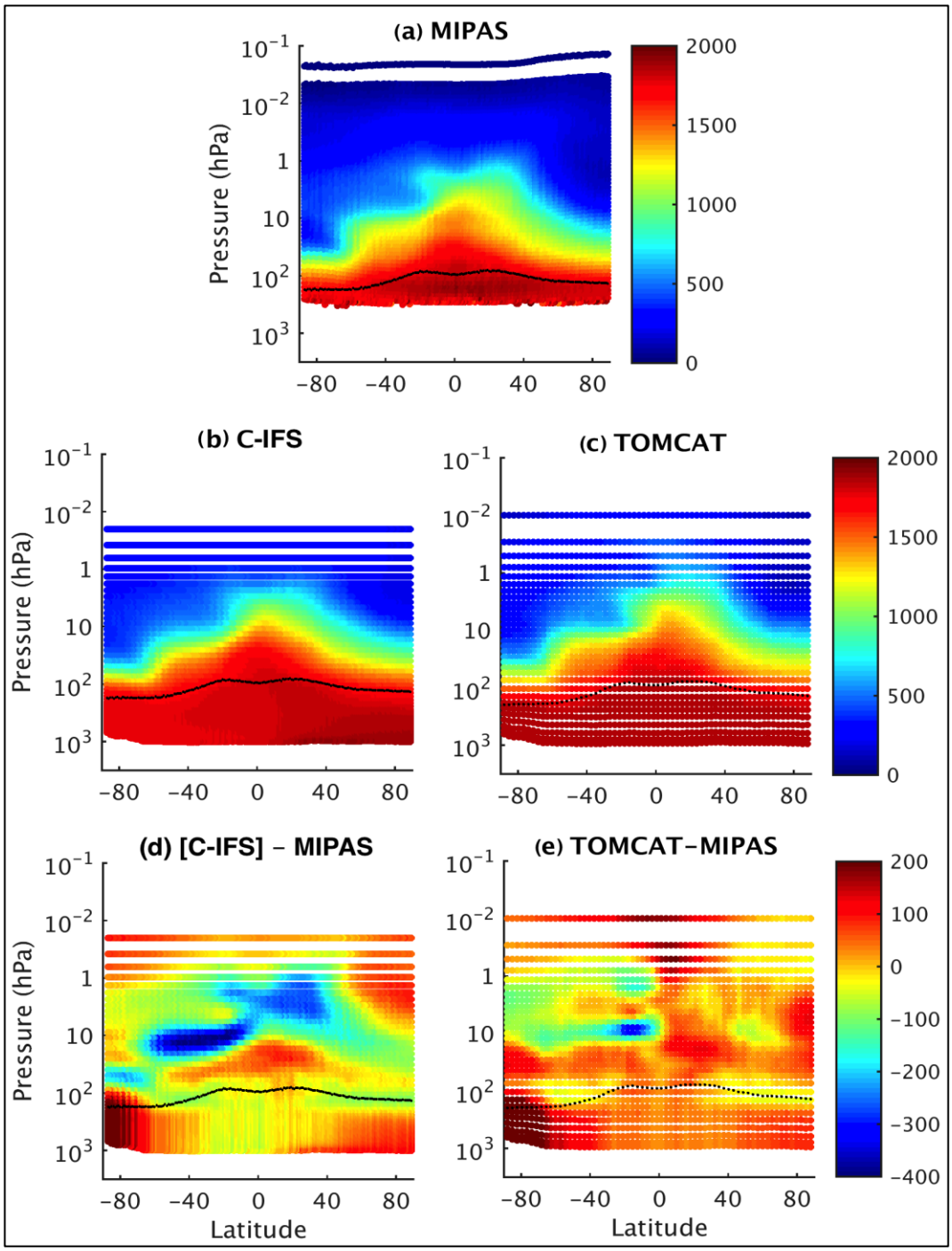

Figure 3.6: Zonal mean latitude-pressure plots of CH_4 (in ppb) for the months September to November 2010. Panel (a) shows the profiles from the MIPAS limb soundings. Panels (b) and (c) show the profiles from the C-IFS and TOMCAT models, respectively, sampled at the location and time of the MIPAS measurement. Panels (d) and (e) show the bias between the models and MIPAS measurements. The tropopause location is shown as black dots.

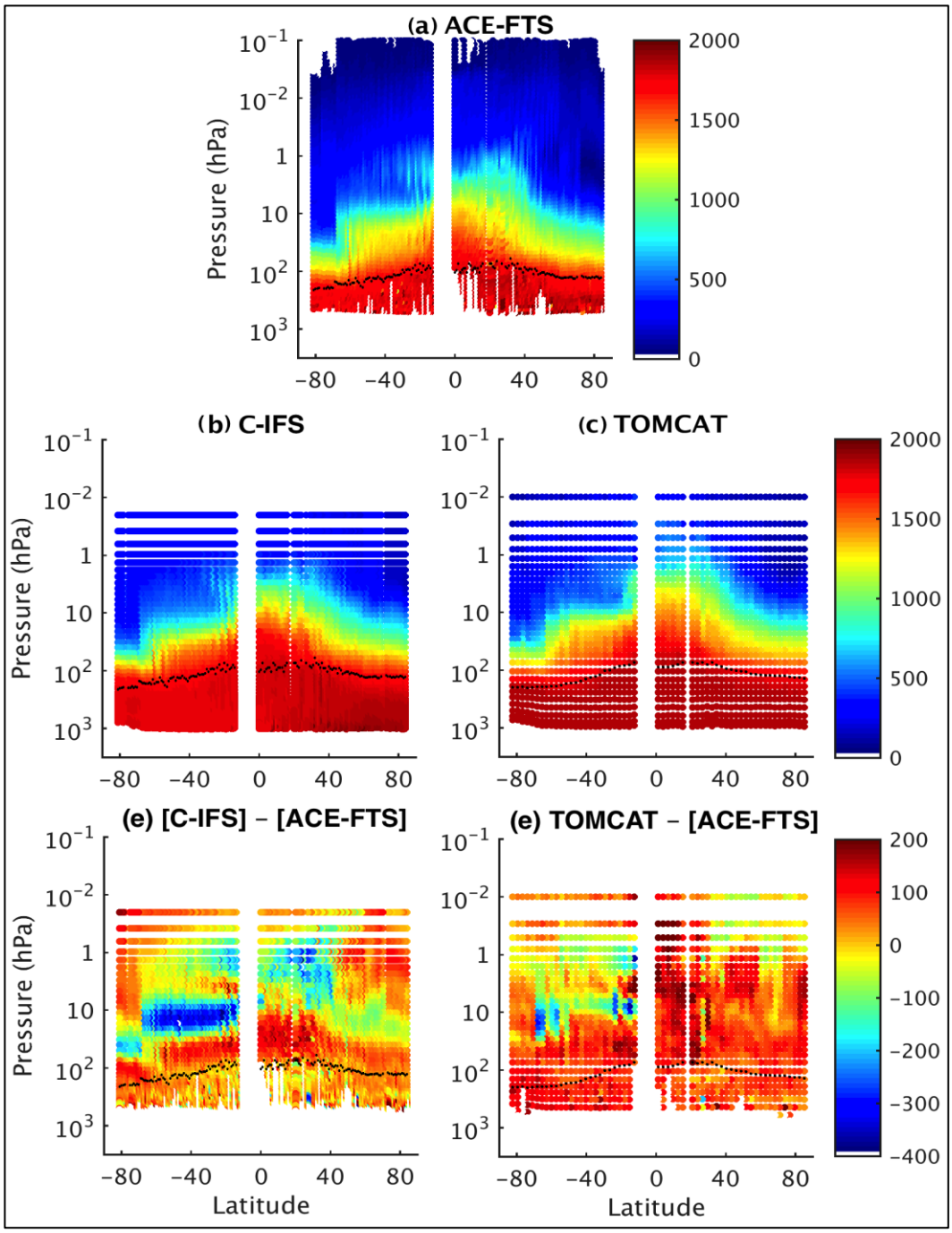

Figure 3.7: Zonal mean latitude-pressure CH_4 profiles (in ppb) for the months September to November 2010 plotted against latitude. Panel (a) shows the profiles from the ACE limb soundings. Panels (b) and (c) show the profiles from the C-IFS and TOMCAT models, respectively, sampled at the location and time of the ACE measurement. Panels (d) and (e) show the bias between the models and ACE measurement. The tropopause location is shown as black dots.

In order to further investigate the spatial patterns of the stratospheric bias, the satellite observed CH_4 concentrations and the models sampled at the locations of the satellite measurements are evaluated at a given pressure level. The 10 hPa pressure level is chosen, since the observed biases are highest around this pressure. From Fig. 3.8(c), 3.8(d) and 3.9(c), 3.9 (d), it can be seen that for both instruments, the bias in the C-IFS model forms zonal bands with little variability. Since the data density from MIPAS is much higher, these patterns are more clearly seen in Fig. 3.8. From Fig. 3.8(e) and 3.9(e) we see that the TOMCAT model bias in the middle stratosphere with reference to the two satellite instruments compare well with each other, with the highest bias during Sep-Nov 2010 being around the North Pole (~400 ppb). The spatial distribution of the bias is not quite as zonal as is seen in the C-IFS and is more irregular in structure. This difference in the bias pattern between the two models can be attributed to the fact that the TOMCAT simulation used here fails to capture the observed zonal structure of the CH_4 distribution (Fig. 3.8(c)) while the C-IFS does a much better job at simulating the longitudinal patterns (Fig. 8(b)) in the satellite data from MIPAS or ACE-FTS measurements.

A similar comparison was made for the two models for the other seasons of the year (not shown) and it was seen that these biases are a constant feature throughout the year with the magnitude and distribution being almost the same for all seasons. The CH_4 profiles from the ACE-FTS instrument and the C-IFS fields were also compared to investigate if the biases obtained by comparison with MIPAS are in agreement (Fig. 3.7). Although MIPAS has much better data coverage than ACE-FTS, with measurements made at all latitudes and the number of MIPAS profiles measured per day being significantly larger than those measured by ACE-FTS, the model bias as observed by ACE-FTS is similar in magnitude and distribution to that observed by MIPAS and the two comparisons are in good agreement with one another. The CH_4 gradient in the vertical as observed by ACE-FTS is also much shallower than that simulated by C-IFS, a feature consistent with that seen by MIPAS.

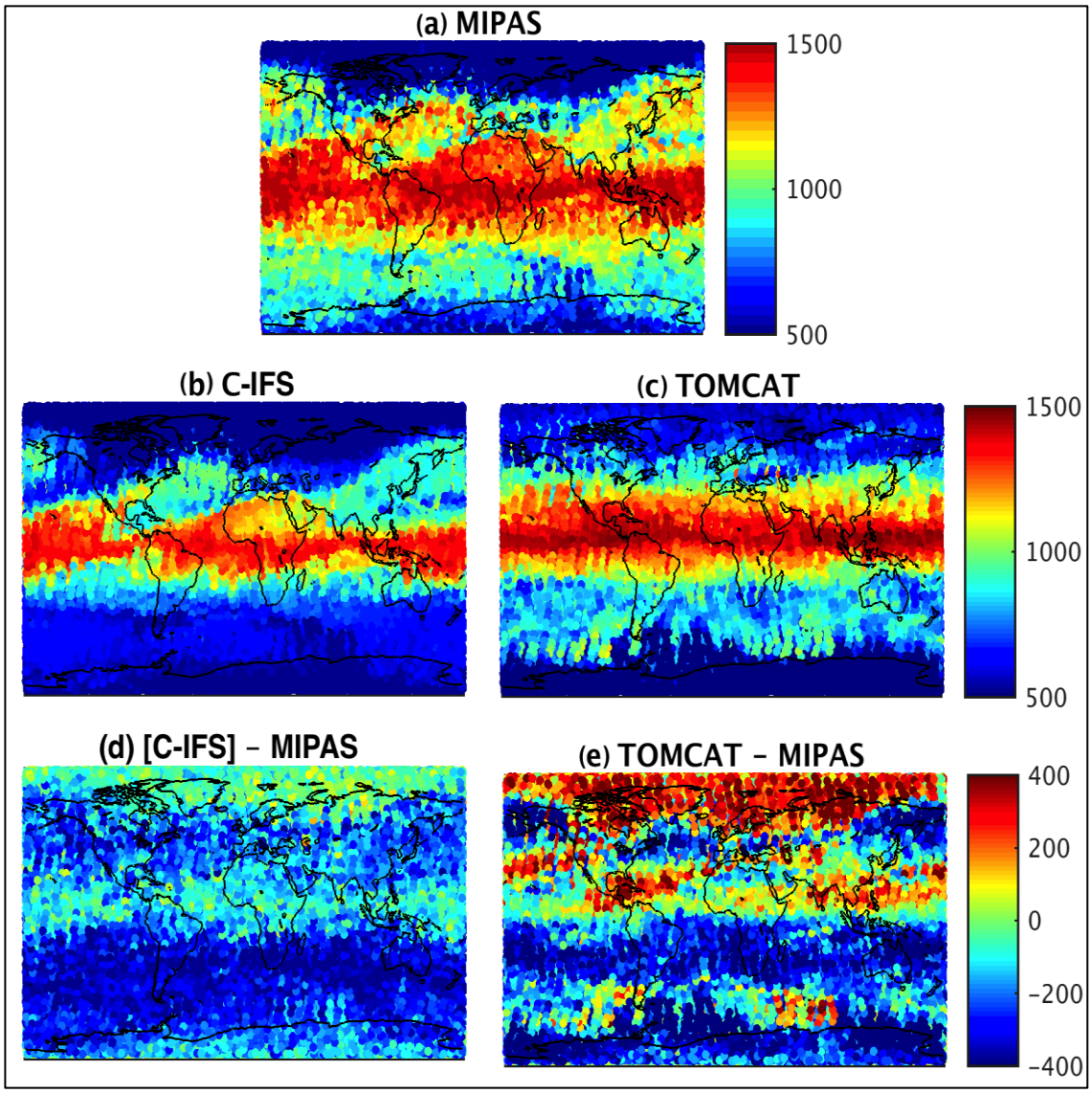

Figure 3.8: Maps showing the CH_4 concentration (in ppb) at the 10 hPa pressure level for the months September to November 2010. Panel (a) shows the CH_4 concentration as measured by MIPAS. Panels (b) and (c) show the CH_4 concentrations modeled by C-IFS and TOMCAT, respectively, sampled at the location and times of the MIPAS measurements. Panels (c) and (d) show the bias between the models and the MIPAS measurements.

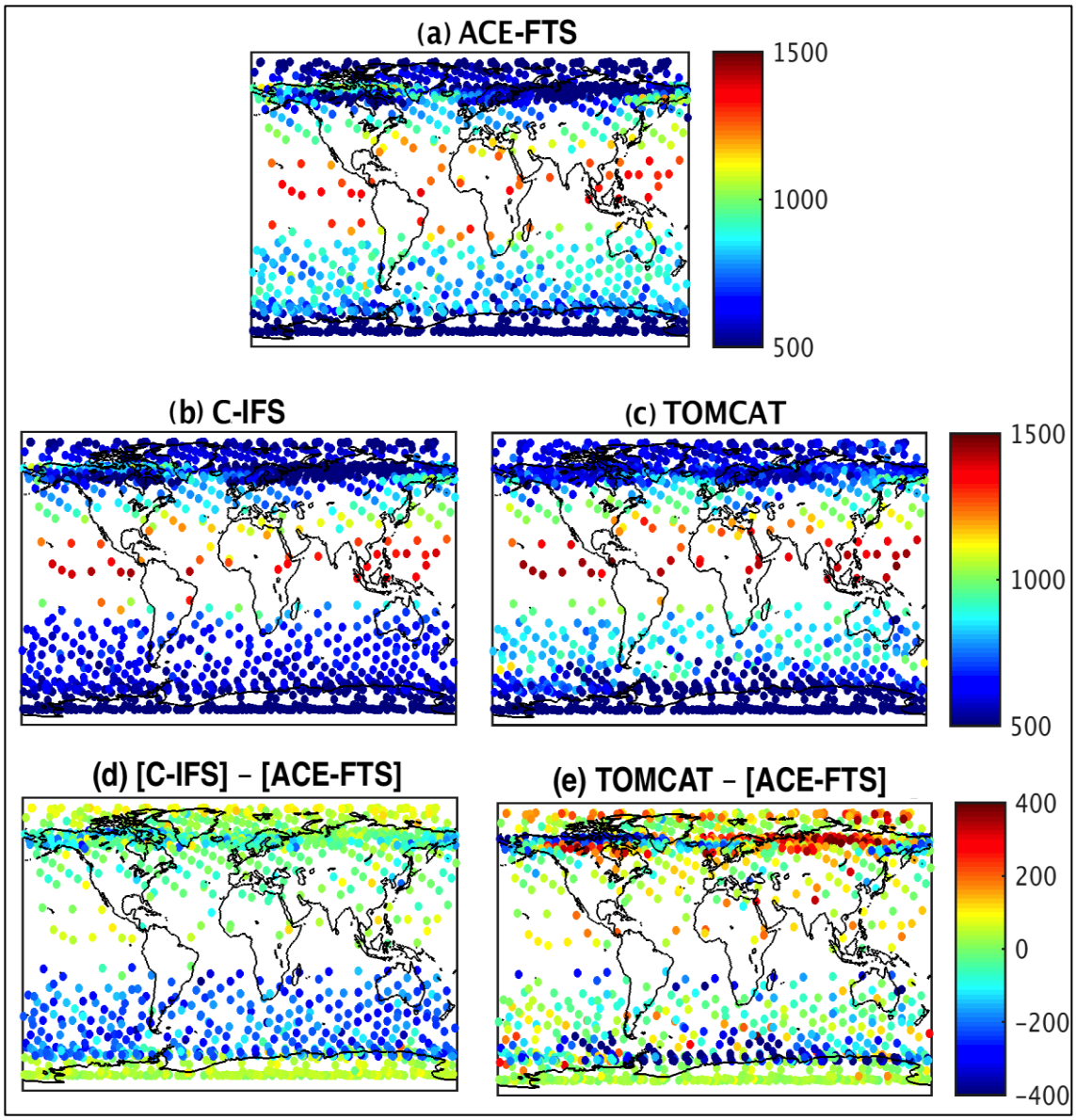

Figure 3.9: Maps showing the CH_4 concentration (in ppb) at the 10 hPa pressure level for the months September to November 2010. Panel (a) shows the CH_4 concentration as measured by ACE. Panels (b) and (c) show the CH_4 concentration modeled by the C-IFS and TOMCAT, respectively, sampled at the location and times of the MIPAS measurements. Panels (c) and (d) show the bias between the models and the ACE measurements.

Next, the column-averaged bias for the stratospheric levels in the C-IFS and TOMCAT models is computed. Comparing the bias allows us to evaluate the sources of model error in the stratospheric extension of aircraft profiles. Here, an implicit assumption that the aircraft profiles reach the altitude of the tropopause and that the entire column above the tropopause height is unmeasured and has to be extended artificially using the model data is made. The MIPAS instrument, offering the advantage of more complete global coverage over ACE-FTS, is used as the reference for the subsequent analysis of stratospheric column bias. The overall bias in the stratospheric column by carrying out a mass-weighted integration of the bias in each model with respect to the satellite soundings from MIPAS for each pressure level above the tropopause. The analysis is restricted to only those latitudes where the aircraft profiles are likely to be measured, i.e. latitudes poleward of 60^{o} S and 80^{o} N are not considered. Thus the polar regions over which no commercial aircraft are likely to fly (see Fig. 3.5) are excluded from the analysis for the purpose of this study.

Figure 3.10 shows the zonally averaged stratospheric column bias relative to MIPAS for C-IFS and TOMCAT. The overall absolute magnitude of the bias in the stratospheric column of the C-IFS is less than 15 ppb. This bias translates to less than 1 % of the total column CH_4 abundance. The bias magnitude changes with season and latitude. Overall, in the Northern Hemisphere the bias is lowest during the autumn months (SON) and highest in spring (MAM). The opposite is observed in the Southern Hemisphere. The errors in the Southern Hemisphere could be partly due to the inability of the model to capture the dynamics of the polar vortex and the extra-tropical storm track that develops in the Southern Ocean during autumn-winter months. These are associated with tropopause folds in the development of synoptic weather systems which are generally not as well captured as those in the northern hemisphere due to a sparser observing system (Bauer et al., 2015; Haiden et al., 2015). The summer and winter bias values lie intermediate to the spring and autumn bias globally. The zonal mean bias in TOMCAT has a similar seasonally- and latitudinally-varying nature as C-IFS albeit with a smaller magnitude. The bias throughout lies between ±5 ppb, which translates to 0.2 % of the total column value, which is much smaller than the C-IFS model bias. This is likely to be due to the fact that these values are averages over all longitudes and, therefore, any variation in the bias along the latitude will be smoothed out.

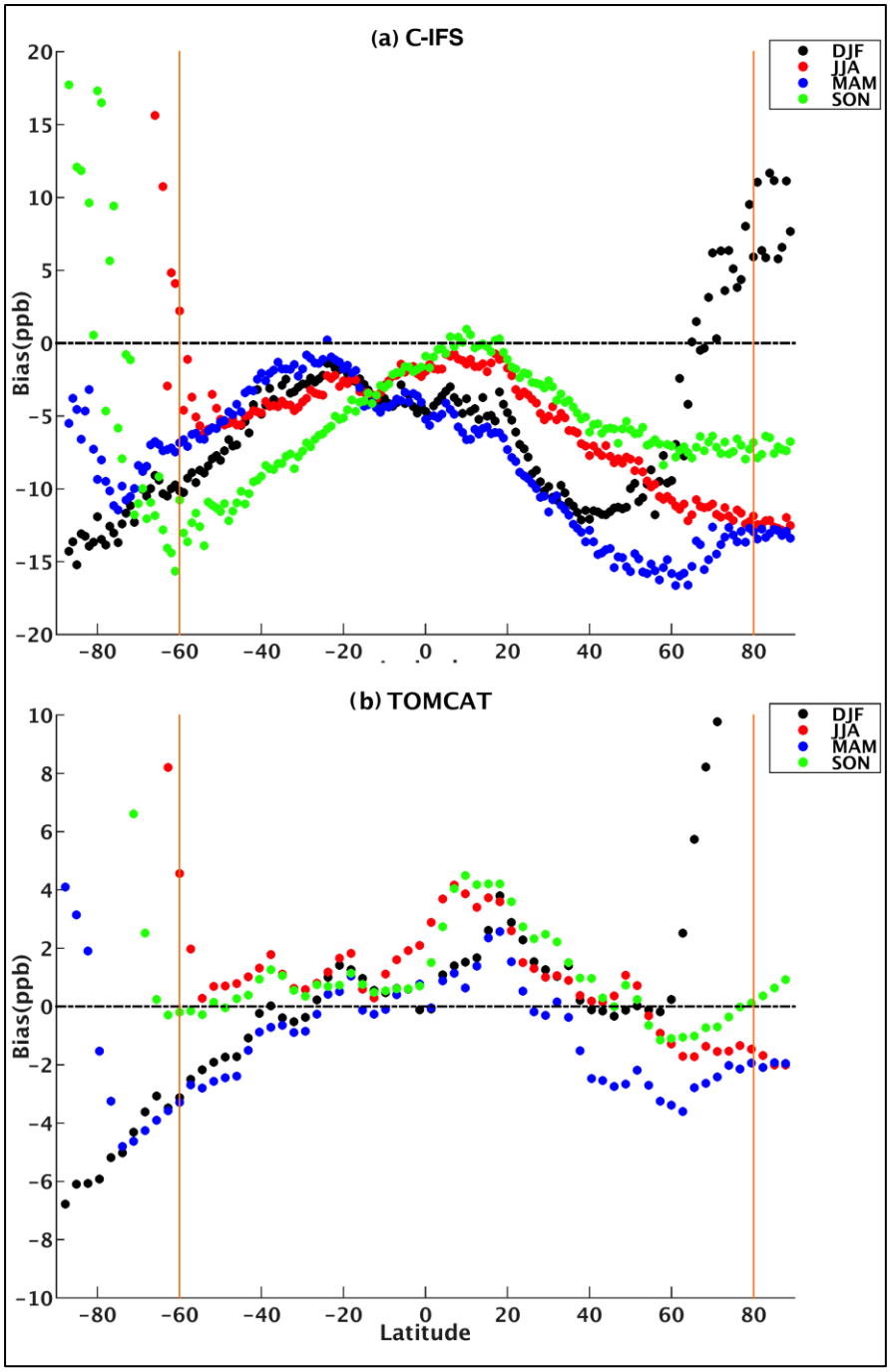

Figure 3.10: Zonal mean CH_4 stratospheric column bias for different seasons of the year 2010 plotted against latitude for the models (a) C-IFS and (b) TOMCAT. MIPAS data are used as reference truth. Note the difference in the scaling of the y-axis.

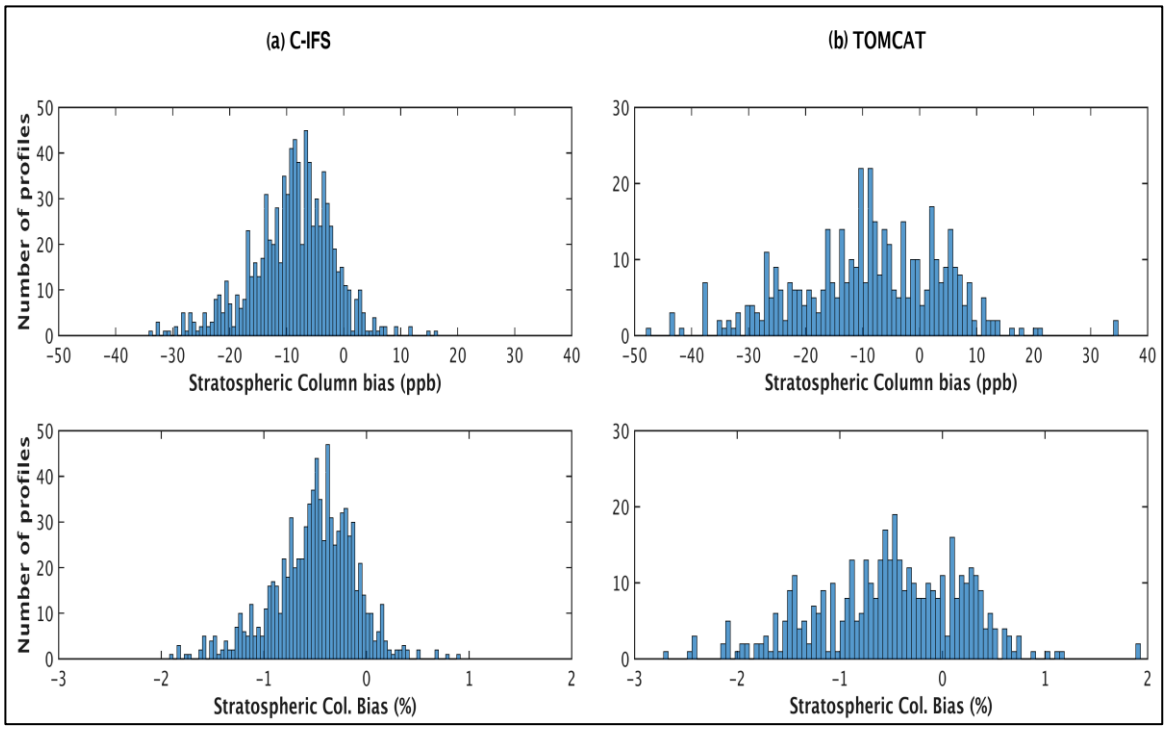

Figure 3.11: Histograms showing the distribution of the stratospheric column bias with respect to MIPAS at the MOZAIC airport locations for the year 2010 for (a) C-IFS model and (b) TOMCAT model.

In order to get a realistic estimate of the bias from both models, the stratospheric column bias is analysed at actual aircraft profile locations from the MOZAIC project. For comparison, MIPAS profiles measured on the same day as the aircraft profiles and within $\pm 2^{o}$ longitude and latitude in space are used. For real aircraft profile locations, both models have the same mean bias (about -9 ppb) in the stratosphere (Fig. 3.11, Table 3.1). The C-IFS bias however has a higher precision (standard deviation of 6.5 ppb) compared to TOMCAT (standard deviation of 12.8 ppb). As per the random error (precision) and systematic error (accuracy) requirements specified in Buchwitz et al., 2011, the errors from both models are lower than the minimum ('threshold') accuracy and precision requirements for XCH_4. In addition, the C-IFS model random error also meets the targeted precision ('goal') requirement (9 ppb).

It is noteworthy that correction of model bias prior to using the fields for completion of aircraft profiles is expected to further improve these error estimates. This is tested by applying a bias-correction to the C-IFS model output for the year 2010. Figure 3.12(a) shows the zonally averaged stratospheric column bias in the C-IFS model after application of the bias correction. The overall magnitude of the bias in the stratospheric column reduces from 15 ppb pre bias-correction to less than about 8 ppb post bias-correction. Figure 3.12(b) shows the distribution of the stratospheric column bias computed at the locations where the MOZAIC aircraft profiles are measured. The bias reduces greatly to -3.7 ppb while the random error reduces slightly to 5.7 ppb

when bias corrected model data is used.

	MEAN BIAS (ppb)	VARIABILITY (ppb)
Model output		
C-IFS	-9.0	6.5
TOMCAT	-9.1	12.8
Climatology-based approaches		
mmC-IFS	-14.2	49.0
mmC-IFS @ MIPAS	3.0	56.7
mmC-IFS @ ACE	-32.0	200.0
GOSAT a-priori profile	-14.7	53.0

Table 3.1: Mean value and variability of the stratospheric column bias due to the different stratospheric extensions at the locations of MOZAIC airports. MIPAS is taken to be the reference truth. The documented 'threshold' requirements of bias/systematic error (as a measure of accuracy) and random error (as a measure of precision) for satellite based XCH_4 to be usable for CH_4 source/sink estimation are 10 ppb and 34 ppb respectively (Buchwitz et al., 2011)

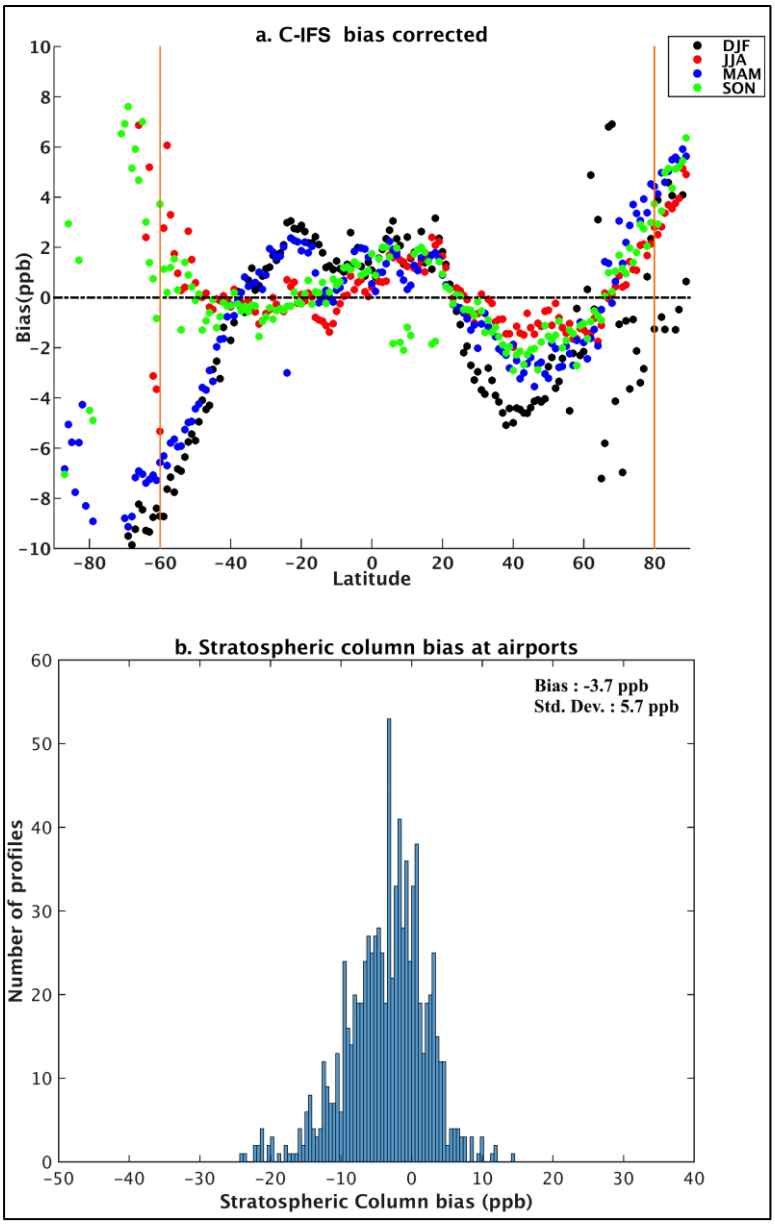

Figure 3.12: Impact of model bias correction. (a) Zonal mean CH_4 stratospheric column bias for different seasons of the year 2010 plotted against latitude. (b) Histogram showing the distribution of the stratospheric column bias in the C-IFS model at the MOZAIC airport locations. MIPAS data are used as reference truth.

3.4.3 Climatology-based approaches

The potential of climatology-based approaches as stratospheric extensions for the aircraft profiles is explored that, for instance, could be based on balloon-based measurements, satellite limb soundings or those from AirCore. Climatology based measurements are typically long term means, having a much sparser global coverage compared to global model output. For this part of the study, no real observations are used and only the contribution of sparse data coverage and temporal averaging to the stratospheric column uncertainty is evaluated. In order to do this, two main cases are analysed:

1. mmC-IFS: In this case, monthly mean C-IFS fields are used as stratospheric assumption instead of full C-IFS fields with 6-hourly output (the FULL C-IFS case). This means that synoptic scale variability in the CH_4 vertical distribution is not accounted for. This helps examine the impact of temporal variability of the data source on the stratospheric column bias.

2. In addition to the temporal variability, the impact of reduced spatial coverage of the data source for the stratosphere is tested. In order to do this, C-IFS CH_4 fields are sampled at measurement locations from two satellite instruments:
(a) mmC-IFS@ACE: Full C-IFS CH_4 fields are sampled at the ACE measurement locations, after which monthly means are obtained and interpolated to obtain global fields at CAMS resolution.
(b) mmC-IFS@MIPAS: Similar to 2(a), using sampling locations and time from the MIPAS instrument.

Comparison of the above three scenarios with the FULL C-IFS case helps draw conclusions about how well the stratospheric column can be captured with limited temporal and/or spatial coverage of the data. Since the MIPAS instrument has much better coverage than ACE, the fields obtained from mmC-IFS@MIPAS are expected to be closer to the truth (in this case FULL C-IFS) than mmC-IFS@ACE. The idea here is to not compare the two instruments but evaluate the impact of high/low data coverage in addition to reduced temporal variability. The histograms (Fig. 3.13) showing the stratospheric column bias and its variability are analysed for each of the above cases with respect to FULL C-IFS and subsequently convert these to values with MIPAS as a reference (Table 3.1). This is done by adding the bias in the FULL C-IFS with respect to MIPAS to the bias values computed for each of the scenarios. The random error or standard deviation is converted by computing the square root of the sum of the variance in the FULL C-IFS and that from each case.

The mean bias increases slightly to -14 ppb in the case where only monthly mean fields from C-IFS (mmC-IFS) are used, and increases to -32 ppb in mmC-IFS@ACE. The variability increases strongly to 49 ppb and 200 ppb for the two cases. In mmC-IFS@MIPAS, the mean reduces to 3 ppb, which is better than the mean bias in the FULL C-IFS (-9 ppb). However, since the variability in the stratospheric column error

is still about 10 times larger than that of the FULL C-IFS (around 57 ppb), it cannot be deemed fit for estimating the stratosphere well. As expected mmC-IFS@ACE performs poorly as compared to mmC-IFS@MIPAS both in terms of the bias and variability, owing to the fact that the monthly sampling from ACE is much sparser than that of MIPAS.

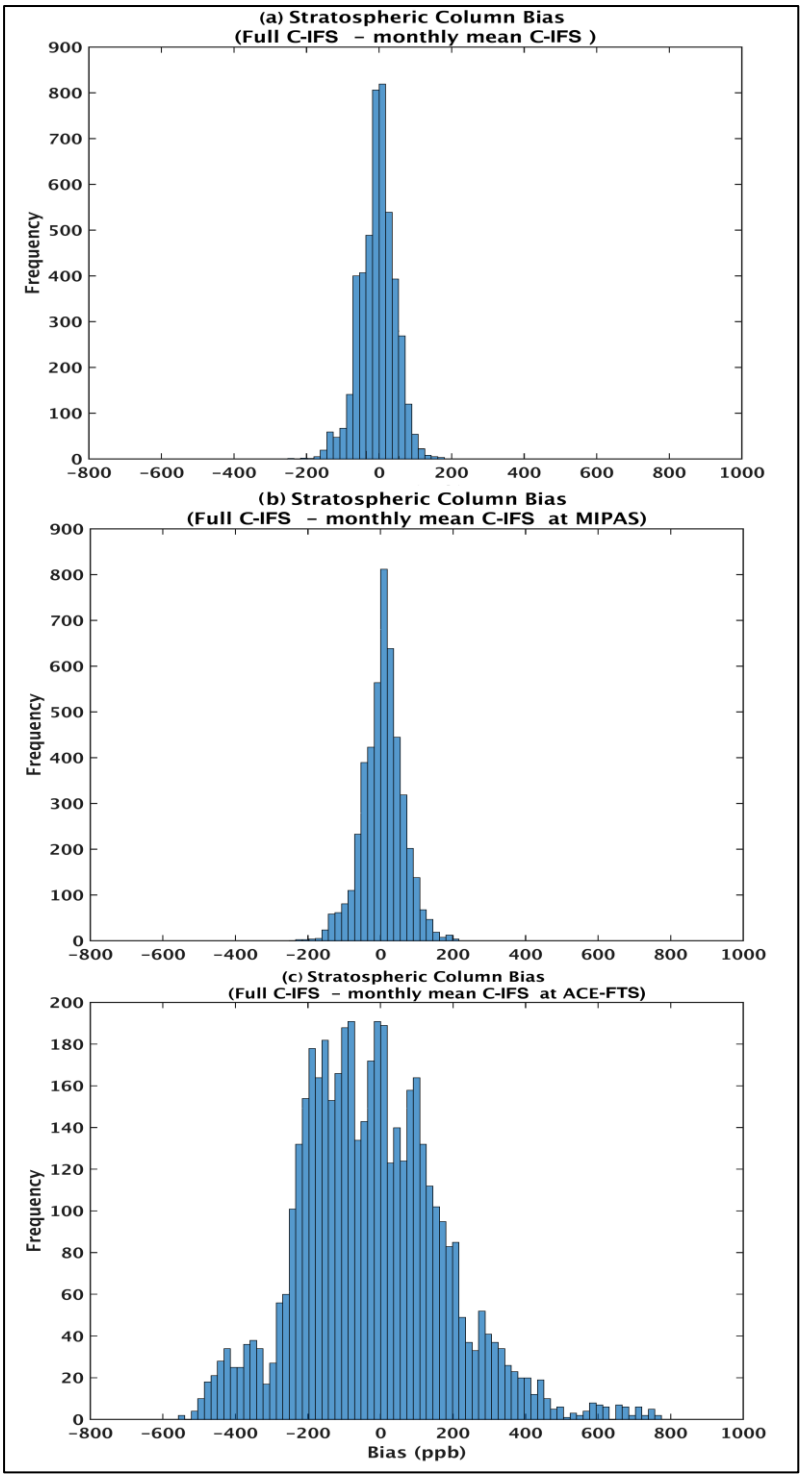

Figure 3.13: Distribution of the stratospheric column bias estimated at the location of the MOZAIC airports and using FULL C-IFS as the reference truth. Panel (a) shows the bias when monthly mean fields from the C-IFS model are used for profile extension. Panels (b) and (c) depict the bias when monthly mean fields from the C-IFS model obtained using the sampling from the MIPAS and ACE instruments are used for profile extension, respectively.

3.4.4 Satellite a-priori profile

Finally, the possibility of using a priori profiles used in satellite data retrievals to extend aircraft profiles into the stratosphere is evaluated. For this, the University of Leicester GOSAT Proxy XCH_4 retrieval (Parker et al., 2011) is used. The CH_4 a-priori profile in this retrieval is based on the TM3 transport model run. Figure 3.14 shows the distribution of the stratospheric column bias at the MOZAIC airport locations, with respect to collocated MIPAS CH_4 profiles. The mean error in the stratospheric column is about -14.7 ppb while the random error amounts to 53 ppb (Table 3.1). These values are comparable to those obtained from the mmC-IFS case in Sect. 3.4 but are still much higher than the bias and random error obtained from the C-IFS and TOMCAT models.

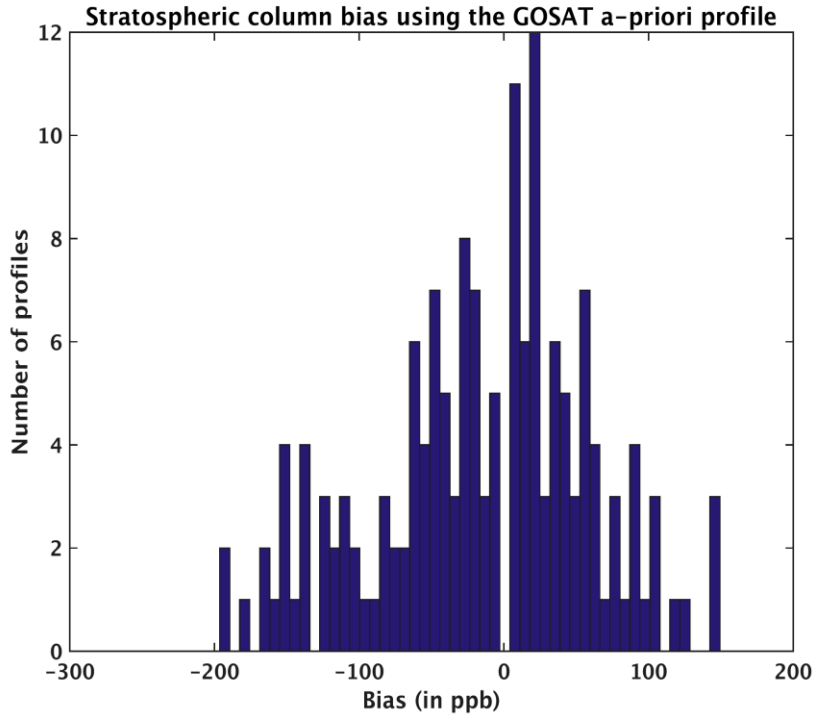

Figure 3.14: Stratospheric column error estimated at the MOZAIC airport locations when the GOSAT CH_4 a-priori profile is used for aircraft profile extension. MIPAS data are taken as reference truth.

3.5 Discussion and conclusions

The suitability of airborne measurements as reference data for the validation of satellite based total column measurements is well documented. Previous studies have shown that the unsampled part of the atmosphere above the aircraft ceiling contributes the largest uncertainty in the total column computed from aircraft profiles (Wunch et al., 2010). In this study, different stratospheric CH_4 data sources that can be used for the purpose of aircraft profile extension by comparing the bias each data source introduces in the total column are analysed. For realistic bias estimation, the value of the bias is computed at the location of the MOZAIC airports.

The results show that the C-IFS and TOMCAT models have smaller biases and standard deviation values of the stratospheric column error at the airport locations than those computed using scenarios that simulate the use of climatology datasets and the satellite a-priori profile. While the bias from both the models in the stratosphere is about -9 ppb, the random error in the C-IFS is smaller in magnitude (6.5 ppb) than that from the TOMCAT model (12.8 ppb). These values are within the minimum requirements for total column CH_4 retrievals from satellites as specified in Buchwitz et al., (2011). The error from the C-IFS model, additionally meets the 'goal' or targeted requirement. Application of latitudinal and seasonal bias correction to the model fields is likely to produce even better results. It is to be kept in mind that while both models seem to be performing equally well in the stratosphere there are significant differences in the datasets from the two models in terms of how they are generated. The C-IFS is a data assimilation model that simulates tropospheric CH_4 in detail. However, since the model initial conditions are constrained by the assimilated observations for NWP, its use could be circular. In addition, the stratospheric chemistry used in the model is parameterized. On the other hand, TOMCAT is a chemical transport model that is driven by the ERA-interim meteorology. The treatment of tropospheric CH_4, however, is simplified in the model. The TOMCAT model improves over the C-IFS model due to the realistic treatment of stratospheric sinks, which is reflected in the lower mid-stratospheric bias (-100 to -200 ppb) in comparison to the C-IFS analysis (200 to 300 ppb). In other words the TOMCAT results show that ongoing developments to include a more realistic implementation of stratospheric chemistry in C-IFS should improve the bias relative to the satellite observations. In addition, the C-IFS model output used here is at a higher horizontal resolution than TOMCAT (approximately 0.8° compared to 2.8°), which is also likely to impact the bias. This can be improved by running the TOMCAT model in a different configuration. It is worth mentioning that since the C-IFS is optimised in the troposphere, unlike the TOMCAT simulation used here, it can also be used as reliable extension for any tropospheric levels that are not measured by the aircraft.

In order to simulate using a climatology, the impact of reduced synoptic scale variability and spatial coverage of the data source used for stratospheric extension is investigated. It is found that the spatial coverage of the data source impacts the bias

greatly, as is clear in the case of mmC-IFS@ACE-FTS (-32 ppb bias, 200 ppb standard deviation) as compared to mmC-IFS@MIPAS (3 ppb bias and 56.7 ppb standard deviation) since the ACE-FTS instrument has poorer spatial coverage compared to the nearly global coverage by MIPAS. It should be noted that the evaluation of the MIPAS and ACE-FTS instruments in this section is only a theoretical exercise to evaluate the influence of spatial sampling and coverage in estimating the bias. In any case, the MIPAS instrument is no longer operational and cannot be used as a potential stratospheric extension data source while ACE-FTS, though currently operational, might not work for much longer (SCISAT-1 has long surpassed its expected lifetime of two years). Hence, other limb sounding instruments measuring trace gas profiles in the UTLS region are needed in the coming years. This analysis also highlights the shortfalls of any climatology based on sparse profile measurements such as those from balloons or AirCore. Lastly, on using the GOSAT a- priori profile for profile extension, the resulting stratospheric uncertainty is comparable to the case where monthly mean C-IFS fields are used. However, the random error in this case is much higher than the case where full fields from the C-IFS model are used making the a-priori profile a less favourable option among other data sources considered in this work.

In summary, this work offers insights into the different data sources that can be used for the purpose of completing the "missing" part of the CH_4 profile from aircraft when using these profiles for satellite validation. Using bias-corrected model fields are likely to produce the best results in the stratosphere for methane. In-situ profiles from balloon borne AirCore measurements can prove to be very useful in this regard. These profiles extend up to an altitude of about 30 km and can be good sources of reference data for model validation and bias correction in the UTLS regions. Thus, this study offers solutions to the main limitation of using altitude-limited aircraft-based greenhouse gas profiles for validating satellite based total column data. Besides having great potential for providing robust validation methodologies of remote sensing observations and atmospheric models, these measurements have applications in NWP (e.g. in bias correction schemes or for data assimilation) as explored by the CAMS system providing for an integrated global observing system and deeper insights into the chemical and physical processes in the atmosphere.

3.6 References

Bauer, P., Thorpe, A., & Brunet, G.: The quiet revolution of numerical weather prediction. Nature, 525(7567), 47–55. doi:10.1038/nature14956, 2015.

Bergamaschi, P., Frankenberg, C., Meirink, J. F., Krol, M., Villani, M. G., Houweling, S., Dentener, F., Dlugokencky, E. J., Miller, J. B., Gatti, L. V., Engel, A. and Levin, I.: Inverse modeling of global and regional CH_4 emissions using SCIAMACHY satellite retrievals, J. Geophys. Res., 114(D22), D22301, doi:10.1029/2009JD012287, 2009.

Bernath, P. F.: Atmospheric Chemistry Experiment (ACE): Mission overview, Geophys. Res. Lett., 32(15), L15S01, doi:10.1029/2005GL022386, 2005.

Boone, C. D., Nassar, R., Walker, K. a, Rochon, Y., McLeod, S. D., Rinsland, C. P. and Bernath, P. F.: Retrievals for the atmospheric chemistry experiment Fourier-transform spectrometer., Appl. Opt., 44, 7218–7231, doi:10.1364/AO.44.007218, 2005.

Buchwitz, M., F. Chevallier, P. Bergamaschi, I. Aben, H. Bösch, O. Hasekamp, J. Notholt, M. Reuter, et al., User Requirements Document for the GHG-CCI project of ESA's Climate Change Initiative, pp. 45, version 1, 3. February 2011.

Butz, A., Hasekamp O. P., Frankenberg, C., Vidot J., Aben I. : CH4 retrievals from space-based solar backscatter measurements: Performance evaluation against simulated aerosol and cirrus loaded scenes, J. Geophys. Res., 115, D24302, doi:10.1029/2010JD014514, 2010

Chauhan, S., Höpfner, M., Stiller, G. P., von Clarmann, T., Funke, B., Glatthor, N., Grabowski, U., Linden, A., Kellmann, S., Milz, M., Steck, T., Fischer, H., Froidevaux, L., Lambert, A., Santee, M. L., Schwartz, M., Read, W. G., and Livesey, N. J.: MIPAS reduced spectral resolution UTLS-1 mode measurements of temperature, O_3, HNO_3, N_2O, H_2O and relative humidity over ice: retrievals and comparison to MLS, Atmos. Meas. Tech., 2, 337–353, doi:10.5194/amt-2-337-2009, 2009

Chipperfield, M. P., Cariolle, D., Simon, P., Ramarosom, R. and Lary, D. J.: A 3-dimensional modeling study of trace species in the arctic lower stratosphere during winter 1989-1990, J. Geophys. Res., 98(D4), 7199–7218, 1993.

Chipperfield, M. P.: Multiannual simulations with a three-dimensional chemical transport model, J. Geophys. Res., 104(D1), 1781–1805, doi:10.1029/98JD02597, 1999.

Chipperfield, M. P.: New version of the TOMCAT/SLIMCAT off-line chemical transport model: Intercomparison of stratospheric tracer experiments, Q. J. R. Meteorol. Soc., 132(617), 1179–1203, doi:10.1256/qj.05.51, 2006.

Chipperfield, M.P., S.S. Dhomse, W. Feng, R.L. McKenzie, G. Velders and J.A. Pyle, Quantifying the ozone and UV benefits already achieved by the Montreal Protocol, Nature Communications, 6, 7233, doi:10.1038/ncomms8233, 2015.

De Laat, A. T. J., Dijkstra, R., Schrijver, H., Nédélec, P., and Aben, I.: Validation of six years of SCIAMACHY carbon monoxide observations using MOZAIC CO profile measurements, Atmos. Meas. Tech., 5, 2133-2142, doi:10.5194/amt-5-2133-2012, 2012.

De Laat, A. T. J., Aben, I., Deeter, M., Nédélec, P., Eskes, H., Attié, J. L., Ricaud, P., Abida, R., El Amraoui, L. and Landgraf, J.: Validation of nine years of MOPITT V5 NIR using MOZAIC/IAGOS measurements: Biases and long-term stability, Atmos.Meas. Tech., 7(11), 3783–3799, doi:10.5194/amt-7-3783-2014, 2014.

Fischer, H., Birk, M., Blom, C., Carli, B., Carlotti, M., von Clarmann, T., Delbouille, L., Dudhia, A., Ehhalt, D., Endemann, M., Flaud, J. M., Gessner, R., Kleinert, A., Koopman, R., Langen, J., López-Puertas, M., Mosner, P., Nett, H., Oelhaf, H., Perron, G., Remedios, J., Ridolfi, M., Stiller, G., and Zander, R.: MIPAS: an instrument for atmospheric and climate research, Atmos. Chem. Phys., 8, 2151-2188, doi:10.5194/acp-8-2151-2008, 2008.

Flemming, J., Huijnen, V., Arteta, J., Bechtold, P., Beljaars, A., Blechschmidt, A.-M., Diamantakis, M., Engelen, R. J., Gaudel, A., Inness, A., Jones, L., Josse, B., Katragkou, E., Marecal, V., Peuch, V.-H., Richter, A., Schultz, M. G., Stein, O., and Tsikerdekis, A.: Tropospheric chemistry in the Integrated Forecasting System of ECMWF, Geosci. Model Dev., 8, 975-1003, doi:10.5194/gmd-8-975-2015, 2015.

Geibel, M. C., Messerschmidt, J., Gerbig, C., Blumenstock, T., Chen, H., Hase, F., Kolle, O., Lavrič, J. V., Notholt, J., Palm, M., Rettinger, M., Schmidt, M., Sussmann, R., Warneke, T., and Feist, D. G.: Calibration of column-averaged CH_4 over European TCCON FTS sites with airborne in-situ measurements, Atmos. Chem. Phys., 12, 8763-8775, doi:10.5194/acp-12-8763-2012, 2012.

Glatthor, N., von Clarmann, T., Fischer, H., Funke, B., Grabowski, U., Höpfner, M., Kellmann, S., Kiefer, M., Linden, A., Milz, M., Steck, T., Stiller, G. P., Mengistu Tsidu, G., and Wang, D. Y.: Mixing processes during the Antarctic vortex split in September/October 2002 as inferred from source gas and ozone distributions from ENVISAT-MIPAS, J. Atmos. Sci., 62, 787–800, 2005.

Haiden, T., et al. Evaluation of ECMWF forecasts, including 2014-2015 upgrades. Technical Report 765, ECMWF, 2015.

Inoue, M., Morino, I., Uchino, O., Miyamoto, Y., Yoshida, Y., Yokota, T., Machida, T., Sawa, Y., Matsueda, H., Sweeney, C., Tans, P. P., Andrews, A. E., Biraud, S. C., Tanaka, T., Kawakami, S., and Patra, P. K.: Validation of XCO_2 derived from SWIR spectra of GOSAT TANSO-FTS with aircraft measurement data, Atmos. Chem. Phys., 13, 9771-9788, doi:10.5194/acp-13-9771-2013, 2013.

Inoue, M., Morino, I., Uchino, O., Miyamoto, Y., Saeki, T., Yoshida, Y., Yokota, T., Sweeney, C., Tans, P. P., Biraud, S. C., Machida, T., Pittman, J. V., Kort, E. A., Tanaka, T., Kawakami, S., Sawa, Y., Tsuboi, K., and Matsueda, H.: Validation of XCH_4 derived from SWIR spectra of GOSAT TANSO-FTS with aircraft measurement data, Atmos. Meas. Tech., 7, 2987-3005, doi:10.5194/amt-7-2987-2014, 2014.

Inoue, M., Morino, I., Uchino, O., Nakatsuru, T., Yoshida, Y., Yokota, T., Wunch, D., Wennberg, P. O., Roehl, C. M., Griffith, D. W. T., Velazco, V. A., Deutscher, N. M., Warneke, T., Notholt, J., Robinson, J., Sherlock, V., Hase, F., Blumenstock, T., Rettinger, M., Sussmann, R., Kyrö, E., Kivi, R., Shiomi, K., Kawakami, S., De Mazière, M., Arnold, S. G., Feist, D. G., Barrow, E. A., Barney, J., Dubey, M., Schneider, M., Iraci, L., Podolske, J. R., Hillyard, P., Machida, T., Sawa, Y., Tsuboi, K., Matsueda, H., Sweeney, C., Tans, P. P., Andrews, A. E., Biraud, S. C., Fukuyama, Y., Pittman, J. V., Kort, E. A., and Tanaka, T.: Bias corrections of GOSAT SWIR XCO_2 and XCH_4 with TCCON data and their evaluation using aircraft measurement data, Atmos. Meas. Tech. Discuss., doi:10.5194/amt-2015-366, in review, 2016.

Janssens-Maenhout, G., Dentener, F., Aardenne, J. Van, Monni, S., Pagliari, V., Orlandini, L., Klimont, Z., Kurokawa, J., Akimoto, H., Ohara, T., Wankmüller, R., Battye, B., Grano, D., Zuber, A. and Keating, T.: EDGAR-HTAP: a harmonized gridded air pollution emission dataset based on national inventories., 2012.

Karion, A., Sweeney, C., Tans, P. and Newberger, T.: AirCore: An innovative atmospheric sampling system, J. Atmos. Ocean. Technol., 27(11), 1839–1853, doi:10.1175/2010JTECHA1448.1, 2010.

Kaiser, J. W., Heil, A., Andreae, M. O., Benedetti, A., Chubarova, N., Jones, L., Morcrette, J.-J., Razinger, M., Schultz, M. G., Suttie, M., and van der Werf, G. R.: Biomass burning emissions estimated with a global fire assimilation sys- tem based on observed fire radiative power, Biogeosciences, 9, 527–554, doi:10.5194/bg-9-527-2012, 2012.

Krol, M., Houweling, S., Bregman, B., van den Broek, M., Segers, A., van Velthoven, P., Peters, W., Dentener, F., and Berga- maschi, P.: The two-way nested global chemistry-transport zoom model TM5: algorithm and applications, Atmos. Chem. Phys., 5, 417–432, doi:10.5194 /acp-5-417-2005, 2005.

Laeng, A., Plieninger, J., von Clarmann, T., Grabowski, U., Stiller, G., Eckert, E., Glatthor, N., Haenel, F., Kellmann, S., Kiefer, M., Linden, A., Lossow, S., Deaver, L., Engel, A., Hervig, M., Levin, I., McHugh, M., Noël, S., Toon, G., and Walker, K.: Validation of MIPAS IMK/IAA methane profiles, Atmos. Meas. Tech., 8, 5251-5261, doi:10.5194/amt-8-5251-2015, 2015.

Massart, S., Agusti-Panareda, A., Aben, I., Butz, A., Chevallier, F., Crevoisier, C., Engelen, R., Frankenberg, C., and Hasekamp, O.: Assimilation of atmospheric methane products into the MACC-II system: from SCIAMACHY to TANSO and IASI, Atmos. Chem. Phys., 14, 6139-6158, doi:10.5194/acp-14-6139-2014, 2014.

Miller, C. E., Crisp, D., DeCola, P. L., Olsen, S. C., Randerson, J. T., Michalak, A. M., Alkhaled, A., Rayner, P., Jacob, D. J., Suntharalingam, P., Jones, D. B. A., Denning, A. S., Nicholls, M. E., Doney, S. C., Pawson, S., Boesch, H., Connor, B. J., Fung, I. Y., O'Brien, D., Salawitch, R. J., Sander, S. P., Sen, B., Tans, P., Toon, G. C., Wennberg, P. O., Wofsy, S. C., Yung, Y. L. and Law, R. M.: Precision requirements for space-based XCO_2 data, J. Geophys. Res. Atmos., 112(10), doi:10.1029/2006JD007659, 2007.

Miyamoto, Y., Inoue, M., Morino, I., Uchino, O., Yokota, T., Machida, T., Sawa, Y., Matsueda, H., Sweeney, C., Tans, P. P., Andrews, A. E., and Patra, P. K.: Atmospheric column-averaged mole fractions of carbon dioxide at 53 aircraft measurement sites, Atmos. Chem. Phys., 13, 5265-5275, doi:10.5194/acp-13-5265-2013, 2013.

Marenco, A., Thouret, V., Nédélec, P., Smit, H., Helten, M., Kley, D., Karcher, F., Simon, P., Law, K. and Pyle, J.: Measurement of ozone and water vapor by Airbus in‐service aircraft: The MOZAIC airborne program, An overview, Journal of Geophysical Research: Atmospheres (1984–2012), 103(D19), 25631–25642, 1998.

Monks, S.A., S.R. Arnold and M.P. Chipperfield, Evidence for El Nino-Southern Oscillation (ENSO) influence on Arctic CO interannual variability through biomass burning emissions, Geophys. Res. Lett., 39, L14804, doi:10.1029/2012GL052512, 2012.

Parker, R., Boesch, H., Cogan, A., Fraser, A., Feng, L., Palmer, P. I., Messerschmidt, J., Deutscher, N., Griffith, D. W. T., Notholt, J., Wennberg, P. O. and Wunch, D.: Methane observations from the Greenhouse Gases Observing SATellite: Comparison to ground-based TCCON data and model calculations, Geophys. Res. Lett., 38(15), doi:10.1029/2011GL047871, 2011.

Petzold, A., Thouret, V., Gerbig, C., Zahn, A., Brenninkmeijer, C. A. M., Gallagher, M., Hermann, M., Pontaud, M., Ziereis, H., Boulanger, D., Marshall, J., Nédélec, P., Smit, H. G. J., Friess, U., Flaud, J.-M., Wahner, A., Cammas, J.-P. and Volz-Thomas, A.: Global-scale atmosphere monitoring by in-service aircraft – current achievements and future prospects of the European Research Infrastructure IAGOS, Tellus B, 67(0), 13801, doi:10.5194/acp-7-4953-2007, 2015.

Plieninger, J., von Clarmann, T., Stiller, G. P., Grabowski, U., Glatthor, N., Kellmann, S., Linden, A., Haenel, F., Kiefer, M., Höpfner, M., Laeng, A., and Lossow, S.: Methane and nitrous oxide retrievals from MIPAS-ENVISAT, Atmos. Meas. Tech., 8, 4657-4670, doi:10.5194/amt-8-4657-2015, 2015.

Plieninger, J., Laeng, A., Lossow, S., von Clarmann, T., Stiller, G. P., Kellmann, S., Linden, A., Kiefer, M., Walker, K. A., Noël, S., Hervig, M. E., McHugh, M., Lambert, A., Urban, J., Elkins, J. W., and Murtagh, D.: Validation of revised methane and nitrous oxide profiles from MIPAS–ENVISAT, Atmos. Meas. Tech., 9, 765-779, doi:10.5194/amt-9-765-2016, 2016.

Prather, M. J.: Numerical advection by conservation of second-order moments, J. Geophys. Res., 91, 6671–6681, doi:10.1029/JD091iD06p06671, 1986.

Rabier, F., Järvinen, H., Klinker, E., Mahfouf, J.-F. and Simmons, A.: The ECMWF operational implementation of four-dimensional variational assimilation. I: Experimental results with simplified physics. Q.J.R. Meteorol. Soc., 126, 1143–1170. doi: 10.1002/qj.49712656415, 2010.

Raspollini, P., Belotti, C., Burgess, A., Carli, B., Carlotti, M., Ceccherini, S., Dinelli, B. M., Dudhia, A., Flaud, J.-M., Funke, B., Höpfner, M., López-Puertas, M., Payne, V., Piccolo, C., Remedios, J. J., Ridolfi, M., and Spang, R.: MIPAS level 2 operational analysis, Atmos. Chem. Phys., 6, 5605-5630, doi:10.5194/acp-6-5605-2006, 2006.

Rayner, P. J. and O'Brien, D. M.: The utility of remotely sensed CO_2 concentration data in surface source inversions, Geophys. Res. Lett., 28(1), 175–178, doi:10.1029/2000GL011912, 2001.

Richards, N.A.D., S.R. Arnold, M.P. Chipperfield, G. Miles, A. Rap, R. Siddans, S.A. Monks and M.J. Hollaway, The Mediterranean summertime ozone maximum: global emission sensitivities and radiative impacts, Atmos. Chem. Phys., 13, 2331-2345, doi:10.5194/acp-13-2331-2013, 2013.

Ridolfi, M., Ceccherini, S., Raspollini, P., and Niemeijer, S.: Technical note: Use of mipas vertical averaging kernels in validation activities. Technical report, Dipartimento di Fisica, Universita di Bologna (Italy), 2011

Stockwell, D.Z., C. Giannakopoulos, P.H. Plantevin, G.D. Carver, M.P. Chipperfield, K.S. Law, J.A. Pyle, D.E. Shallcross and K.Y. Wang, Modelling NO_x from lightning and its impact on global chemical fields, Atmospheric Environment, 33, 4477-4493, doi:10.1016/S1352-2310(99)00190-9, 1999.

Tiedtke, M.: A comprehensive mass flux scheme for cumulus parameterization in large-scale models, Mon. Weather Rev., 117(8), 1179–1800, doi:10.1175/1520-0493(1989)117<1779:ACMFSF>2.0.CO;2, 1989.

von Clarmann, T., Höpfner, M., Kellmann, S., Linden, A., Chauhan, S., Funke, B., Grabowski, U., Glatthor, N., Kiefer, M., Schieferdecker, T., Stiller, G. P., and Versick, S.: Retrieval of temperature, H_2O, O_3, HNO_3, CH_4, N_2O, $ClONO_2$ and ClO from MIPAS reduced resolution nominal mode limb emission measurements, Atmos. Meas. Tech., 2, 159-175, doi:10.5194/amt-2-159-2009, 2009.

Wunch, D., Toon, G. C., Wennberg, P. O., Wofsy, S. C., Stephens, B. B., Fischer, M. L., Uchino, O., Abshire, J. B., Bernath, P., Biraud, S. C., Blavier, J. F. L., Boone, C., Bowman, K. P., Browell, E. V., Campos, T., Connor, B. J., Daube, B. C., Deutscher, N. M., Diao, M., Elkins, J. W., Gerbig, C., Gottlieb, E., Griffith, D. W. T., Hurst, D. F., Jiménez, R., Keppel-Aleks, G., Kort, E. A., MacAtangay, R., MacHida, T., Matsueda, H., Moore, F., Morino, I., Park, S., Robinson, J., Roehl, C. M., Sawa, Y., Sherlock, V., Sweeney, C., Tanaka, T. and Zondlo, M. A.: Calibration of the total

carbon column observing network using aircraft profile data, Atmos. Meas. Tech., 3(5), 1351–1362, doi:10.5194/amt-3-1351-2010, 2010.

Wunch, D., Toon, G. C., Blavier, J. F. L., Washenfelder, R. A., Notholt, J., Connor, B. J., Griffith, D. W. T., Sherlock, V. and Wennberg, P. O., The Total Carbon Column Observing Network, Philosophical Transactions of the Royal Society A: Mathematical, Physical and Engineering Sciences, 369(1943), 2087–2112, doi:10.1098/rsta.2010.0240, 2011.

Yokota, T., Yoshida, Y., Eguchi, N., Ota, Y., Tanaka, T., Watanabe, H. and Maksyutov, S.: Global Concentrations of CO_2 and CH_4 Retrieved from GOSAT: First Preliminary Results, Sola, 5, 160–163, doi:10.2151/sola.2009-041, 2009.

Yoshida, Y., Ota, Y., Eguchi, N., Kikuchi, N., Nobuta, K., Tran, H., Morino, I., and Yokota, T.: Retrieval algorithm for CO_2 and CH_4 column abundances from short-wavelength infrared spectral observations by the Greenhouse gases observing satellite, Atmos. Meas. Tech., 4, 717-734, doi:10.5194/amt-4-717-2011, 2011.

Chapter 4

Using aircraft profiles for validation of satellite-based column-averaged mole fraction measurements of CO_2

4.1 Abstract

Satellite-based measurements of tropospheric greenhouse gases like CO_2 and CH_4 form an integral part of the Earth observing system. However, these measurements must be highly precise and accurate in order to be useful for applications in atmospheric research like inverse modelling. Therefore, in order to assess the quality of these measurements these observations need to be continuously calibrated and validated using independent observations of even higher precision. In this chapter, the validation of the column-averaged dry air mole fraction CO_2 data (XCO_2) from two satellite-products — GOSAT RemoTeC and SCIAMACHY-BESD — is presented. The dataset used as reference truth is obtained from vertical profiles of CO_2 measured onboard commercial airliners from the CONTRAIL project. The general methodology and approach for using aircraft profiles for satellite XCO_2 validation and the impact of different stratospheric extensions used to complete the aircraft profile are discussed. Subsequently, the bias and the random error in the XCO_2 data from the two satellite products, with respect to the aircraft-derived XCO_2 are compared. Further, CO_2 fields from the mesoscale chemical transport model WRF-GHG model (Weather Research and Forecasting-Greenhouse Gas model) are analysed to investigate the variability of the XCO_2 measurements along the aircraft profile path. This analysis helps address the question of how representative the slant aircraft profiles that span a certain horizontal distance are of the nadir column as seen by the satellite.

4.2 Introduction

The usefulness of space-based observations of atmospheric greenhouse gases for enhancing our current knowledge about global carbon cycle is well documented and well investigated. For example, satellite-based measurements can be assimilated in an inverse modelling framework in order to derive surface fluxes. (Rayner and O'Brian, 2001; Pak et al., 2001; Houweling et al., 2004; Chevallier et al., 2005; Miller et al., 2007). These satellite measurements are obtained as column-averaged dry air mole fractions of greenhouse gases (XGHG) like CO_2 and CH_4. These measurements are

available from the TANSO-FTS instrument onboard GOSAT, SCIAMACHY on Envisat and the OCO-2 satellite. In addition to this, satellite-based observations are continuously being assimilated in numerical weather prediction (NWP) models in order to make improved predictions about the state of the atmosphere (Massart et al., 2014)

However, these measurements are subject to uncertainties arising from the instrument itself, the retrieval algorithm (which derives XGHG from the spectral measurement), and spatio-temporal sampling and averaging, among others. Therefore, prior to using satellite products for atmospheric research and monitoring it is essential to understand and characterize the capabilities and limitations of the data, assess data quality, and provide users with quality indicators enabling them to judge the fitness of the data for their purpose. For example, a precondition for the use of satellite-based column-averaged mole fractions in inverse modelling studies is that these measurements must meet certain minimum accuracy and precision requirements. According to Rayner and O'Brien (2001) the precision requirement for remotely sensed XCO_2 to be useful in constraining surface fluxes is less than 1% (3 to 4 ppm) while that suggested by Miller et al., (2007) is even lower (1 to 2 ppm). Buchwitz et al., (2011) specify the threshold and goal requirements for the precision (random error) of XCO_2 to be around 8 ppm and 1 ppm respectively while those for the accuracy (systematic error) are specified to be 0.5 ppm and 0.2 ppm respectively

Therefore, satellite XCO_2 measurements must be validated and calibrated prior to use, which involves characterizing the uncertainty associated with the data through comparison with an independent reference dataset with known and documented uncertainties. This process of validation allows users to decide whether a particular data product is adequate for its intended use in the specific research or application area. Besides quantifying the bias and uncertainty associated with the satellite measurement, it helps answer pertinent questions regarding the representativeness of the satellite-retrieved products for the actual atmospheric state.

The validation dataset that is used as a reference truth for comparison with the satellite data must fulfill certain requirements. These include the following:

1. The data must be obtained independently.
2. They must be more accurate and precise than the satellite measurements.
3. They should measure the same air mass as the satellite measurement.
4. They should be easily and continuously available during the lifetime of the satellite instrument.

In the last decade, the most popular source of reference data for validation of satellite based column-averaged retrievals has been the Total Carbon Column Observing Network (TCCON), a network of ground-based Fourier Transform Spectrometers providing total column measurements of CO_2, CH_4 and CO (among other species) at 23 sites across the globe (Wunch et al., 2011). However, these remotely sensed

measurements, in turn depend on in-situ measurements from other sources like aircraft or AirCore (Karion et al., 2010) for calibration (Geibel et al., 2012; Messerchmidt et al., 2011). Also, since the TCCON network is still sparse and there exist large areas across the globe that remain unsampled, airborne measurements can provide useful auxiliary data in locations where the TCCON stations do not measure.

So far, dedicated aircraft and balloon campaigns have been the major source of obtaining accurate, in-situ atmospheric observations for validation. However, airborne measurements made by sensors onboard commercial aircraft are a relatively new concept in the field of global atmospheric monitoring. Globally, there are currently a few ongoing projects that deploy hi-tech instruments onboard commercial airliners that make regular in-situ measurements of the atmosphere during long distance flights, thus providing a view of the horizontal and vertical distribution of the measured trace gases at high temporal and spatial resolution. For instance, projects like the In-Service Aircraft for a Global Observing System (IAGOS) (Petzold et al., 2015) and the Comprehensive Observation Network for TRace gases by AIrLiner (CONTRAIL) project (Machida et al., 2008; Matsueda et al., 2008) provide a large database of observations that have applications in the field of atmospheric modelling, validation of satellite observations and carbon cycle science.

The common approach used in most validation studies involves four steps: (1) quality filtering of data sets, (2) colocation with certain distance and time-difference criteria, and (3) application of a-priori and averaging kernel to the reference data, and (4) comparison with reference data. However, using aircraft profiles for validation of satellite total column trace gas abundances involves additional steps in order to account for the fact that aircraft profiles do not reach the top of the atmosphere. They are limited in altitudinal extent and only reach a height of about 9 -13 km.Therefore, they need to be extended synthetically into the stratosphere and upper layers of the atmosphere. The various steps involved in using aircraft profiles for validation of satellite-based total column CO_2 are shown in Fig. 4.1.

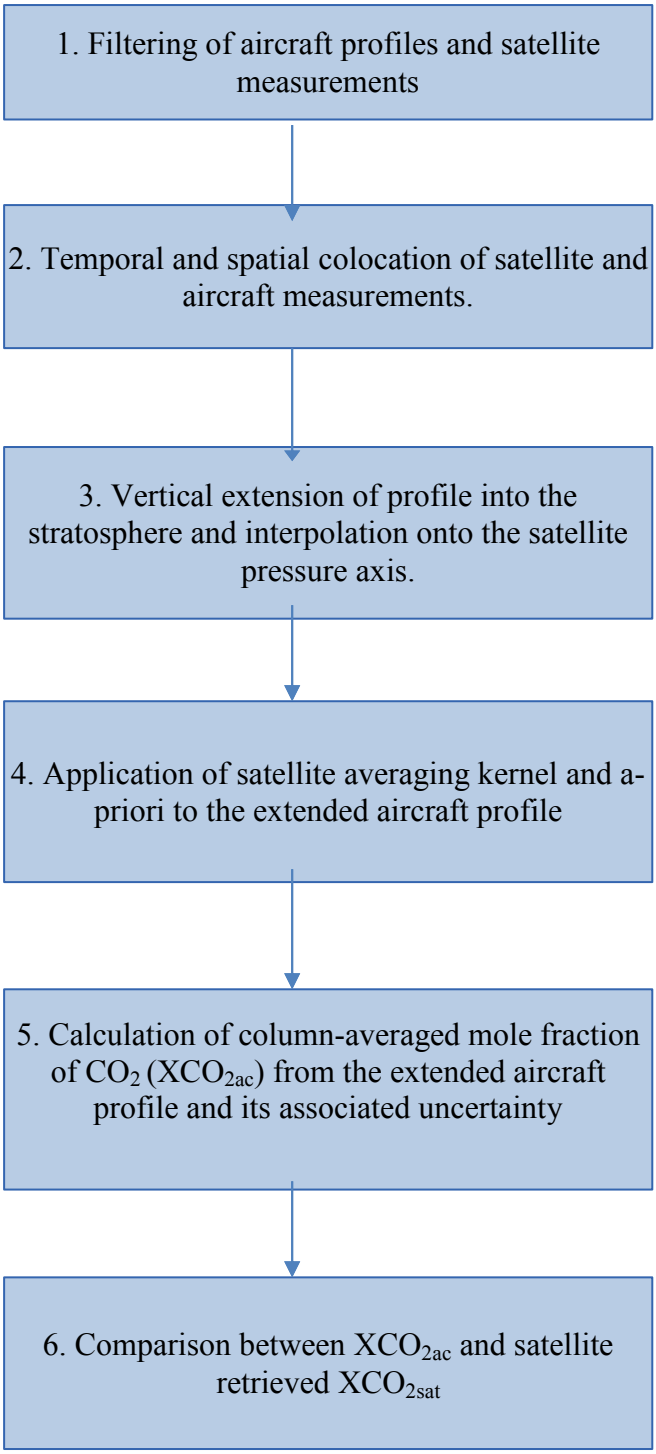

Figure 4.1: Steps involved in the validation of satellite-based column-averaged mole fraction using aircraft vertical profiles.

Aircraft profiles need to be extended into the upper atmospheric layers using other data sources. These could be model output, the a-priori profile from the satellite retrieval etc. The column-averaged abundance is especially sensitive to the choice of this data source for tracers like CH_4 that are chemically active in the stratosphere and therefore have a stratospheric sink (as discussed in Chapter 3). However CO_2, being an inert tracer in the stratosphere does not pose such challenges and therefore this profile extension is not likely to significantly influence the total column mole fraction. This is demonstrated in this study by using three different model outputs as stratospheric extensions and comparing the XCO_2 value obtained using each.

This chapter describes the method for using vertical profiles of CO_2 measured by commercial aircraft from the CONTRAIL project for validation of satellite observed XCO_2. We use this approach for comparing two satellite products: the BESD retrieval of XCO_2 from the SCIAMACHY sensor (Reuter et al., 2011; hereafter referred to as SCIAMACHY-BESD) and the RemoTeC retrieval from the TANSO instrument (Guerlet et al., 2013) onboard the GOSAT satellite (hereafter referred to as GOSAT-RemoTec). These are compared in terms of the bias and random error in the retrieved column averaged mole fraction (XCO_{2sat}) to the XCO_2 computed using the aircraft profiles (XCO_{2ac}).

Furthermore, this chapter also investigates the issue of the representativeness of the aircraft vertical profiles with respect to the column-averaged mixing ratio as seen by the satellite. Most validation studies (e.g. Inoue et al., 2016, 2013, Miyamoto et al., 2013) using commercial aircraft-based profiles as reference assume the aircraft profile to be vertical from the ground up to the cruise height for the calculation of XCO_{2ac}. However, in reality, the aircraft spans a certain horizontal distance (200 - 400 km) during the take off and landing ('profile flight path') (Fig. 4.2). The impact that this large horizontal distance covered by the aircraft profiles has on validation needs to be investigated and the error due to the assumption of the vertical aircraft profile needs to be accounted for in the validation process. While this issue has been explored in de Laat et al., 2014 for CO, it has not yet been addressed for CO_2. In this chapter, high-resolution CO_2 model fields from the WRF-GHG model (Weather Research and Forecasting- Greenhouse Gas model; Beck et al. 2011) for the Europe domain are analysed. The aircraft profile locations and times are obtained from the MOZAIC project (Measurement of Ozone and Water Vapour on Airbus in-service Aircraft; Marenco et al., 1998) for this part of the study because of significant coverage of the MOZAIC fleet in the Europe region.

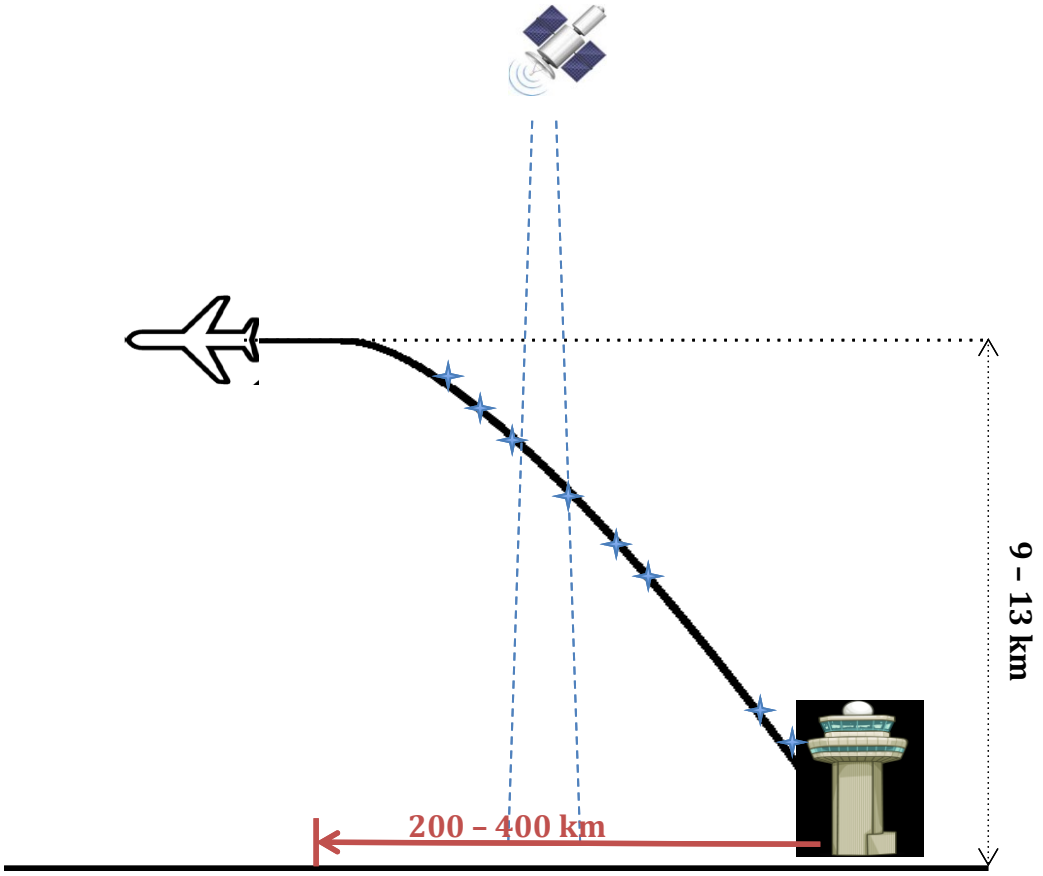

Figure 4.2: Illustration showing the problem of representativeness of slant aircraft profiles of the true vertical column as seen by the satellite.

The outline of this chapter is as follows: Section 4.3 provides a brief overview of the datasets used in this study and the methodology adopted and steps involved in computing XCO_{2ac} and its associated uncertainty is discussed in Section 4.4. In Sect. 4.5, statistical analyses and comparison between the XCO_2 computed from the aircraft profiles and those from GOSAT-RemoTeC and SCIAMACHY-BESD retrievals are presented. Results from the WRF-GHG model analysis for the representation error of the slant aircraft CO_2 profiles are also presented in this section. Finally, these results are summarized in Section 4.6.

4.3 Datasets

4.3.1 CONTRAIL CO_2 data

The CONTRAIL project was started in late 2005 with the aim of using the existing commercial aviation infrastructure for obtaining free tropospheric CO_2 mixing ratios systematically for long periods of time over a large geographical space (Machida et al., 2008; Matsueda et al., 2008). Five Japan Airlines Corporation (JAL) commercial aircraft were instrumented with continuous CO_2 measuring equipment (CME) and most flights originate from Narita International Airport in Chiba, Japan. The data observed during the ascent and descent of the aircraft are taken as vertical CO_2 profiles over each observation site (airport), and have an overall uncertainty of 0.2 ppm. Typical observing altitudes are 1–11 km with vertical resolutions of 30 - 100 m. The CONTRAIL airports used for the validation of the satellite data products used in this study are listed in Table 4.1 and shown in Fig. 4.3.

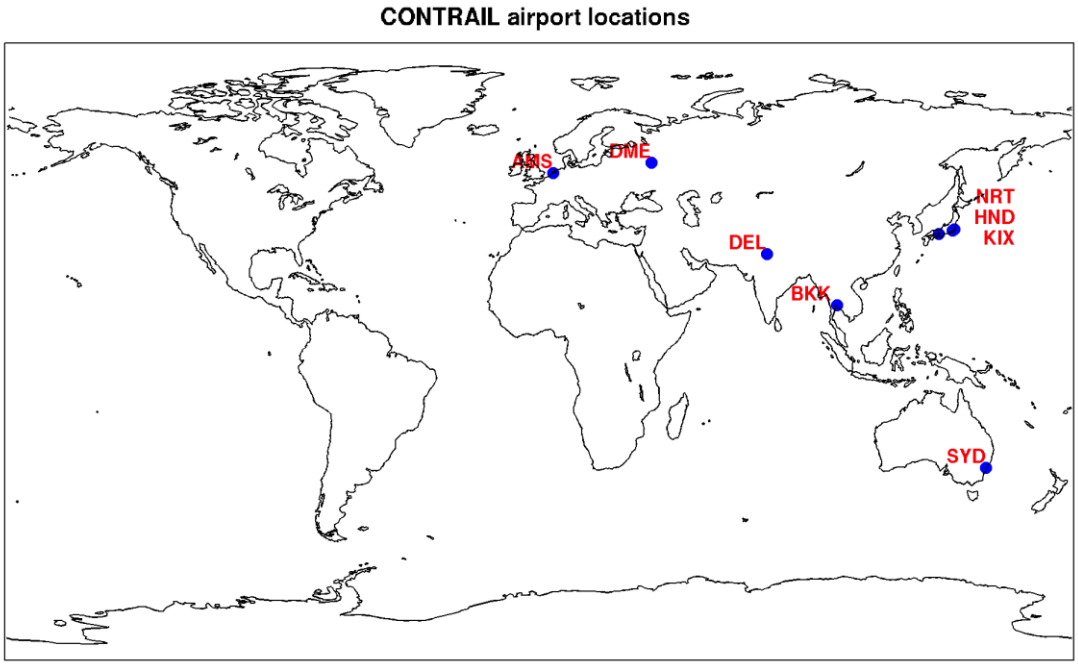

Figure 4.3: Location of CONTRAIL airports used for validation.

	Latitude	Longitude	Name of airport
AMS	52.3	4.8	Schiphol Airport, the Netherlands
BKK	13.7	100.7	Suvarnabhumi International Airport, Thailand
DEL	28.6	77.1	Indira Gandhi International Airport, India
DME	55.4	37.9	Domodedovo Airport, Moscow
HND	35.6	139.8	Tokyo International Airport, Japan
KIX	34.4	135.2	Kansai International Airport, Japan
NRT	35.8	140.4	Narita International Airport, Japan
SYD	-33.9	151.2	Kingsford Smith Airport, Australia

Table 4.1: Location and names of the CONTRAIL airports used for validation.

4.3.2 GOSAT-RemoTeC CO_2 observations

GOSAT, a joint project of the National Institute for Environmental Studies (NIES), the Japanese Space Agency (JAXA), and the Ministry of the Environment (MOE), was launched in January 2009 as the world's first satellite dedicated to greenhouse gas monitoring. GOSAT follows a polar sun-synchronous orbit with a 3-day repeat pattern and crosses the equator at around 1 p.m. local time. The TANSO-FTS instrument onboard GOSAT measures short-wavelength infrared (SWIR) light reflected from the Earth's surface, along with the thermal infrared (TIR) radiation emitted from the surface and atmosphere using a Fourier transform spectrometer (Kuze et al., 2009). It has three narrow bands in the SWIR region centered at 0.76, 1.6 and 2.0 μm and a wide TIR band (5.5–14.3 μm) at a spectral resolution of about 0.2 cm^{-1}. The TANSO-FTS instantaneous field of view (IFOV) is 15.8 mrad, corresponding to a nadir footprint diameter of 10.5 km.

Several retrieval algorithms have been developed to retrieve the column-averaged CO_2 from the GOSAT spectra. In this study, the full-physics version of the RemoTeC algorithm (SRFP (Full physics) v2.3.6) developed by the Netherlands Institute for Space Research (SRON) and the Karlsruhe Institute of Technology (KIT) has been used. RemoTeC is a flexible algorithm developed to accurately retrieve CO_2, CH_4 , and other absorbing species from SWIR satellite observations of backscattered sunlight. This algorithm is based on a radiative transfer model developed by Hasekamp and Butz, 2008. Scattering particles are parameterized as spherical particles with a fixed refractive index ($1.400 - i \times 0.003$), and their size distribution follows a power law, $n(r) \propto r^{-\alpha}$ where r is the particle radius and the exponent α is the size parameter. The height distribution of particle optical thickness is a Gaussian function of center height z_S. 12-layer vertical profiles of the CO_2 and CH_4 column number densities are retrieved, among other parameters. XCO_2 and XCH_4 quantities are calculated by summing the respective column number densities over the 12 retrieval layers and dividing by the dry air column.

4.3.3 SCIAMACHY-BESD CO_2 observations

The satellite instrument SCIAMACHY (Burrows et al., 1995; Bovensmann et al., 1999) was part of the atmospheric chemistry payload onboard Envisat that was operational between January 2003 and May 2012. Envisat flew on a sun-synchronous daytime (descending) orbit with an equator crossing time of 10:00 local time. The SCIAMACHY instrument used passive remote sensing to measure sunlight transmitted, reflected and scattered by the Earth's atmosphere or surface in the wavelength range between 240 nm and 2400 nm with a spectral resolution between 0.2 and 1.4 nm. The main atmospheric species measured by the SCIAMACHY

instrument were O_3, NO_2, CH_4 and CO_2 as well as clouds and aerosols, ocean colour and land parameters. It was capable of measuring in three different viewing geometries: nadir, limb and solar/lunar occultation and operated at a typical spatial resolution of ~60 km across track and ~30 km along track.

The Bremen Optimal Estimation DOAS (BESD) retrieval algorithm has been developed at the University of Bremen to retrieve XCO_2 from SCIAMACHY nadir measurements. The product version of 02.00.08 has been used in this study. The theoretical basis of BESD and a study of synthetic retrievals is presented in the publication of Reuter et al. (2010) and validation results are presented in Reuter et al., (2011). The algorithm uses measurements in the O_2-A absorption (755-775 nm) band to retrieve scattering information of clouds and aerosols. This information is transferred to the CO_2 absorption band (1558-1594 nm) by simultaneously fitting the spectra measured in both spectral regions. An optimal-estimation-based inversion technique is used to derive the most probable atmospheric state from a SCIAMACHY measurement using some a priori knowledge

A 10-layered CO_2 mixing ratio profile, which is separated in equally spaced pressure intervals, is fitted in the CO_2 fit window. Although BESD has been designed to minimise scattering-related retrieval errors, clouds are still an important potential error source and strict cloud filtering is necessary. BESD filters clouds by using cloud information based on measurements from the Medium Resolution Imaging Spectrometer (MERIS).

4.3.4 Integrated Forecasting system for Composition (C-IFS)

The Integrated Forecasting System for Composition (C-IFS) (Flemming et al. 2015; Massart et al., 2014) is a comprehensive, high-resolution numerical weather prediction (NWP) and Earth system model developed at the European Centre for Medium Range Weather Forecasts (ECMWF). It assimilates data from a wide range of different observation networks and satellite instruments in order to produce optimal estimates of the state of the atmosphere. The model has been discussed in detail in Section 3.3.1.
In this study, 6-hourly CO_2 profiles from C-IFS having $1° \times 1°$ spatial resolution are utilized for the spatial colocation of measurements from the aircraft profiles and satellites. Furthermore, they are also used to synthetically extend the aircraft profiles into the stratosphere for computing the column averaged mole fraction.

In addition, model profiles from two other models − Carbon Tracker and Jena CarboScope – have been used to test the impact of different stratospheric extensions of aircraft profiles on the estimated value of XCO2ac. The details of these models are given below:

4.3.5 Carbon Tracker CO_2 profiles

CarbonTracker (Peters et al., 2007) is a CO_2 measurement and inverse modelling system, developed by the National Oceanic and Atmospheric Administration (NOAA), that simulates the CO_2 fluxes at the Earths surface using atmospheric observations and knowledge of atmospheric transport. CarbonTracker is based on the offline transport model TM5 (Krol et al., 2005) and is driven by meteorology from the European Centre for Medium-Range Weather Forecasts (ECMWF) operational forecasting model and reanalysis. The model runs at a $3° \times 2°$ resolution globally. Once the optimized fluxes are estimated, the model is sampled at 3-hourly time interval on the native vertical grid of 34 levels to obtain 3-D fields of CO_2.

4.3.6 Jena CarboScope CO_2 profiles

Jena CarboScope (or the Jena Inversion System) (Roedenbeck et al., 2005) is a Bayesian inversion framework that is used to estimate trace gas fluxes at the surface of the Earth from measured atmospheric concentrations and knowledge of atmospheric transport. It employs the global atmospheric tracer model TM3 to simulate atmospheric transport (Heimann and Körner, 2003). In this study, 6-hourly model CO_2 profiles have been used that have been obtained from simulations carried out at a $4° \times 5°$ spatial resolution using the ERA-Interim (European Centre for Medium Range Weather Forecasts (ECMWF) Reanalysis-Interim) meteorology. Further details of this model have been discussed in Sect. 2.3.1.

4.3.7 Weather Research and Forecasting − Greenhouse Gas Model (WRF-GHG)

The WRF-GHG model (Beck et al., 2011) is a high-resolution chemical transport model that provides hourly concentration fields at 6 km spatial resolution for the tracers CO_2, CH_4 and CO tracers at 41 vertical levels. The model boundary conditions for meteorological fields are obtained from the European Centre for Medium-Range Weather Forecasts (ECMWF) model analysis data at 0.125° spatial resolution and 6-hourly temporal resolution. As the initial and boundary conditions for CO_2, CH_4 and CO, analysed fields from the C-IFS, interpolated onto the WRF grid are used. Biospheric fluxes in the model are computed online using the Vegetation Photosynthesis and Respiration Model (VPRM), driven by satellite and meteorological data at high temporal and spatial resolutions (Mahadevan et al., 2008). The anthropogenic fluxes are based on the Institut für Energiewirtschaft und Rationelle Energieanwendung (IER inventory), University of Stuttgart, (http://carboeurope.ier.uni-stuttgart.de) available at 10 km horizontal resolution,

extrapolated using the BP (British Petroleum) statistics. Biomass burning emissions in the model are obtained from the Global Fire Emissions Database (GFED v4.1s).

In this study, the WRF-GHG fields for the period July 2014 to October 2014 have been used to investigate the representation error of the CO_2 columns derived from aircraft profiles− that span a certain horizontal distance – compared to the nadir column abundance of CO_2 as seen by the satellite.

4.4 Validation Methodology

4.4.1 Filtering input data

The first step in the validation tool is to filter the usable aircraft profiles. In order to do this, the criteria based on those used in de Laat et al. (2014), were used. Only those profiles are selected that (1) reach at least 300 hPa altitude level, (2) have at least one measurement in every 100 hPa altitude bin and (2) start below 800 hPa. This way all profiles with large data gaps are neglected. While filtering the satellite data, only those measurements with the 'good' quality flag indicated by the number zero were selected.

4.4.2 Spatial and Temporal Colocation

Since the satellite data and the aircraft profiles are rarely perfectly coincident in space and time, certain spatial and temporal colocation criteria need to be defined that help select only those observations from the two observing systems that are close in both space and time. This ensures that the same air mass is being compared.
In this study, the first coarse temporal filter selects all those satellite observations that lie between ± 12 hours from the time at which the aircraft profile is measured. This time is taken to be the mean of the time at which the aircraft starts measuring the profile and the end time when it reaches cruise altitude (for profiles measured during take off) or when it reaches the ground (for profiles measured during landing). The colocations are not restricted to the same calendar date.
There are several spatial colocation methodologies that have been used in different studies.

1. The simplest approach for colocation is using the geographical colocation method where a neighborhood region (for instance $\pm 5°$, or 500 km) is defined around the location of interest (i.e the aircraft profile location) and all satellite measurements lying within the this region are taken to be colocations or matches (Inoue et al., 2013).
2. The T700 colocation technique is a more sophisticated approach that uses the mid tropospheric potential temperature at 700 hPa at the location of interest, in addition to the horizontal spatial and temporal criteria used in the geographical

colocation method (Wunch et al., 2011b, Keppel-Aleks et al., 2011). However, this method only works well at the Northern Hemisphere mid-latitudes since the correlation between potential temperature and XCO_2 is less effective at low latitudes.

3. Nguyen et al., (2014) used a modified Euclidian distance weighted average of distance, time, and mid-Tropospheric temperature at 700 hPa.

In this study, the spatial colocation methodology is based on that implemented for validation of GOSAT XCO_2 with TCCON data in Guerlet et al. (2013). This method takes into account the fact that the observed total column CO_2 value (XCO_2) is impacted by atmospheric transport in addition to the surface fluxes. First, a coarse geographical filter is applied that selects all those satellite measurements that lie within ± 22.5 degrees longitude and ± 7.5 degrees latitude of the aircraft profile location. Further, model XCO_2 fields from the CarbonTracker system are used to define a contiguous area within this larger box, **A**, around the aircraft profile location, inside the larger geographical area, within which the modeled XCO_2 ($XCO_{2,mod}$) lies within a certain tolerance value from the modeled XCO_2 value at the aircraft profile location ($XCO_{2,mod,ac}$). Thus, the following condition must be satisfied:

$$| XCO_{2,mod} - XCO_{2mod,ac} | < \delta \qquad (4.1)$$

where the tolerance value δ is set to 0.5 ppm.

Once the area **A** around the aircraft profile is identified all the satellite observations that lie within this area are considered to be colocated with the corresponding total column from the aircraft profile.

4.4.3 Vertical extension of the aircraft profile

Since aircraft profiles from CONTRAIL are obtained over a limited altitudinal range (1 km to about 11 km) they have to be extended both to the surface and into the upper atmospheric layers. This has been achieved by extrapolating the profiles to the surface from the lowest measured aircraft data. Similarly, the profiles that did not reach up to the tropopause are extended using the CO_2 observation at the highest measurement altitude, assuming the concentration to be constant up to the tropopause. This assumption is reasonable for a tracer like CO_2 since it is well mixed in the troposphere and stratospheric layers of the atmosphere.

Beyond the tropopause, into the stratospheric and mesospheric layers of the atmosphere, the aircraft profiles are extended using the Integrated Forecasting System for Composition (C-IFS) model profiles. In order to identify the tropopause, temperature profiles from the Carbon Tracker model are used. For each profile, the tropopause is defined as the height at which the gradient of the temperature begins to change sign from negative to positive with time.

The extended profiles are then interpolated on to the satellite pressure axis. This is achieved by taking a pressure-weighted mean of all the aircraft measurements that lie between adjacent satellite pressure levels.

4.4.4 Application of satellite a-priori and averaging kernel

According to Rodgers and Connor (2003) the comparison of two XCO_2 observations requires that the retrievals be computed about a common a priori profile. The effect of smoothing must be taken into account by applying the averaging kernels, which allows us to account for the vertical sensitivity of the satellite instrument. Therefore, the satellite a-priori profile and the averaging kernel are applied to the extended profiles using the following equation:

$$XCO_{2,ac} = \Sigma_{i=1}^{m} [\, VMR_i^{pri} + AK_i(VMR_i^{ac} - VMR_i^{pri})].pw_i \qquad (4.2)$$

where the sum is over m atmospheric layers, pw_i is the layer dependent weight, VMR_i^{pri} is the satellite a priori layer averaged volume mixing ratio between pressure levels p_i and p_{i+1}, VMR_i^{ac} is the corresponding aircraft value (From step 3) and AK_i is the satellite XCO_2 averaging kernel for layer i.

4.4.5 Estimation of uncertainty of the computed XCO_{2ac}

An estimate of the uncertainty of the aircraft computed XCO_{2ac} due to the different profile assumptions is made for each profile. The methodology is adopted from Miyamoto et al., (2013), who computed CO_2 total columns using vertical profiles from aircraft at the CONTRAIL airports. According to this approach, the aircraft profile is divided into four domains and a uniform uncertainty value is assumed for each based on the analysis of the observed data (Table 4.2). Domain I is the part of the profile that lies within the boundary layer. Domain II lies above the boundary layer with observed data; Domain III lies above the boundary layer and has no observed data. Domain IV: includes the stratospheric part of the profile without any observations.

The total uncertainty of for each profile (Equation 4.3) is computed as an average of the assumed uncertainty for each domain weighted by the fractional amount of CO_2 in that domain, calculated using the Carbon Tracker model profiles.

Domain	Standard Deviation (in ppm)
I (No observed data in boundary layer)	15
I (With observed data in boundary layer)	2.89
II	0.4
III	1.73
IV	1.73

Table 4.2: The assumed standard deviation of partial XCO_2 for each domain

$$uncertainty = \frac{\sqrt{\Sigma_j N(j)^2 \times \sigma(j)^2}}{N} \quad (j = I, II, III, IV) \qquad (4.3)$$

4.5 Results

4.5.1 Impact of model profiles in the stratosphere on the calculation of aircraft based XCO_{2ac}

In order to test the impact of the stratospheric extension of the aircraft profile on the computed total column XCO_{2ac}, CO_2 profiles from two other models – Jena CarboScope and Carbon Tracker − in addition to the fields from the C-IFS model were used for the stratosphere. XCO_{2ac} was computed at four airports: Bangkok, New Delhi, Narita and Sydney. Column abundances calculated using the profiles from the three models mentioned above for stratospheric extension are referred to as CIFS XCO_{2ac}, JCS XCO_{2ac} and CT XCO_{2ac}. Figure 4.4 shows an example of an aircraft profile measured at Narita on 23 January 2010 and extended using the three model profiles from the Integrated Forecasting System for Composition (C-IFS), Carbon Tracker (CT), Jena CarboScope (JCS) models.

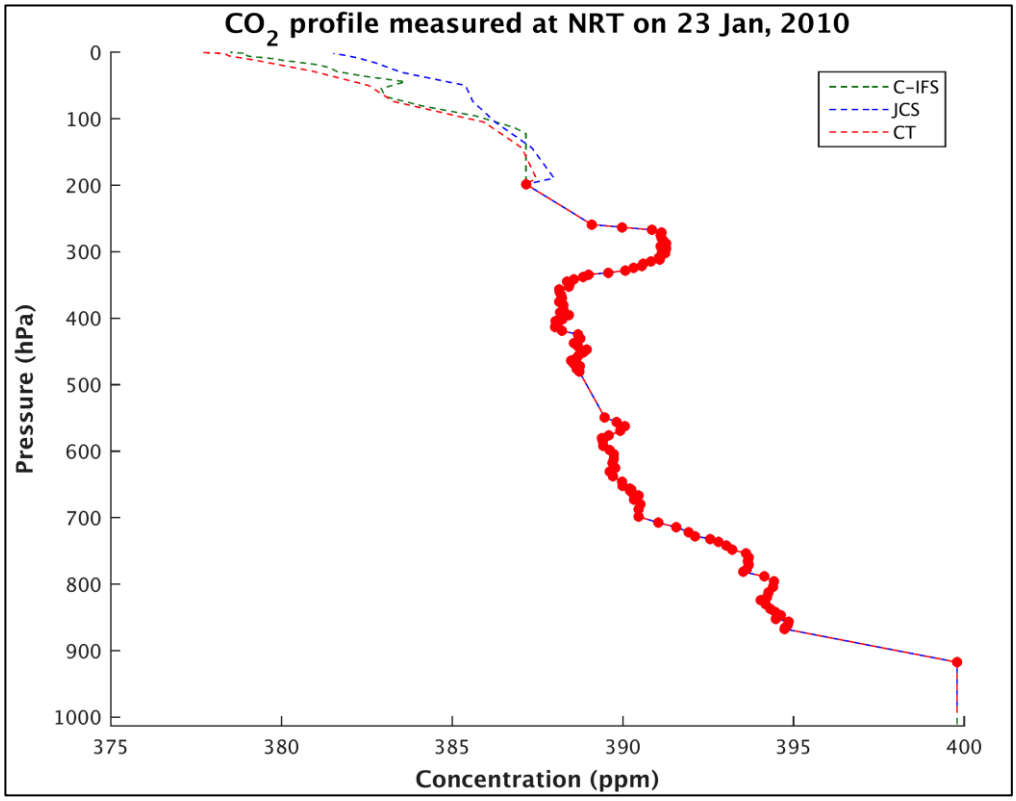

Figure 4.4: Vertical profiles of CO_2 over Narita on 23 January, 2010. The green, blue and red dashed lines above the tropopause represent model profiles from the Integrated Forecasting system for Composition (C-IFS), Jena CarboScope (JCS) and the Carbon Tracker (CT) model respectively. The red dots represent the measurements made by the aircraft.

		C-IFS XCO_{2ac} – JCS XCO_{2ac}		C-IFS XCO_{2ac} – CT XCO_{2ac}	
	Number	Mean (ppm)	Std. Dev. (ppm)	Mean (ppm)	Std. Dev. (ppm)
DME	8	0.048	0.073	-0.161	0.055
DEL	30	0.035	0.240	-0.261	0.537
NRT	67	-0.014	0.267	-0.118	0.271
SYD	62	0.042	0.082	-0.090	0.082
All data	167	-0.018	0.204	-0.131	0.289

Table 4.3. The average and standard deviation of the differences of aircraft-based XCO_2 calculated by using CO_2 profiles from Integrated Forecasting System for Composition (C-IFS), Jena CarboScope (JCS) and the CarbonTracker (CT) in the stratosphere at each aircraft observation site during the year 2010.

The averages of the differences (C-IFS XCO_2 - JCS XCO_2) and (C-IFS XCO_2 - CT XCO_2) obtained at the four respective airports are listed in Table 4.3. The average of (C-IFS XCO_2 - JCS XCO_2) over Narita was −0.014 ± 0.267 ppm while that of (C-IFS XCO_2 - CT XCO_2) was -0.118 ± 0.271 ppm. For the Southern hemisphere airport of Sydney, these values are as small as 0.042 ± 0.082 ppm and -0.090 ± 0.082 ppm. It can be seen from the table that although the differences vary with location, the values for all the sites taken together are quite small. This is due to the fact that the amount of CO_2 above the tropopause is small and therefore different representations of the stratosphere used for the extension of aircraft profiles are not likely to impact the computed total column $XCO2_{ac}$ greatly.

4.5.2 Validation results and comparison of satellite products

The comparison between the satellite retrieved column-averaged CO_2 abundance XCO_{2sat} for the two satellite products — GOSAT RemoTeC and SCIAMACHY-BESD — and XCO_{2ac} computed at the CONTRAIL airports is carried out. The following statistical parameters have been computed from the comparisons of the datasets at the CONTRAIL airports (i) the number of collocated data points, (ii) the mean difference (bias) between the data sets, (iii) the standard deviation of the difference (as an estimate of the precision when compared with XCO_{2ac}) and (iv) the linear correlation coefficient between the data sets (Table 4.4). Biases are computed by subtracting the aircraft computed XCO_2 from the satellite retrieved XCO_2.

It can be seen from Table 4.4 that the number of satellite matches are higher for the SCIAMACHY instrument compared to GOSAT since more measurements per day

were performed by SCIAMACHY. The statistics are likely to be most robust for the sites SYD, NRT, DEL and DME since these have a high number of collocated matches for both instruments throughout the time period considered in this study. For the other stations, the applied filtering and the colocation criteria cause significant gaps in the usable aircraft and satellite data that hinder the statistical analysis. In addition to that the cloud screening of pixels applied in the satellite retrievals also reduces the "good quality" satellite pixels. This screening is more stringent for the SCIAMACHY-BESD retrieval as compared to GOSAT-RemoTeC.

Figure 4.5 shows scatter plots between the aircraft computed XCO_2 at all the airports and the colocated XCO_2 values retrieved from the GOSAT and SCIAMACHY satellite products. The slope and the intercept of the regression line shown in the figure have been calculated taking into account errors in both x- and y-axis (York et al. 2004). The typical uncertainty range of the satellite retrieved XCO_{2sat} from the two products lies between 2 to 4 ppm, while that of the aircraft-derived XCO_{2ac} (as discussed in Sect. 4.4.5) is estimated to be around 0.8 to 1.5 ppm. We see that the mean bias between the XCO_{2sat} and XCO_{2ac} for both satellite products is positive, which implies that the satellite products overestimate the value of XCO_2. The value of this bias is higher for GOSAT RemoTeC (0.40 ppm) than for the SCIAMACHY-BESD retrieval (0.19 ppm). These bias values are much smaller in magnitude as compared to the satellite measurement uncertainty. The standard deviation (or random error) of the difference for the two products is comparable, with SCIAMACHY-BESD (1.96 ppm) performing marginally better than GOSAT-RemoTeC (2.01 ppm). The discrepancies in the bias and precision between the two retrievals are likely to be due to differences of the scattering modules used in the inversion and cloud removal methods in the retrievals. Further, for both the retrievals, the slope of the linear regression line is far from unity. This is likely to be due to the inability of the satellite retrieval to represent the truth or the problem of representativeness of the aircraft measurements.

Table 4.4: The statistical results of comparison between satellite retrieved (GOSAT-RemoTeC and SCIAMACHY-BESD) XCO_2 data and that computed from aircraft profiles from the CONTRAIL project (taken to be the truth) during the period January 2010 to October 2011.

			Standard Deviation (ppm)		Correlation coefficient		Total number of satellite matches	
	GOS	HY	GOSAT	SCIAMACHY	GOSAT	SCIAMACHY	GOSAT	SCIAMACHY
AMS	0.0		1.74	1.90	0.78	0.78	32	154
BKK	0.9		1.43	2.34	0.73	0.59	56	246
DEL	1.2		2.26	2.18	0.45	0.50	392	989
DME	0.9		1.99	2.24	0.84	0.74	121	1129
HND	-0.1		2.10	2.30	0.53	0.50	97	235
KIX	0.4		1.27	2.62	0.62	0.67	28	46
NRT	0.5		2.67	2.71	0.58	0.60	626	1702
SYD	0.0		1.84	1.85	0.54	0.42	1385	10790

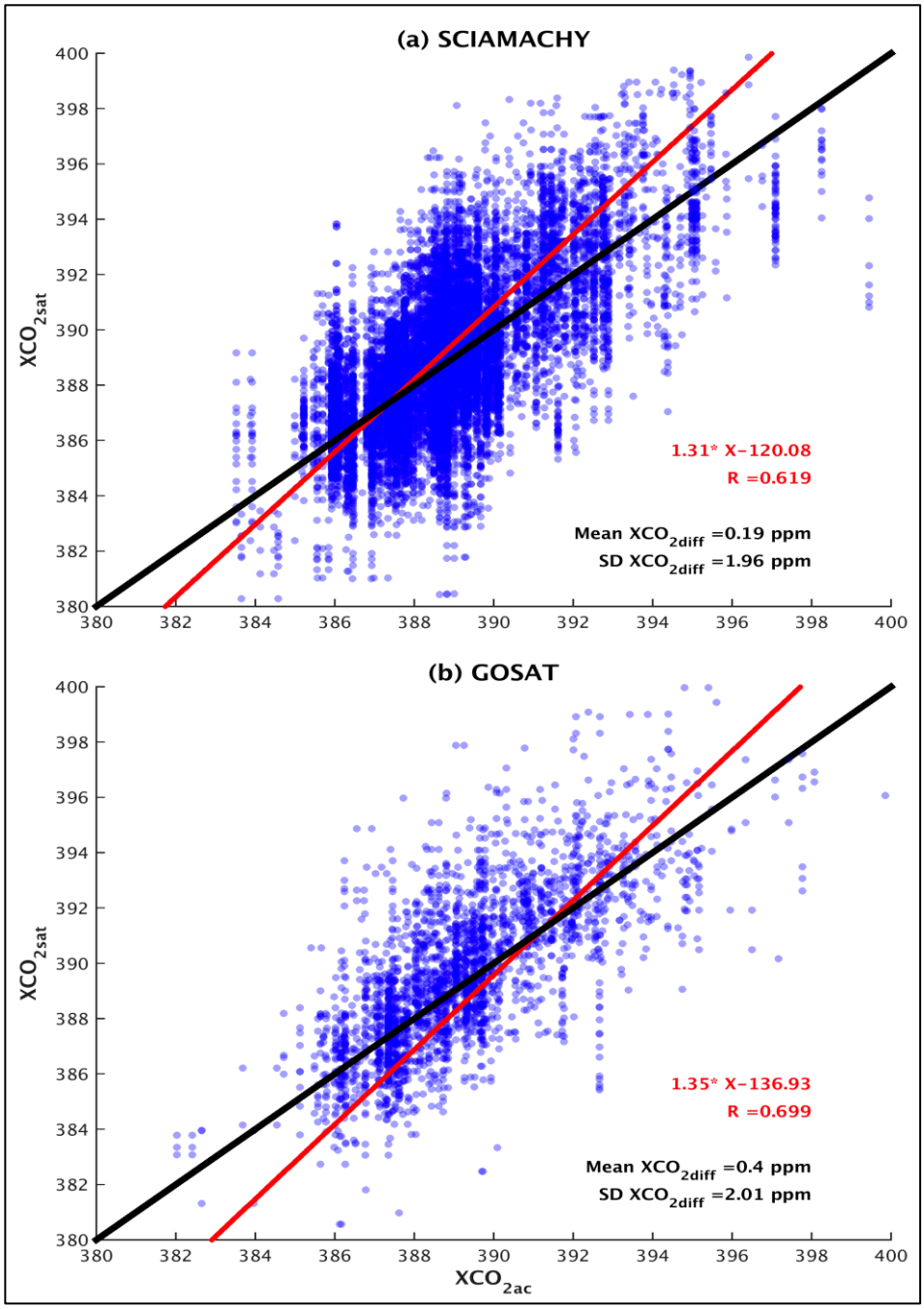

Figure 4.5: Scatter plot between XCO_{2ac} computed at the CONTRAIL airports against the collocated XCO_{2sat} from the (a) SCIAMACHY-BESD and (b) GOSAT-RemoTeC retrieval during January 2010 to October 2011.

The time series of XCO_{2ac} and XCO_{2sat} from the two satellite products as well as their uncertainties at four airports is shown in Fig. 4.6 and Fig. 4.7. In general, both satellite retrievals capture the temporal and spatial patterns observed in the validation data well. The satellite data have the same seasonal fluctuations as that shown by the reference observations from CONTRAIL, with a decrease in XCO_2 in the boreal summer months and increasing trend during boreal winter. This seasonality in the XCO_2, as shown at the Northern Hemisphere airports of DME, DEL and NRT is largely driven by photosynthesis, which is at its peak during summer. During the boreal winter, due to decreased photosynthesis, the atmospheric CO_2 builds up, as reflected in the XCO_2 increase during the winter to spring months. Overall, the maximum value of XCO_2 is observed in the months of April and May. On the other hand, Sydney lacks a pronounced XCO_2 seasonal cycle, which can be attributed to milder seasons and lesser landmass in the Southern Hemisphere and hence smaller amplitudes in the CO_2 annual cycle.

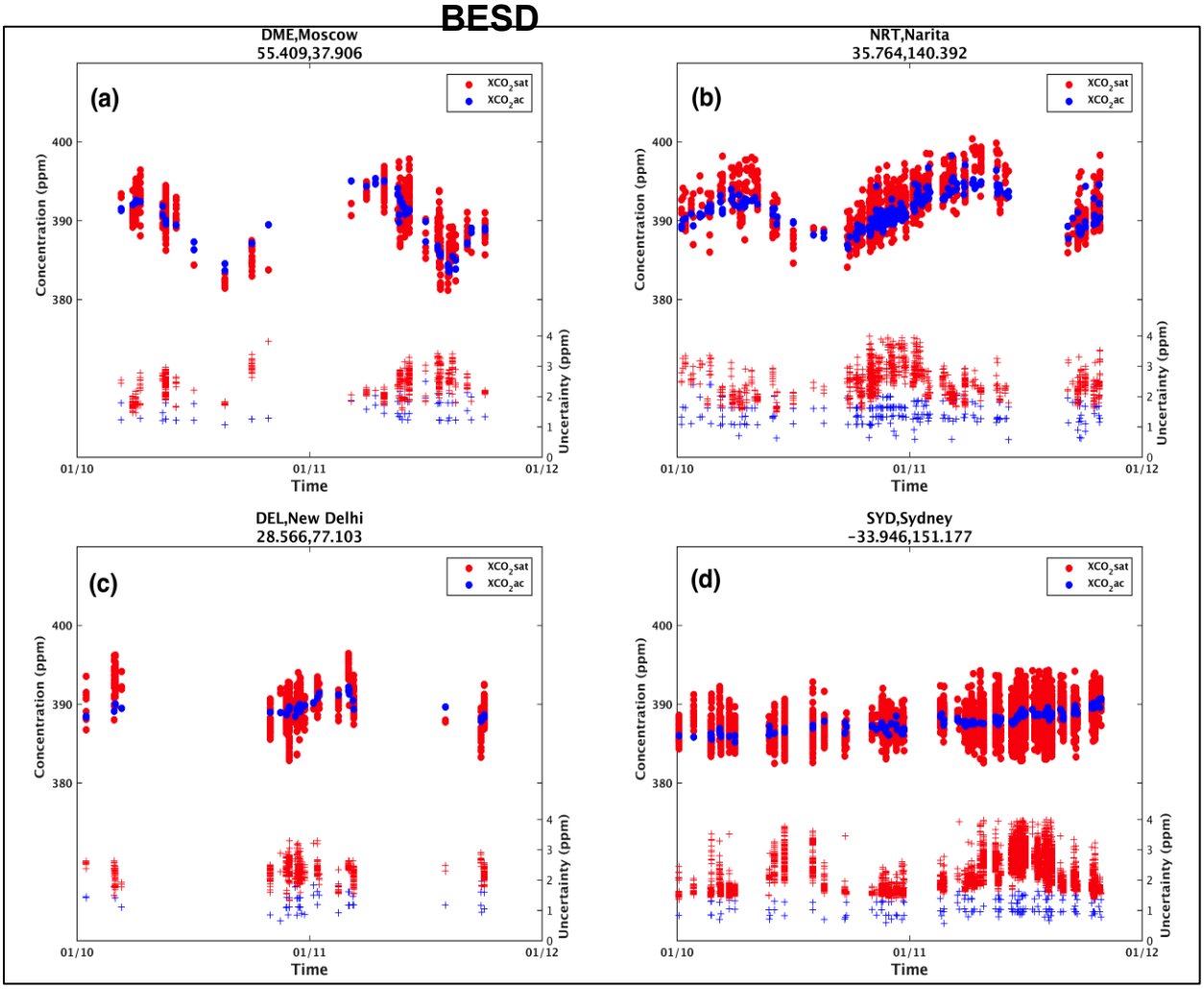

Figure 4.6: Time series of XCO_{2ac} (blue dots) and XCO_{2sat} (red dots) from the SCIAMACHY-BESD retrieval during January 2010 to October 2011. The y-axis on the bottom right of each panel shows the uncertainties in the XCO_{2sat} and XCO_{2ac} as red and blue crosses.

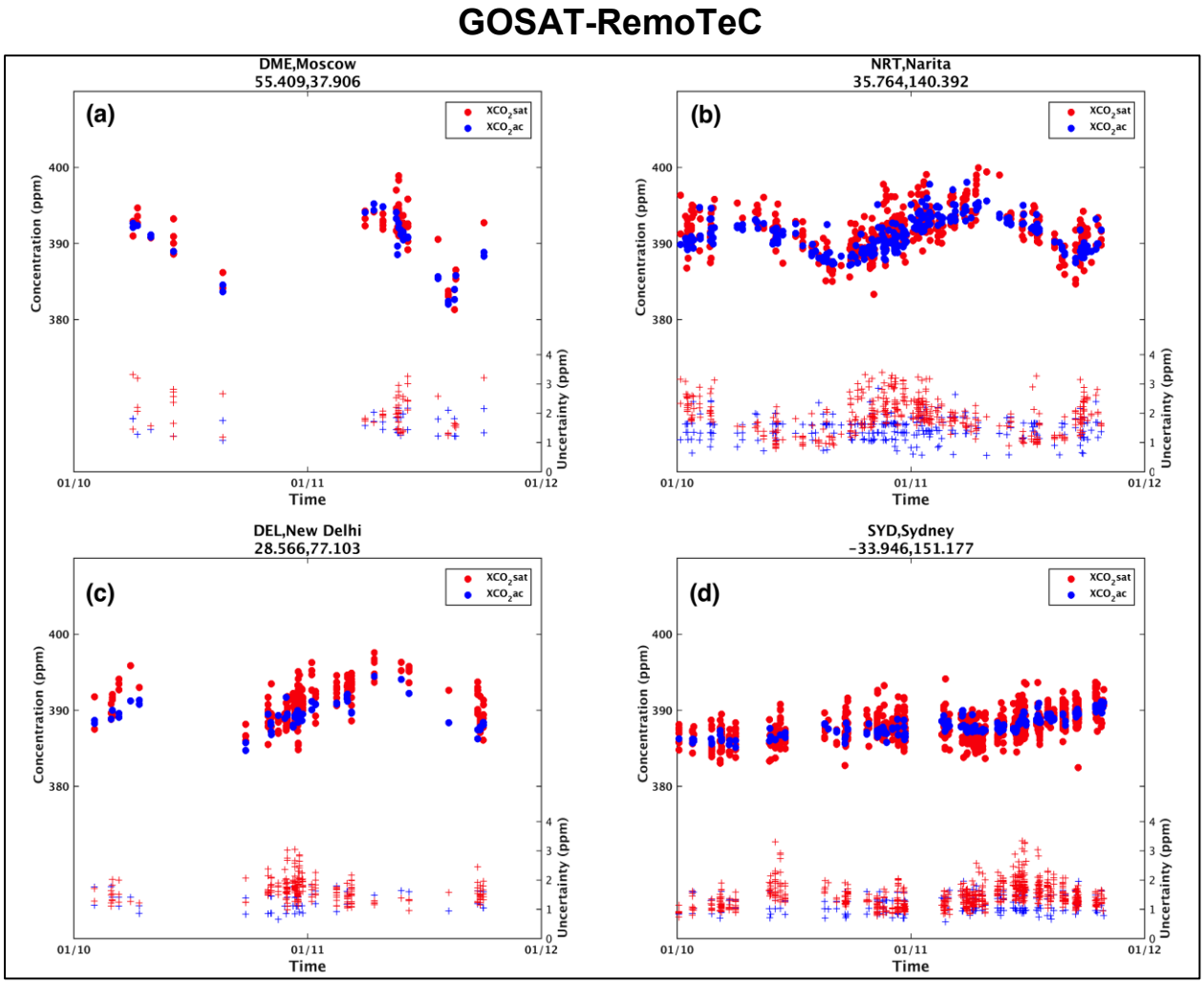

Figure 4.7: Time series of XCO_{2ac} (blue dots) and XCO_{2sat} (red dots) from the GOSAT-RemoTeC retrieval during January 2010 to October 2011. The y-axis on the bottom right of each panel shows the uncertainties in the XCO_{2sat} and XCO_{2ac} as red and blue crosses.

4.5.3 Model analysis: Representativeness of aircraft profiles

High resolution CO_2 model fields from the WRF-GHG model were analysed for the months of July to October, 2014 for the Europe domain to estimate the impact of the horizontal distance covered by an aircraft while measuring CO_2 profiles during take off and landing on the comparison between XCO_{2sat} and $XCO_{2ac.}$ The time and location of aircraft profile measurements were obtained from vertical profiles from the MOZAIC project.

First, the model was sampled at the representative location of the aircraft profile used for satellite validation. The coordinates of this "representative location" were obtained by taking the mean of the coordinates of the measurements in the profile, weighted by the pressure difference between the measurement levels. Subsequently, the column-averaged mole fraction is computed from the model profile at the aircraft location ($XCO_{2,vert}$). In order to estimate the impact of the slant aircraft profile, the actual slant column-averaged abundance ($XCO_{2,slant}$) was computed for each aircraft profile by sampling the model at actual measurement locations for each profile. The highest and lowest measurement point of the slant profile was extended upwards and ground wards for each aircraft profile prior to computing the $XCO_{2,slant}$. The difference ($XCO_{2,vert}$ - $XCO_{2,slant}$) was computed for each profile (Fig. 4.8).

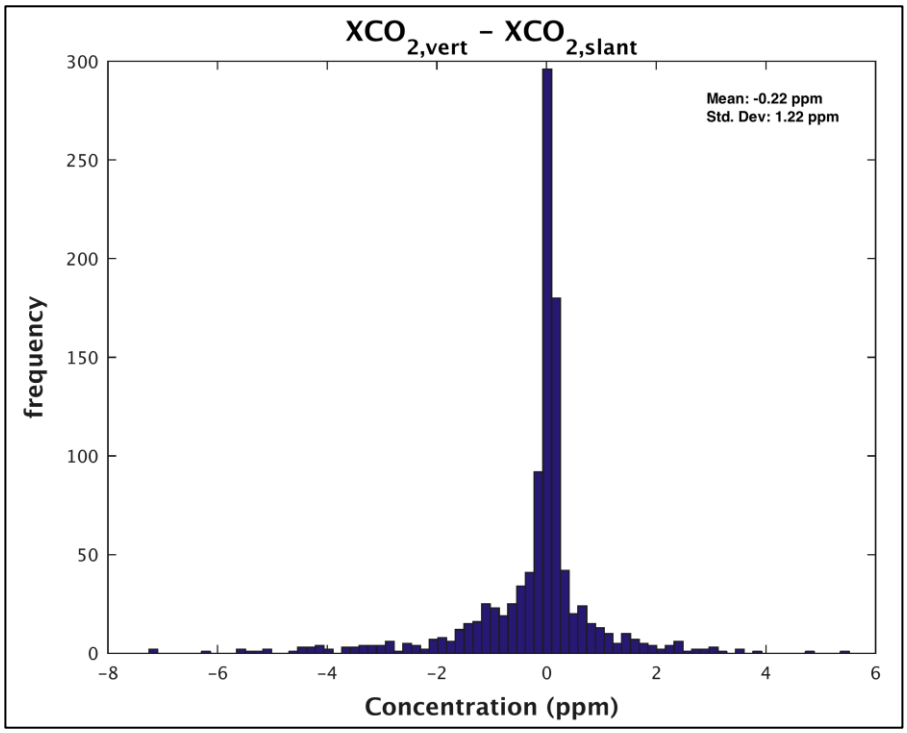

Figure 4.8: Histogram showing the distribution of the difference between the vertical column XCO_{2ac} computed at the representative location of the aircraft profile and the slant column $XCO_{2ac.}$

For assessing whether the variability in the aircraft-derived column due to the horizontal extent of the aircraft profile is likely to impact satellite validation, the variability of modeled XCO_2 within the colocation region for each aircraft profile ($XCO_{2,coloc}$) is computed. In order to do this, the WRF-GHG fields were first aggregated to 1° × 1° resolution and the colocation method, as explained in Sect. 4.4.2, was applied. Figure 4.9 is a histogram showing the probability distribution of ($XCO_{2,vert} - XCO_{2,coloc}$) for all aircraft profiles within the WRF-GHG model domain.
It can be seen from Fig. 4.8 that the variability of XCO_{2ac} due to the slant aircraft profile is about 1.220 ppm. This value is lower than the typical variability of the XCO_2 in the colocation region (about 3.64 ppm) as shown by Fig. 4.9.

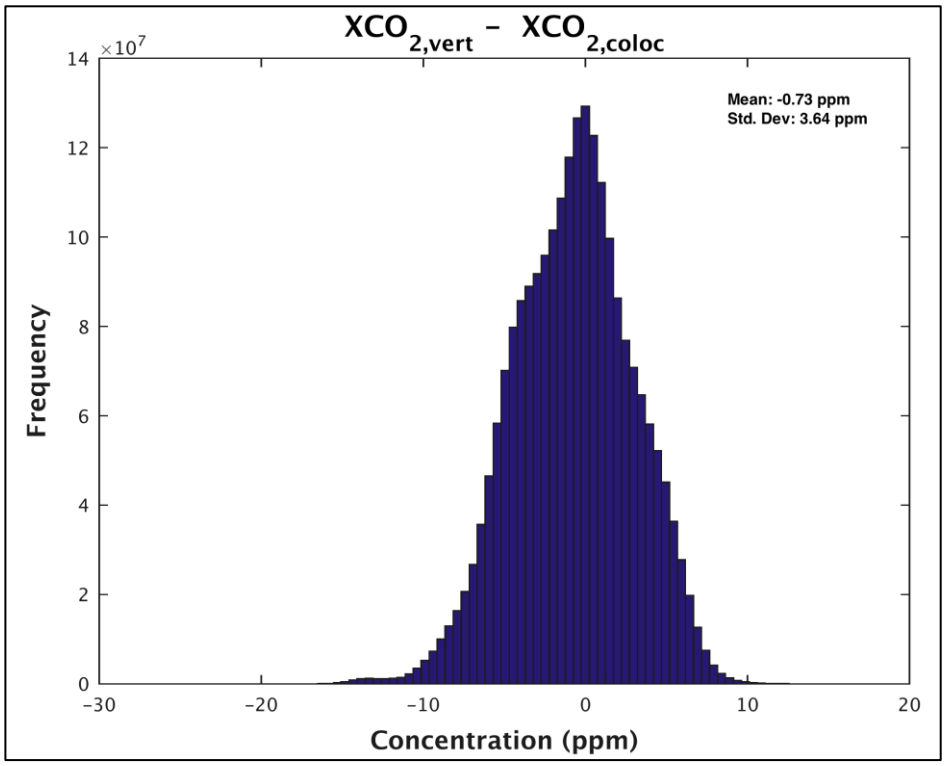

Figure 4.9: Histogram showing the distribution of the difference between the vertical column XCO_{2ac} computed at the representative location of the aircraft profile and modelled XCO_2 in the colocation region for each aircraft profile.

This indicates that the error due to the slant aircraft profile is well within the variability range of $XCO_{2,coloc}$ for each profile. Therefore, it is not likely to impact the comparison between XCO_{2ac} and XCO_{2sat} and the aircraft-derived columns are representative of the true vertical columns as seen by the satellites.

4.6 Summary and Conclusion

The application and general approach for using aircraft profiles for the validation of satellite based total column abundances of CO_2 (XCO_2) is discussed. Aircraft profiles measured near airports from the CONTRAIL project are used as reference data in order to characterize the errors in the total column abundance data from the SCIAMACHY-BESD and GOSAT-RemoTeC retrievals. The impact of different stratospheric extensions of aircraft profiles on the computed total column abundance (XCO_{2ac}) is assessed. In order to investigate this, output from three different models is used to complete the aircraft partial column. It is seen that there is only a marginal impact of the stratospheric data on the computed total column. This is likely to be because of the fact that the most of the CO_2 is concentrated in the tropospheric layers of the atmosphere and also since CO_2 is a chemically inactive tracer in the stratosphere.

Overall, both satellite retrievals capture the spatial and temporal patterns in the aircraft validation data well. In the Northern hemisphere, the XCO_2 seasonal cycle with late summer minimum and spring maximum is clearly seen from the XCO_2 time series at Narita and New Delhi. At the southern hemisphere airport of Sydney, the seasonal cycle has almost no amplitude. Both retrievals overestimate XCO_2 compared to CONTRAIL as shown by the positive bias. The value of this bias is only 0.19 ppm for the SCIAMACHY-BESD product, which is much smaller than that of GOSAT RemoTeC (0.40 ppm). These values lie well within the uncertainty ranges of the measurements. The standard deviation of the difference between the satellite measurement and CONTRAIL derived XCO_{2ac} is also found to be slightly better for SCIAMACHY (1.96 ppm) as compared to GOSAT (2.01 ppm). These are comparable to the results from other validation studies that use TCCON as reference truth. Detmers and Hasekamp (2015) reported standard deviations of the GOSAT-TCCON difference to be around 1.93 ppm. Kulawik et al. (2016) validated SCIAMACHY-BESD XCO_2 using TCCON measurements and found this value to be close to 2.1 ppm.

At this point, it is worth mentioning that one of the general open questions pertaining to the use of aircraft profiles for validation of satellite-based column abundances is regarding the representativeness of these measurements. These profiles are generally measured near airports, which form areas of high emissions. This is unlike TCCON stations that are situated outside the cities or at remote locations where the impact of local pollution sources on the observations is likely to be low. The agreement between the validation results obtained in this study and those that use TCCON measurements indicates that the despite being measured near polluted areas, the aircraft profiles perform equally well as reference data for the validation of satellite-based column-averaged greenhouse gas mole fractions as TCCON.

On investigating the impact of the slant aircraft profiles on satellite validation, it was

found that the error due to the horizontal distance spanned by the aircraft during the ascent and descent of the aircraft in XCO_{2ac} lies within the variability of the XCO_2 in the region defined for colocation of satellite and aircraft measurements and is therefore not likely to have a large impact on satellite validation. In other words, the assumption of the vertical aircraft-derived column is reasonable for the comparison of XCO_{2ac} and XCO_{2sat}.

These results demonstrate the utility of these observations for validation of satellite-based column-averaged greenhouse gas mole fractions. This new data stream can go a long way in complementing the existing network of in-situ and TCCON-based measurements for use as valuable reference data for validation studies. While this study only uses profiles from the CONTRAIL project, more aircraft observations are expected to be available within projects like IAGOS in the near future. The IAGOS instruments are expected to provide continuous measurements in the boundary layer thus reducing the uncertainty on the aircraft-derived XCO_{2ac} thus providing more accurate reference data for satellite validation.

4.7 References

Beck, V., T. Koch, R. Kretschmer, J. Marshall, R. Ahmadov, C. Gerbig, D. Pillai, and M. Heimann : The WRF Greenhouse Gas Model (WRF-GHG). Technical Report No. 25, Max Planck Institute for Biogeochemistry, Jena, Germany, 2011

Bovensmann, H., Burrows, J. P., Buchwitz, M., Frerick, J., Noël, S., Rozanov, V. V., Chance, K. V. and Goede, a. P. H.: SCIAMACHY: Mission Objectives and Measurement Modes, J. Atmos. Sci., 56(2), 127–150, doi:10.1175/1520-0469(1999)056<0127:SMOAMM>2.0.CO;2, 1999.

Burrows, J. P., Hölzle, E., Goede, A. P. H., Visser, H. and Fricke, W.: SCIAMACHY—scanning imaging absorption spectrometer for atmospheric chartography, Acta Astronaut., 35(7), 445–451, doi:10.1016/0094-5765(94)00278-T, 1995.

Chevallier, F., M. Fisher, P. Peylin, S. Serrar, P. Bousquet, F.-M. Bréon, A. Chédin, and P. Ciais: Inferring CO_2 sources and sinks from satellite observations: Method and application to TOVS data, J. Geophys. Res., 110, D24309, doi:10.1029/2005JD006390, 2005

de Laat, A. T. J., Aben, I., Deeter, M., Nédélec, P., Eskes, H., Attié, J. L., Ricaud, P., Abida, R., El Amraoui, L. and Landgraf, J.: Validation of nine years of MOPITT V5 NIR using MOZAIC/IAGOS measurements: Biases and long-term stability, Atmos.Meas. Tech., 7(11), 3783–3799, doi:10.5194/amt-7-3783-2014, 2014

Detmers, R., Hasekamp, O. : Product User Guide (PUG) for the RemoTeC XCO_2 Full Physics GOSAT Data Product for the Essential Climate Variable (ECV) Greenhouse Gases (GHG) ; www.esa-ghg-cci.org/?q=webfm_send/292, 2015

Hasekamp, O. P. and Butz, A.: Efficient calculation of intensity and polarization spectra in vertically inhomogeneous scattering and absorbing atmospheres, J. Geophys. Res. Atmos., 113(20), doi:10.1029/2008JD010379, 2008.

Flemming, J., Huijnen, V., Arteta, J., Bechtold, P., Beljaars, A., Blechschmidt, A.-M., Diamantakis, M., Engelen, R. J., Gaudel, A., Inness, A., Jones, L., Josse, B., Katragkou, E., Marecal, V., Peuch, V.-H., Richter, A., Schultz, M. G., Stein, O., and Tsikerdekis, A.: Tropospheric chemistry in the Integrated Forecasting System of ECMWF, Geosci. Model Dev., 8, 975-1003, doi:10.5194/gmd-8-975-2015, 2015.

Geibel, M. C., Messerschmidt, J., Gerbig, C., Blumenstock, T., Chen, H., Hase, F., Kolle, O., Lavrič, J. V., Notholt, J., Palm, M., Rettinger, M., Schmidt, M., Sussmann, R., Warneke, T., and Feist, D. G.: Calibration of column-averaged CH4 over European TCCON FTS sites with airborne in-situ measurements, Atmos. Chem.

Phys., 12, 8763-8775, doi:10.5194/acp-12-8763-2012, 2012.

Houweling, S., Breon, F.-M., Aben, I., Rödenbeck, C., Gloor, M., Heimann, M., and Ciais, P.: Inverse modeling of CO_2 sources and sinks using satellite data: a synthetic inter-comparison of measurement techniques and their performance as a func- tion of space and time, Atmos. Chem. Phys., 4, 523–538, doi:10.5194/acp-4-523-2004, 2004.

Karion, A., Sweeney, C., Tans, P. and Newberger, T.: AirCore: An innovative atmospheric sampling system, J. Atmos. Ocean. Technol., 27(11), 1839–1853, doi:10.1175/2010JTECHA1448.1, 2010.

Krol, M., Houweling, S., Bregman, B., van den Broek, M., Segers, A., van Velthoven, P., Peters, W., Dentener, F., and Berga- maschi, P.: The two-way nested global chemistry-transport zoom model TM5: algorithm and applications, Atmos. Chem. Phys., 5, 417–432, doi:10.5194 /acp-5-417-2005, 2005.

Kulawik, S., Wunch, D., O'Dell, C., Frankenberg, C., Reuter, M., Oda, T., Chevallier, F., Sherlock, V., Buchwitz, M., Osterman, G., Miller, C. E., Wennberg, P. O., Griffith, D., Morino, I., Dubey, M. K., Deutscher, N. M., Notholt, J., Hase, F., Warneke, T., Sussmann, R., Robinson, J., Strong, K., Schneider, M., De Mazière, M., Shiomi, K., Feist, D. G., Iraci, L. T. and Wolf, J.: Consistent evaluation of ACOS-GOSAT, BESD-SCIAMACHY, CarbonTracker, and MACC through comparisons to TCCON, Atmos. Meas. Tech., 9(2), 683–709, doi:10.5194/amt-9-683-2016, 2016.

Kuze, A., Suto, H., Nakajima, M. and Hamazaki, T.: Thermal and near infrared sensor for carbon observation Fourier-transform spectrometer on the Greenhouse Gases Observing Satellite for greenhouse gases monitoring., Appl. Opt., 48(35), 6716–6733, doi:10.1364/AO.48.006716, 2009.

Machida, T., Matsueda, H., Sawa, Y., Nakagawa, Y., Hirotani, K., Kondo, N., Goto, K., Nakazawa, T., Ishikawa, K. and Ogawa, T.: Worldwide Measurements of Atmospheric CO2 and Other Trace Gas Species Using Commercial Airlines, J. Atmos. Ocean. Technol., 25, 1744–1754, doi:10.1175/2008JTECHA1082.1, 2008.

Mahadevan, P., Wofsy, S. C., Matross, D. M., Xiao, X., Dunn, A. L., Lin, J. C., Gerbig, C., Munger, J. W., Chow, V. Y. and Gottlieb, E. W.: A satellite-based biosphere parameterization for net ecosystem CO_2 exchange: Vegetation Photosynthesis and Respiration Model (VPRM), Global Biogeochem. Cycles, 22(2), doi:10.1029/2006GB002735, 2008.

Makoto, I., Isamu, M., Osamu, U., Yuki, M., Yukio, Y., Tatsuya, Y., Toshinobu, M., Yousuke, S., Hidekazu, M., Colm, S., Pieter P., T., Arlyn E., A., Sebastien C., B., Tomoaki, T. and Shuji Kawakami and Prabir K., P.: Validation of XCO_2 derived from SWIR spectra of GOSAT TANSO-FTS with aircraft measurement data, Atmospheric

Chemistry and Physics, Atmos. Chem. Phys., 13(19), 9771–9788, doi:10.5194/amt-7-2987-2014, 2013.

Matsueda, H., Machida, T., Sawa, Y., Nakagawa, Y., Hirotani, K., Ikeda, H., Kondo, N., and Goto, K.: Evaluation of atmospheric CO_2 measurements from new flask air sampling of JAL airliner observations, Pap. Meteorol. Geophys., 59, 1–17, 2008.

Massart, S., Agusti-Panareda, A., Aben, I., Butz, A., Chevallier, F., Crevosier, C., Engelen, R., Frankenberg, C. and Hasekamp, O.: Assimilation of atmospheric methane products into the MACC-II system: From SCIAMACHY to TANSO and IASI, Atmos. Chem. Phys., 14(12), 6139–6158, doi:10.5194/acp-14-6139-2014, 2014.

Messerschmidt, J., Geibel, M. C., Blumenstock, T., Chen, H., Deutscher, N. M., Engel, A., Feist, D. G., Gerbig, C., Gisi, M., Hase, F., Katrynski, K., Kolle, O., Lavrič, J. V., Notholt, J., Palm, M., Ramonet, M., Rettinger, M., Schmidt, M., Sussmann, R., Toon, G. C., Truong, F., Warneke, T., Wennberg, P. O., Wunch, D. and Xueref-Remy, I.: Calibration of TCCON column-averaged CO2: The first aircraft campaign over European TCCON sites, Atmos. Chem. Phys., 11(21), 10765–10777, doi:10.5194/acp-11-10765-2011, 2011.

Miller, C. E., Crisp, D., DeCola, P. L., Olsen, S. C., Randerson, J. T., Michalak, A. M., Alkhaled, A., Rayner, P., Jacob, D. J., Suntharalingam, P., Jones, D. B. A., Denning, A. S., Nicholls, M. E., Doney, S. C., Pawson, S., Boesch, H., Connor, B. J., Fung, I. Y., O'Brien, D., Salawitch, R. J., Sander, S. P., Sen, B., Tans, P., Toon, G. C., Wennberg, P. O., Wofsy, S. C., Yung, Y. L. and Law, R. M.: Precision requirements for space-based XCO_2 data, J. Geophys. Res. Atmos., 112(10), doi:10.1029/2006JD007659, 2007.

Marenco, A., Thouret, V., Nédélec, P., Smit, H., Helten, M., Kley, D., Karcher, F., Simon, P., Law, K., Pyle, J., Poschmann, G., Von Wrede, R., Hume, C. and Cook, T.: Measurement of ozone and water vapor by Airbus in-service aircraft: The MOZAIC airborne program, an overview, J. Geophys. Res., 103(D19), 25631, doi:10.1029/98JD00977, 1998.

Miyamoto, Y., Inoue, M., Morino, I., Uchino, O., Yokota, T., Machida, T., Sawa, Y., Matsueda, H., Sweeney, C., Tans, P. P., Andrews, A. E. and Patra, P. K.: Atmospheric column-averaged mole fractions of carbon dioxide at 53 aircraft measurement sites, Atmos. Chem. Phys., 13(10), 5265–5275, doi:10.5194/acp-13-5265-2013, 2013.

Nguyen, H., Osterman, G., Wunch, D., O'Dell, C., Mandrake, L., Wennberg, P., Fisher, B. and Castano, R.: A method for colocating satellite XCO_2 data to ground-based data and its application to ACOS-GOSAT and TCCON, Atmos. Meas. Tech., 7(8), 2631–2644, doi:10.5194/amt-7-2631-2014, 2014.

Pak, B. C. and Prather, M. J.: CO_2 source inversions using satellite observations of the

upper troposhere, Geophys. Res. Lett., 28, 4571–4574, 2001.

Peters, W., Jacobson, A. R., Sweeney, C., Andrews, A. E., Conway, T. J., Masarie, K., Miller, J. B., Bruhwiler, L. M. P., Pétron, G., Hirsch, A. I., Worthy, D. E. J., van der Werf, G. R., Randerson, J. T., Wennberg, P. O., Krol, M. C. and Tans, P. P.: An atmospheric perspective on North American carbon dioxide exchange: CarbonTracker., Proc. Natl. Acad. Sci. U. S. A., 104(48), 18925–18930, doi:10.1073/pnas.0708986104, 2007.

Petzold, A., Thouret, V., Gerbig, C., Zahn, A., Brenninkmeijer, C. A. M., Gallagher, M., Hermann, M., Pontaud, M., Ziereis, H., Boulanger, D., Marshall, J., Nédélec, P., Smit, H. G. J., Friess, U., Flaud, J.-M., Wahner, A., Cammas, J.-P. and Volz-Thomas, A.: Global-scale atmosphere monitoring by in-service aircraft - current achievements and future prospects of the European Research Infrastructure IAGOS, Tellus B, 67, 1–24, doi:10.3402/tellusb.v%v.28452, 2015.

Rayner, P. J. and O'Brien, D. M.: The utility of remotely sensed CO2 concentration data in surface source inversions, Geophys. Res. Lett., 28(1), 175–178, doi:10.1029/2000GL011912, 2001.

Reuter, M., Buchwitz, M., Schneising, O., Heymann, J., Bovensmann, H., and Burrows, J. P.: A method for improved SCIAMACHY CO2 retrieval in the presence of optically thin clouds, Atmos. Meas. Tech., 3, 209-232, doi:10.5194/amt-3-209-2010, 2010.

Reuter, M., Bovensmann, H., Buchwitz, M., Burrows, J. P., Connor, B. J., Deutscher, N. M., Griffith, D. W. T., Heymann, J., Keppel-Aleks, G., Messerschmidt, J., Notholt, J., Petri, C., Robinson, J., Schneising, O., Sherlock, V., Velazco, V., Warneke, T., Wennberg, P. O. and Wunch, D.: Retrieval of atmospheric CO_2 with enhanced accuracy and precision from SCIAMACHY: Validation with FTS measurements and comparison with model results, J. Geophys. Res. Atmos., 116(4), doi:10.1029/2010JD015047, 2011.

Rödenbeck, C. : Estimating CO_2 sources and sinks from atmospheric mixing ratio measurements using a global inversion of atmospheric transport. Technical Report 6, Max Planck Institute for Biogeochemistry, Jena, 2005.

Rodgers, C. D.: Intercomparison of remote sounding instruments, J. Geophys. Res., 108(D3), 46–48, doi:10.1029/2002JD002299, 2003.

Wunch, D., Toon, G. C., Blavier, J.-F. L., Washenfelder, R. A., Notholt, J., Connor, B. J., Griffith, D. W. T., Sherlock, V. and Wennberg, P. O.: The Total Carbon Column Observing Network, Philos. Trans. R. Soc. A Math. Phys. Eng. Sci., 369(1943), 2087–2112, doi:10.1098/rsta.2010.0240, 2011.

Yokota, T., Yoshida, Y., Eguchi, N., Ota, Y., Tanaka, T., Watanabe, H. and

Maksyutov, S.: Global Concentrations of CO2 and CH4 Retrieved from GOSAT: First Preliminary Results, Sola, 5, 160–163, doi:10.2151/sola.2009-041, 2009.

York, D., Evensen, N. M., Martínez, M. L. and De Basabe Delgado, J.: Unified equations for the slope, intercept, and standard errors of the best straight line, Am. J. Phys., 72(3), 367, doi:10.1119/1.1632486, 2004.

Yoshida, Y., Ota, Y., Eguchi, N., Kikuchi, N., Nobuta, K., Tran, H., Morino, I., and Yokota, T.: Retrieval algorithm for CO_2 and CH_4 column abundances from short-wavelength infrared spectral observations by the Greenhouse gases observing satellite, Atmos. Meas. Tech., 4, 717-734, doi:10.5194/amt-4-717-2011, 2011.

Chapter 5

Summary and outlook

This thesis is based on atmospheric greenhouse gas measurements made by sensors onboard commercial aircraft and investigates the applications of this unique and novel dataset for addressing hitherto open issues in carbon cycle science. Vertical profiles of CO_2 and CH_4, measured near airports during ascent and descent of the aircraft, are used for two main applications. These are: 1. Estimation of carbon flux sources and sinks using inverse modelling; 2. Validation of satellite-based column-averaged dry air mole fractions. The work has been organized into three main chapters and the main results obtained in each of these are summarized and discussed in the subsequent paragraphs.

In chapter 2, vertical profiles of CO_2 from aircraft are assimilated into an inverse modelling framework. Large discrepancies exist in the simulation of important atmospheric processes like vertical mixing by the current crop of transport models, which causes large uncertainties in the retrieved flux estimates. In this study, the sensitivity of the posterior fluxes obtained using aircraft profiles to erroneous vertical transport is assessed and compared to that obtained using ground-based measurements. It is observed that the flux retrieved using aircraft-based measurements is less sensitive to errors in vertical transport as compared to the flux estimated using ground-based measurements. This means that using aircraft-based measurements for surface flux estimation is likely to reduce the overall uncertainty in flux estimates by reducing the error due to transport models. This highlights the advantage of aircraft profiles over surface measurements for the estimation of fluxes and provides a simple and flexible approach for reducing the error contributed by inaccurate transport models to retrieved flux estimates. Further, the reduction in the uncertainty of the retrieved posterior flux on augmenting the existing surface-based network with the vertical profiles from aircraft is estimated and it is seen that overall, the uncertainty reduction is greatest for the tropics, and therefore it can be said that these regions will benefit the most from these measurements. In the near future, projects like IAGOS are expected to measure greenhouse gas mole fractions globally using airborne sensors. In light of this fact, it can be said that instrumenting aircraft flying preferentially tropical routes would provide the greatest incremental increase in the knowledge of fluxes.

Chapters 3 and 4 are based on the second application of aircraft-based profiles i.e. satellite validation. Chapter 3 deals with the main challenge posed by aircraft measurements, which is the fact that these profiles only sample the tropospheric air

and the stratosphere is not represented at all. In order to overcome this limitation, assumptions have to be made about the stratospheric contribution to the column and the profiles must be extended upwards synthetically before using them for validation of column-averaged mixing ratios provided by the satellites. This problem is more critical for tracers such as CH_4 that are chemically reactive in the stratosphere and hence have a steeper gradient. This chapter discusses three different data sources that may be used as potential data sources for the extension of CH_4 aircraft profiles and compares the error that each of them introduces into the aircraft column. The error is computed with respect to CH_4 profiles from the MIPAS satellite instrument. It is seen that the C-IFS model of the ECMWF, a high-resolution data assimilation system and TOMCAT/SLIMCAT, a CTM (Chemical Transport Model) optimized for the stratosphere perform better in the stratosphere than climatology-based data and a-priori profiles from the satellite retrievals. The error introduced in the total column using the output from the two models for stratospheric extension is well within the documented minimum precision requirements for satellite measurements to be useful for source-sink estimation using inverse modelling. However, these error estimates can be further improved by using latitudinal and seasonal bias correction schemes. Thus, this analysis provides an assessment of the different potential candidates that are available for the artificial extension of aircraft profiles and can help future validation work using commercial aircraft profiles.

Having addressed the shortcoming related to altitudinal extent, the general approach and methodology for using these profiles to validate satellite measurements of column-averaged abundances (XGHG) is presented in Chapter 4. CO_2 profiles from the CONTRAIL project are used to validate XCO_2 from GOSAT-RemoTeC and SCIAMACHY-BESD retrievals. The two retrievals are compared in terms of the overall error that each of them has with respect to the aircraft computed total column. The time series of XCO_2 from the two retrievals at the CONTRAIL airports show that both the satellite products capture the spatial and temporal patterns of XCO_2 obtained from the aircraft profiles well. The offset in the SCIAMACHY-BESD product is around 0.19 ppm while that in the GOSAT retrieval amounts to 0.40 ppm. The random error is also slightly lower for SCIAMACHY-BESD (1.96 ppm) than for GOSAT-RemoTeC (2.01 ppm). These values are consistent with past studies that have used data from the TCCON network as reference. The agreement between the results highlights the usefulness of aircraft profiles for future validation efforts. These profiles are measured near airports, associated with high emissions, unlike TCCON measurements that are often located in less polluted and even remote environments. This chapter also investigates the issue of the representativeness of the aircraft profiles. The aircraft profiles are not truly vertical in space and span a certain horizontal distance during the take off and landing, which could potentially hamper the validation of the vertical satellite-based columns. This was assessed with realistic concentration fields at 6 km resolution produced by a mesoscale model. It is seen that the influence of the slant profile on the aircraft-derived XCO_2 is much smaller than the variability of XCO_2 in the defined colocation region. This means that the impact

of the horizontal distance spanned by the profile can be neglected and is not likely to impact the comparison between satellite- and aircraft-based column abundances.

These studies demonstrate how airborne measurements made onboard commercial aircraft can help fill the existing observational gap between surface and space-based measurements and hence aid in achieving an integrated global climate observing system. Utilizing these data for atmospheric research can help provide a more complete picture of atmospheric composition and processes on global scales. However, there exist unexplored issues that have not been dealt with in this thesis, which should form the basis of future work. One of the main open questions pertains to the data-gaps in the aircraft profiles used for validation of satellite XGHG. The vertical profiles of trace gases, available currently, do not provide continuous data at all atmospheric levels where the aircraft fly. There sometimes exist gaps in the profiles, which may impact satellite XGHG validation. This is especially true if the gaps are within the highly variable boundary layer. In the study described in Chapter 4, these have been dealt with using interpolation and filtering. However, the error contribution of these data gaps needs to be quantified so that a more accurate estimate of the aircraft-derived column-averaged mixing ratio can be made. This would ensure robust and realistic results from the validation of satellite measurements using these aircraft profiles. Secondly, this thesis does not utilize cruise level measurements but rather only the vertical profiles measured near the airports during the take off and landing. The altitude of these cruise level observations lies near the tropopause region, which could potentially provide valuable insights into atmospheric dynamics and transport in the UTLS (Upper Troposphere Lower Stratosphere), a region that currently remains under explored.

Acknowledgements

First and foremost, I'd like to express my sincere gratitude to my supervisors at MPI-BGC−Dr. Julia Marshall and Dr. habil. Christoph Gerbig− for their constant support and encouragement. Thanks Julia, for your patience and involvement at every stage of my Ph.D.; for believing in me and always pushing me to do better. I also appreciate your help with the proof reading of this manuscript. Thank you Christoph, for your friendly attitude and enthusiasm all along. Your timely guidance and sound advice have been precious for the development of this thesis.

I also wish to sincerely thank my supervisor at the university- Prof. Dr. Kai Uwe Totsche for his cooperation, valuable inputs and inspiring suggestions during the PAC meetings.

I am indebted to my colleagues at the institute−Dr. Christian Roedenbeck, Dr. Thomas Koch, Dr. Ute Karstens, Friedemann Reum, Tonatiuh Guillermo Nunez Ramirez− for their assistance with modelling and data retrieval that made this work possible; as well as other group members−Fabio Boschetti, Panagiotis Kountouris, Dr. Dhanyalekshmi Pillai and Annette Filges. Special thanks to Thomas and Martin Kunz for helping with the German translation of the abstract of this thesis. I would like to thank Dr. Mark Parrington, Dr. Sebastien Massart and Dr. Anna Agusti-Panareda at the ECMWF and Dr. Michael Buchwitz and Dr. Maxmillan Reuter at the University of Bremen. It was truly a pleasure working with you during my research stay.

I gratefully acknowledge the funding sources that made my Ph.D. work possible. This work was funded by European Community's Seventh Framework Programme ([FP7/2007-2013]) under grant agreement n° 312311 for the IGAS project (IAGOS for the GMES Atmospheric Service).

During my Ph.D., I have had the opportunity of interacting with a number of warm-hearted people. I would like to express my heartfelt gratitude to Ulrike Schleier for her unfailing support and kind concern right from my very first day in Germany. Special thanks to Steffi Rothhardt, John Schmidt and Anna Görner for all their help in making life easier in this new country. A big thank you to all my friends and fellow Ph.D. students at the department −Min Jung Kwon, Sung-Bin Park, Annette Filges, Sabrina Arnold, Martin Kunz, Ina Burjack, Fanny Kittler, Chirag Dhara, Karel Castro-Morales, Sandra Bölck, Steffen Schmidt−and all other colleagues at MPI-BGC.

I would like to thank my family−my grandma, my parents−Geeta Verma and Sanjay Verma−and my brother, Sohael−for their unconditional love and blessings. Thank you for always encouraging me to follow my dreams and never letting me give up. I would not have made it this far without you all. My friend, Sirisha, whose words of motivation and encouragement kept me going. Last but not the least, I would like to thank my fiancé, Himanshu for being my biggest cheerleader. Your faithful support during the final stages of this Ph.D. is so appreciated. Thank you.

Curriculum Vitae

Date of Birth: 6 July, 1988

Nationality: Indian

Education:

Sep. 2013-present	Ph.D. Thesis: International Max Planck Research School (IMPRS) for Global Biogeochemical Cycles, Max Planck Institute for Biogeochemistry, Jena, Germany. / Friedrich-Schiller University, Jena
2011-2013	Master of Technology (Climate Science): Indian Institute of Science, Bangalore, India.
2006-2010	Bachelor of Engineering (Electrical and Electronics): Panjab University, Chandigarh, India.
2004-2006	Higher-Secondary School: Moti Ram Arya Sr. Secondary School, Chandigarh, India.
2004	High School: Carmel Convent School, Chandigarh, India.

Publications:

Verma, S., Marshall, J., Gerbig, C., Roedenbeck, C., and Totsche, K. U.: The constraint of CO2 measurements made onboard passenger aircraft on surface-atmosphere fluxes: the impact of transport model errors in vertical mixing, Atmos. Chem. Phys. Discuss., doi:10.5194/acp-2016-597, in review, 2016

Verma, S., Marshall, J., Parrington, M., Agustí-Panareda, A., Massart, S., Chipperfield, M.P., Wilson, C., Gerbig, C. Extending methane profiles from aircraft into the stratosphere for satellite total column validation: A comparative analysis of different data sources, Atmos. Chem. Phys., (submitted), 2016.

Shreeya Verma

Selbstständigkeitserklärung

Ich erkläre, dass ich die vorliegende Arbeit selbstständig und nur unter Verwendung der angegebenen Hilfsmittel, persönlichen Mitteilungen und Quellen angefertigt habe.

Shreeya Verma